University of Stellenbosch

Department of Civil Engineering

Investigation into a beam-column connection in pre-cast concrete

JIN ZANG

Thesis presented in partial fulfilment of the requirements for the degree of Master of Science in Structural Engineering at the University of Stellenbosch

Study Leader:

Prof. J. A. Wium

March 2010

DECLARATION

I, the undersigned, hereby declare that the work contained in this thesis is my own original work and that I have not previously in its entirety or in part submitted it at any university for a degree.

Signature: ..... Date: .....

Abstract

Pre-cast sections have the advantages of structural efficiency, better quality control and less construction time, which enable them to be widely used in building structures. The connections of pre-cast buildings play a vital role for the stability and strength of structures.

Nowadays, more attention is drawn to the aesthetical appearance of building structures, especially by architects. The Hidden Corbel Connection (HCC) was then developed to make the building structures stable and aesthetically pleasing. A modified HCC was designed and investigated in this study.

Amongst all the mechanisms in the connection zone, the mechanism of the end anchorage length of tension reinforcement plays a key role in the economy of the connection and is hence further investigated.

In order to investigate whether the end anchorage length of tension reinforcement can be reduced for a simply supported beam, a 2D non-linear finite element model is used to analyze the stress distribution inside the connection zone. Based on the stress distribution in the connection zone, the tensile force was calculated at the face of the support, which directly correlates to the required end anchorage length of tension reinforcement.

The confinement in the connection zone increases the bond stress, which in turn reduces the required anchorage length of tension reinforcement. Therefore, a 3D model is used to analyze the region inside the modified HCC to find the position of the best confinement.

By comparing the finite element (FE) results with Eurocode 2 (2004), and SABS

0100-1 (2000), it is demonstrated that the FE results require the shortest anchorage length, while the longest anchorage length is specified in SABS 0100-1 (2000). Based on the comparison between the FE results and the design codes, a laboratory experiment was then performed to determine if the end anchorage length of tension reinforcement can be reduced. Four beams with different support conditions and with different end anchorage length of tension reinforcement were tested. The results of the laboratory experiment indicate that the end anchorage length for simply supported beams can be shortened from the specification of SABS 0100-1 (2000).

ACKNOWLEDGEMENTS

This research could not be completed without the support of many individuals and organizations. I appreciate the support of the following people and organizations and sincerely thank them for their time, guidance, and their expertise.

- My promoter Professor Jan Wium, for his time, guidance, patience, support and encouragement.
- Professor van Zijl, for his information about concrete mix.
- Dr. Strasheim, for his ideas.
- University of Stellenbosch, for support and financial assistance.
- All the others who helped me with my research.

TABLE OF CONTENTS

LIST OF TABLES

LIST OF FIGURES

LIST OF ABBREVATIONS

2D:	Two dimensional
3D:	Three dimensional
BCF:	Beam, Column and Freely-supported
FE:	Finite element
FEM:	Finite element methods
FEA:	Finite element analysis
Fib:	International Federation for Structural Concrete
HCC:	Hidden Corbel Connection
N-R:	Newton-Raphson
SASCH:	South African Steel Construction Handbook

TERMINOLOGY

Bond stress:	The shear stress acting parallel to the reinforcement bar on the interface between the bar and the concrete.
Connection zones:	The connection zones are the end regions of the structural elements that meet and are connected at the joint.
Mechanisms:	A natural or established process by which the forces transfer takes place. In this research investigation, mechanisms refer to force transfer mechanisms in the connection zone.

CHAPTER 1

INTRODUCTION

Pre-cast concrete sections have been used by ancient Roman builders and are widely used for modern structures. The British National Pre-cast Concrete Association (2005:28) indicates one hundred advantages of pre-cast concrete including structural efficiency, better quality control, less construction time, unaffected by weather conditions, less labour and less skilled labour are required. These advantages make the use of pre-cast concrete sections a preferred design concept.

The International Federation for Structural Concrete (fib, 2008:31) indicates that connections are essential parts in pre-cast structures. The reaction forces at supports are the dominant shear force that should be considered by designers when doing structural design. Fib (2008:31) further explains that high concentrated loads induced by concrete elements will make the connection zones to be strongly influenced by this force transfer. Therefore, stress distribution near the connection area plays a vital role for the stability and strength of structures.

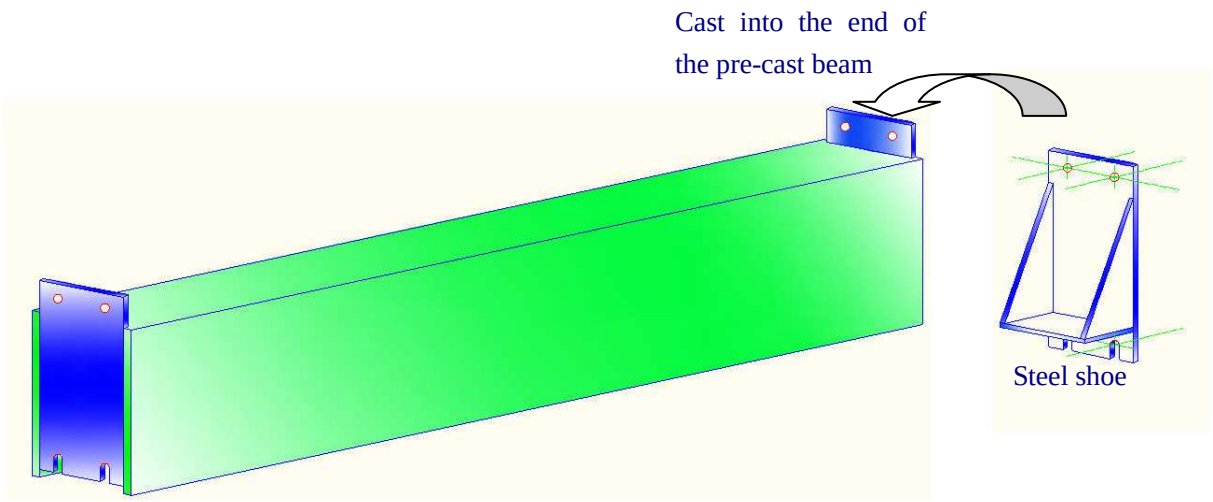

Figure 1.1: Pre-cast beams with built in steel shoe.

Besides stability of the building, more attention is paid to the aesthetic appearance nowadays than before. Traditional corbels for pre-cast beam and column connections are not aesthetically pleasing so it is difficult to make them meet the requirements from architects. In order to meet the requirements from architects and structural engineers, the concept of a hidden corbel was introduced.

A substantial amount of research about hidden corbels has been conducted to meet the requirements from architects. However, some of them are too complicated to make or install, especially in South Africa where the manufacturing industry is still developing. Research by Jurgens (2008:38) introduced the idea of a hidden corbel for South Africa.

The modified hidden corbel is shown in Figure 1.1. The right part of the picture shows steel plates are welded together to form a steel shoe, which acts as a hidden corbel. The left part of the picture shows the steel shoes cast into the end of a pre-cast concrete beam. With the shoe, the pre-cast beam can then be fixed to the column through high strength bolts. For concrete columns, the bolts can pass through sleeves in the columns. In this way, force transfer is accomplished between structural elements in a pre-cast system.

This research focuses on mechanisms in the connection zone of pre-cast beams for skeletal frames. Stress concentrations occur near the support following the *Saint-Venant's Principle*. The stress concentration makes it difficult to analyze stress conditions near the support area through linear static analysis of concrete members. In this study, a non-linear finite element (FE) model is used to analyze the stress distribution inside pre-cast beams near connection areas. A better understanding of the stress distribution in pre-cast beams near the connection areas was thus obtained through analyses using the non-linear FE model. Based on the FE analysis (FEA), the mechanisms in the connection zone can be identified and verified to see whether the force transfer can meet the specification from the current South Africa design code

SABS 0100-1 (2000). Through comparison with other design codes, it is evaluated whether the specifications for reinforcement anchorage at support locations can be reduced as specified in SABS 0100-1 (2000). The end tension anchorage length directly affects the size of the modified hidden corbel and hence will lead determining if the modified hidden corbel can be used economically and practically. The following paragraphs will introduce the main research problem and sub problems of this thesis.

1.1 Context of the research project

This study considered issues which influence the design of the hidden corbel in a pre-cast connection. One such aspect is the requirement for anchorage at the tensile reinforcement.

South African standard SABS 0100-1 (2000) gives a formulation which can be used to design pre-cast connections. Some specifications are mainly based on experimental results. SABS 0100-1 (2000) specify that reinforcement should be anchored for a length of 12 times the diameter of the main reinforcement after the centre of the support for a simply supported beam. If this is the case, the length of a modified hidden corbel in the direction of span can potentially be quite large. Therefore, the length of the corbel should be at least 24 diameters of reinforcement for straight bars and 8 diameters of reinforcement for 90 degree bent-up bars as shown in Figure 1.2 plus concrete cover. If these specifications are followed, then the increased size of the modified hidden corbel is not economic to use.

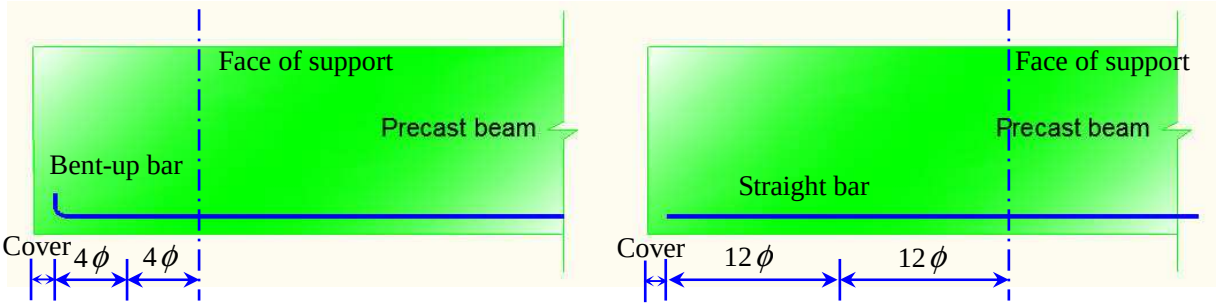

Figure 1.2: Sketch for tension reinforcement that extends into the support.

Mosley, Bungey & Hulse (2007:100) indicate that *The Variable Strut Inclination Methods* was applied in Eurocode 2 (2004) to calculate shear resistance in tension to make the design more economical. In the connection zone, the shear force contributes to the tensile force in the tension reinforcement which in turn affects the required anchorage length. The methods on how to calculate tensile force will be explained in detail in section 2.4.1 of the literature study.

The location of the critical sections beyond which a bar needs to be anchored at an end support is also not clear. SABS 0100-1 (2000) specifies that the critical section is the centre of the corbel and Eurocode 2 (2004) indicate the critical section is measured from the face of the support.

The stress concentration near the support area has a big influence on how the stress is distributed. The formula for calculating the end tensile force includes the parameter theta in the method in Eurocode 2 (2004). Theta is the angle between the concrete compression strut and the beam axis perpendicular to the shear force. Eurocode 2 (2004) is based on linear material methods and specifies the theta value to be between 22 and 45 degrees which does not make sense for the stress concentration area (Figure 2.10). However, in actual conditions, the theta rather should be close to 90 degrees when the cross section is located next to the face of the support (Figure 5.19).

As mentioned above, the true stress distribution near the support is difficult to analyze through linear material analysis because of the stress concentration effect. In order to calculate the end anchorage length, the stress distribution near the support area needs to be analyzed. Based on the stress distribution in the connection zone, the requirement for reinforcement and stirrups can be calculated. Eurocode 2 (2004) indicates that the confinement will affect the anchorage length. Therefore, effects of the stress distribution in the beam end zone on the anchorage length of reinforcement have to be analyzed.

1.2 The statement of the main subject of research

The main subject of research in this study is to determine if the end anchorage length of tension reinforcement can be reduced when using the modified hidden corbel for pre-cast concrete beams.

1.3 The statement of the sub-problems:

- The first sub-problem is to determine the stress distribution in the connection zone.
- The second sub-problem is to determine the impact of the stress in the connection zone on the choice of the layout of reinforcement bars and stirrups.
- The third sub-problem is to determine the impact of the stress distribution on the end anchorage length of tension reinforcement.

1.4 Research objectives

The intention of this research is to obtain a better understanding of the mechanisms in the connection zones of pre-cast beams with a built-in hidden corbel. Parameters identified to play a role:

- Anchorage length;
- Confinement: Horizontal and vertical directions;
- Support flexibility;
  - Rebar type;
  - Concrete parameters;
  - HCC geometry;
  - HCC plate thickness.

To satisfy this intention, the following objectives are identified:

- To analyze the stress distribution in the connection zone;
- Through analyzing the stress distribution in the connection zone, to get a better understanding of the required reinforcement and stirrups;
- Through analyzing the stress distribution in the connection zone, to identify the reasonable critical section for calculating the end anchorage length;
- Through analyzing the stress distribution in the connection zone, to determine how the confinement in the transverse and vertical direction will affect the end anchorage length.

1.5 Hypotheses

For this study, a few hypotheses were set:

- The first hypothesis is that the principal stress distributes in a beam to form a curved compressive stress arc and a tensile stress with the slop of a suspended chain.
- The second hypothesis is that compressive stress is taken up by concrete and the tensile stress is taken up by reinforcement and stirrups.
- The third hypothesis is that the required anchorage length for reinforcement at the support can be shortened from the specification of SABS 0100-1 (2000) for simply supported beams.

1.6 Delimitations of the research

The design conditions vary with different types of buildings. Due to the time restriction, this research focused on:

- Static uniformly distributed loads along the length of a beam instead of concentrated loads near the connection zone, dynamic loads or seismic loads.
- Skeletal frame type of pre-cast concrete building.
- Stress distributed in pre-cast beams with built-in hidden corbel.
- Short term effects.
- Mechanisms that affect end anchorage length of tension reinforcement.

However, this research was limited to a specific range. The research did not consider:

- Axial forces and torsion in the beam.
- Long term effects like creep and shrinkage.
- The material characteristics that affect anchorage length.

1.7 Research methodology

In order to understand the stress distribution in the connection zone, a non-linear material FE model is needed.

Before setting up the FE model, a skeletal frame model is selected so that some practical calculations can be done based on the selected model. With detailed dimensions for the selected model available, the detailed information about the required reinforcement and stirrups can be calculated according to SABS 0100-1 (2000). Subsequently, the detailed information such as the layout of reinforcement, stirrups, and section will serve as the reference data for the FE model.

A two dimensional (2D) plane stress FE model is then set up. By analyzing the results from the FE model, principal stress is obtained on each element. Based on the theory of *Mohr's circle*, the values of normal stress and shear stress can be calculated for each element of the FE model. After analysing the FE model, theoretical calculations are needed to verify the results from the FE model. The analyses of a FE model

assisted to obtain a better understanding of the mechanisms in the connection zone. Subsequently, a three dimensional (3D) model is setup using brick elements. Based on the results from the 2D model, corresponding loads were applied to the 3D model to simulate the effect of the modified hidden corbel. The factors that will affect the end anchorage length can be determined by analyzing the stress distribution in the 3D model.

The FE results were then used to compare with the design codes. In order to determine whether the end anchorage length of the tension reinforcement can be reduced, a laboratory experiment was performed to further verify the theoretical results.

1.8 Overview of this study

The layout of the dissertation is illustrated in Figure 1.3. Chapter 1 presents an introduction to the research, the background knowledge, the main subject of research, the limitations and the objectives of this investigation. Chapter 2 presents a literature review of mechanisms near the support areas. Chapter 3 reviews the methodology of this investigation. Chapter 4 presents the non-linear material FE model of this investigation. Chapter 5 presents the numerical results obtained from the FEA. A comparison between the numerical FE results and the theoretical hand calculations are then presented. Chapter 6 compares the experimental results with the current design code and confirmed the analysis by a laboratory experiment. Chapter 7 concludes this dissertation and identifies possible future research needs.

Figure 1.3: Layout of Dissertation.

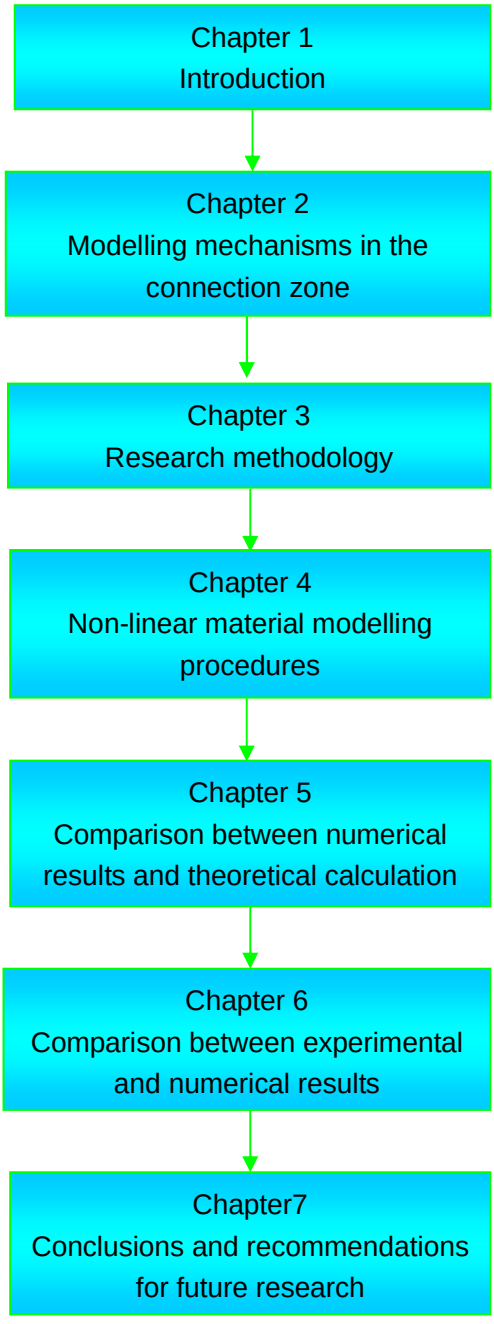

CHAPTER 2

MODELLING MECHANISMS IN THE CONNECTION ZONE

2.1 Introduction

The main purpose of this chapter is to determine and define the types of mechanisms in beam section component interaction. Advantages of pre-cast concrete from the report of the British National Pre-cast Concrete Association are that pre-cast sections have better quality control and less construction time amongst others. Fib (2008:31) shows that connection zones are strongly influenced by considerable concentrated load introduced by connecting concrete elements. Based on the above reasons, connection zones for pre-cast sections are comparatively critical for the design of pre-cast buildings. Therefore, types of mechanisms in the connection zone will be analyzed in this chapter. By applying the design codes for these mechanisms, it can be determined whether a further investigation is needed.

This chapter is divided into seven parts. The first part introduces different types of pre-cast structures and it selects skeletal frames for this research. The second part introduces skeletal frames. The third part compares some previous studies about Hidden Corbel Connections (HCC) and selects a modified HCC for this investigation. The fourth part identifies the mechanisms in the connection zone of the modified HCC. The fifth part selects a frame model for the analysis of mechanisms in the connection zone. The sixth part analyses the mechanisms in the connection zone that are defined from the fourth part. Finally, the contents of this chapter are summarized and it is shown that a non-linear material FE model is needed for the analysis of connection zone.

2.2 Skeletal frames

Fib (2008:31) states that the main purpose of structural connections is to transfer forces between the pre-cast concrete elements. The behaviour of the superstructure and the pre-cast subsystems should interact together as an integrated system to transfer loads in the system. Force transfer between pre-cast concrete elements for different types of pre-cast concrete buildings is not the same.

Fib (2008:1) introduces three types of pre-cast buildings. These are skeletal frames, wall frames and portal frames. Because skeletal frames have great potential to be used in industrial and high-rise buildings, skeletal frames are selected for this research. Figure 2.1 gives an example of skeletal frames.

Figure 2.1: Skeletal frames (Courtesy Trent Concrete Ltd., UK).

As shown in Figure 2.1, skeletal frames mainly consist of pre-cast beams, pre-cast columns and pre-cast slabs. Pre-cast concrete beams connect with pre-cast columns to form a framework. Then, pre-cast floors are installed on top of the pre-cast beams to form the whole structure.

2.3 Previous research on HCC

Amongst research on various type of HCC, three typical types of HCC are discussed and presented here. The three types of HCC will be introduced in the following paragraphs.

2.3.1 Beam, Column and Freely-supported connection: Type Ⅰ

According to Vamberski, Walraven and Straman (cited in Jurgens, 2008: 31), the Beam, Column and Freely-supported (BCF) corbel has the advantage of simple formwork, saving on erection time and a good fire resistance. JVI (2009: 2) describes that the BCF connection was developed in Norway in 1987 by Partek-Ostspenn and has successfully been used in Europe for more than 5 years after the first usage. The new version of BCF was introduced in 1993 with a reduced cost and increased ultimate capacity. A typical BCF connection is shown in Figure 2.2.

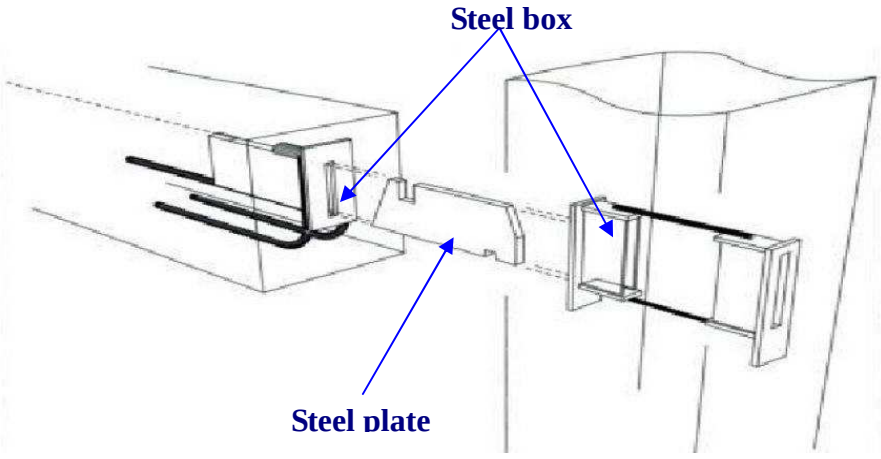

Figure 2.2: BCF connections (Vamberski et al., 2005).

From Figure 2.2, it can be seen that a high precision is needed when the steel plate links between pre-cast beams and pre-cast columns. If the opening of a steel box is too wide, the beam tends to have torsional moment. If the opening of the steel box is too narrow, it is difficult for workers to connect the steel plate between pre-cast beams and columns. Therefore, high costs would be incurred to provide the high precision of BCF connections in South Africa. In addition, the welding of reinforcement to the steel box is also an expensive component in South Africa. For the reasons, BCF connections are currently not suitable for use in South Africa.

2.3.2 HCC: Type Ⅱ

Research done by Kooi (2004: 63) indicates another type of hidden corbel as shown in Figure 2.3. The conclusion from Kooi (2004: 63) is that a dowel bar which is used in the connection should not be too stiff in order to prevent the failing of grout around the dowel bar.

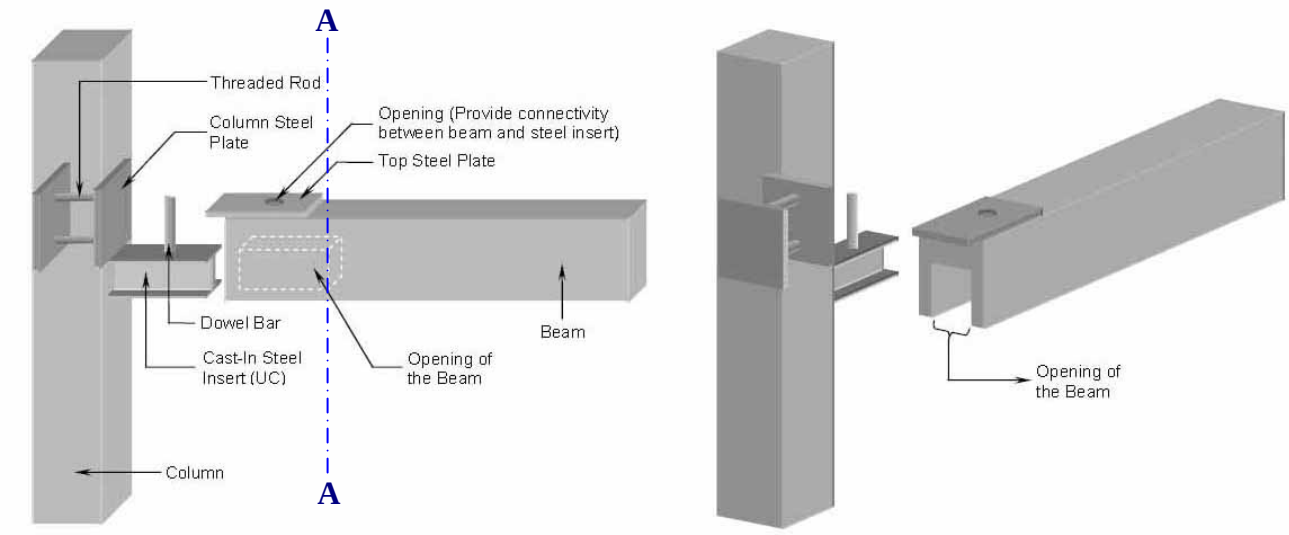

Figure 2.3: HCC Type Ⅱ (Kooi, 2004).

For this type of hidden corbel, special measurements are needed to fix the Cast-In Steel Insert into the column. Installation is easy but the corbel itself is expensive. In

addition, there is no concrete cover below the extreme bottom fibre of the Cast-In Steel Insert, which makes it unable to meet the specification of fire resistance from the design code except if special treatment is applied.

Beams are divided into simply support beams and continuous beams according to their usage. For a simply supported beam, the shear force in the corbel is the dominant force for design. Shear resistance mainly depends on the height of Cast-In Steel Inserts and depends on the classification of the steel used. The cross sectional area between the interface of the Cast-In Steel Insert and the pre-cast beam (marked A-A in Figure 2.3) is relatively small. This reduced section makes shear failure in this type of HCC a critical aspect. In addition, the tension reinforcement needs a certain anchorage length after the critical section, which is difficult to achieve in this type of HCC.

For the continuous beam, there is no problem for HCC because the bottom reinforcement is in compression and the top reinforcement is in tension. The negative bending moment and the redistribution of the negative bending moment will be high in the Cast-In Steel Insert and the dimension of the Cast-In Steel Insert is dependent on the designer. Therefore, the anchorage of bottom reinforcement for continuous beams is not a problem.

Based on the above reasons, HCC Type Ⅱ is also not suitable to be used in South Africa at present.

2.3.3 HCC: Type Ⅲ

Based on the current industry status in South Africa, Jurgens (2008:38) introduced the concept of HCC by using a steel shoe into the end of a pre-cast beam as shown in Figure 2.4. Jurgens (2008:39) mentioned that this type of HCC has the characteristics of economy and ease of manufacture as well as being aesthetically pleasing.

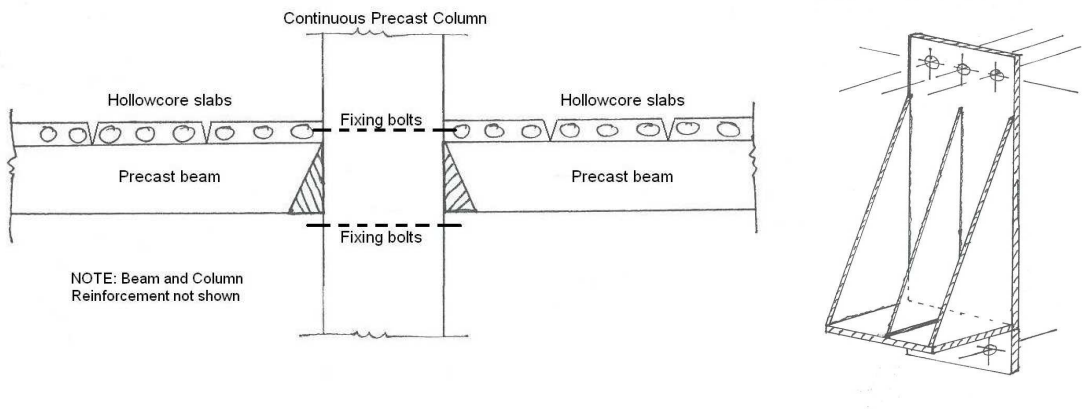

Figure 2.4: HCC Type III (Jurgens, 2008).

As shown in Figure 2.4, the right part of the picture is the steel shoe and the left part indicates how the pre-cast beam is connected with the pre-cast column. Through a bolted connection, the pre-cast beam can be easily fixed to the column on site.

However, part of the fixing bolts and nuts at the bottom of the pre-cast beam is exposed after fixing the pre-cast beam to the column. This makes the appearance of this type of HCC not completely aesthetically pleasing and hard to meet the requirements from architects. The nuts exposed to the air make the connection easy to corrode depending on the ambient air conditions. The bottom face of the hidden corbel and the fixing bolts lack of concrete cover prevent them from failure during a fire accident. Therefore, a modified HCC will be introduced in the following section.

2.3.4 Modified HCC for this investigation

Based on the above analysis of three types of HCC, this research will focus on the proposed HCC by Jurgens (2008), which is considered more suitable to be used in South Africa.

For ease of manufacturing and economy, the steel shoe, which acts as a hidden corbel, has been slightly modified as shown in Figure 2.5. The width of the pre-cast

beam is normally limited for economical design. The limited space makes the welding of the central triangular plate in the middle area difficult and unnecessary (Figure 2.4). Therefore, the triangular plate in the middle is excluded from the modified version of the HCC. The welding of triangular side plates are comparatively easier to be manufactured. The bottom part of the back plate has holes to enable easy installation.

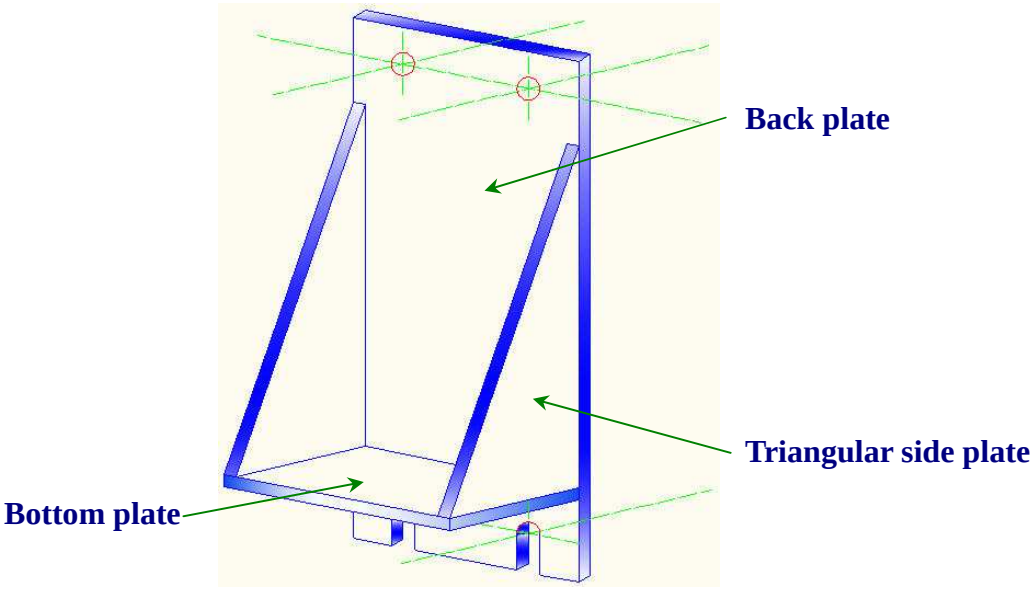

Figure 2.5: Sketch for the hidden corbel.

Considering fire resistance, the hidden corbel is shifted up a certain distance (as compared to the HCC by Jurgens) to ensure the bottom surface of the hidden corbel have enough concrete cover. This distance measures from the bottom fibre of the pre-cast beam to the bottom surface of the hidden corbel. The modified version of the HCC of pre-cast beam is shown in Figure 2.6.

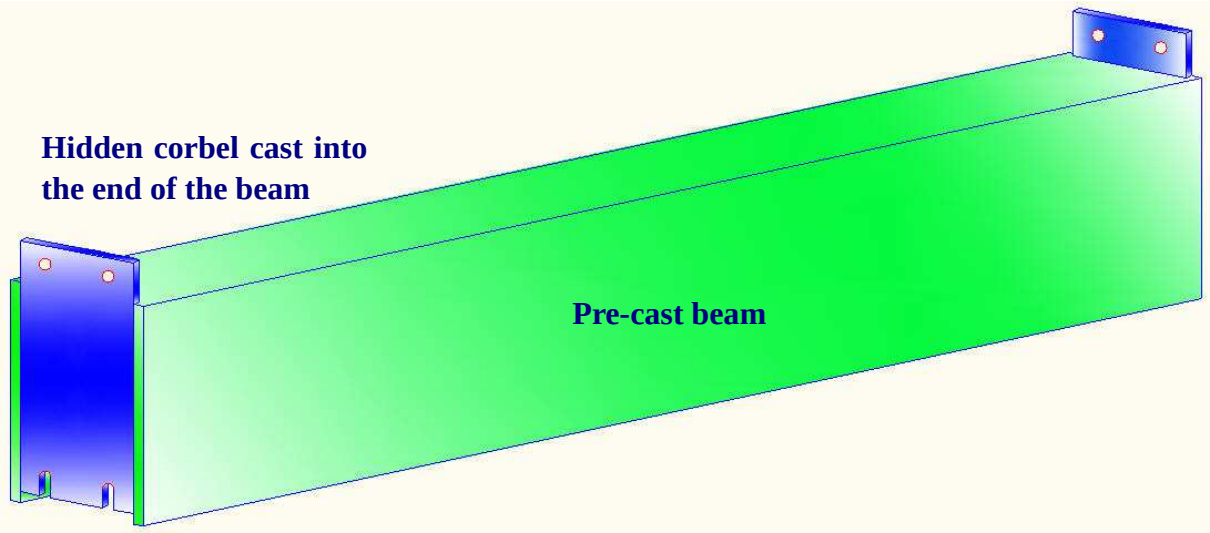

Figure 2.6: Layout of pre-cast beam with built-in hidden corbel.

The opening at the bottom of the hidden corbel enables the pre-cast beam to be laid directly onto the bottom part of the high strength bolts. The top part of the high strength bolts can then be placed in position. After that, the nuts are used to fix the pre-cast beam to the pre-cast column which makes the installation much easier on the construction site. After fixing the pre-cast beam to the column, the gap at the bottom of the plate can be filled with grout (Figure 2.7). The grout will ensure that the bottom plate of the hidden corbel has enough concrete cover, which guarantees sufficient fire resistance. The grout also reduces problems which may arise due to lack of fit.

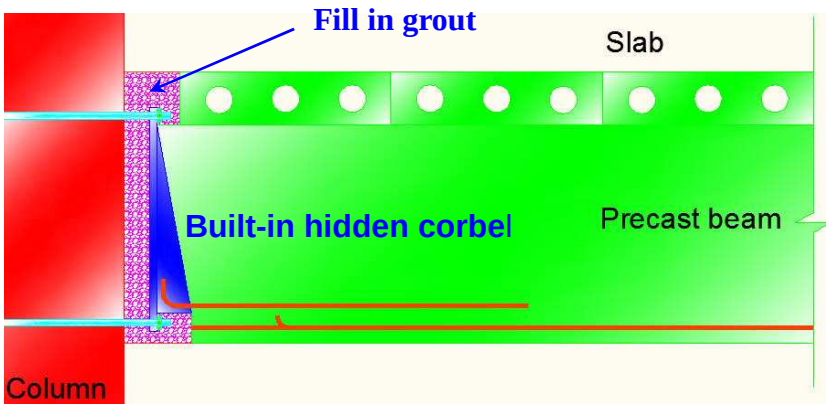

Figure 2.7: Sketch fill in grout.

2.4 Mechanisms of pre-cast beams in the connection zone

Considering the concrete cover and the economy of design, tension reinforcement should be as close to the bottom fibre of the beam as possible. According to SABS 0100-1 (2000), 50% of the tension reinforcement should extend into the support and extend 12 diameters beyond the centre of the support to ensure enough anchorage. Because the spacing is limited, additional reinforcement will be used. The additional reinforcement extends into the hidden corbel, and is then connected to the main reinforcement through a lap splice as indicated in Figures 2.8 and 2.9.

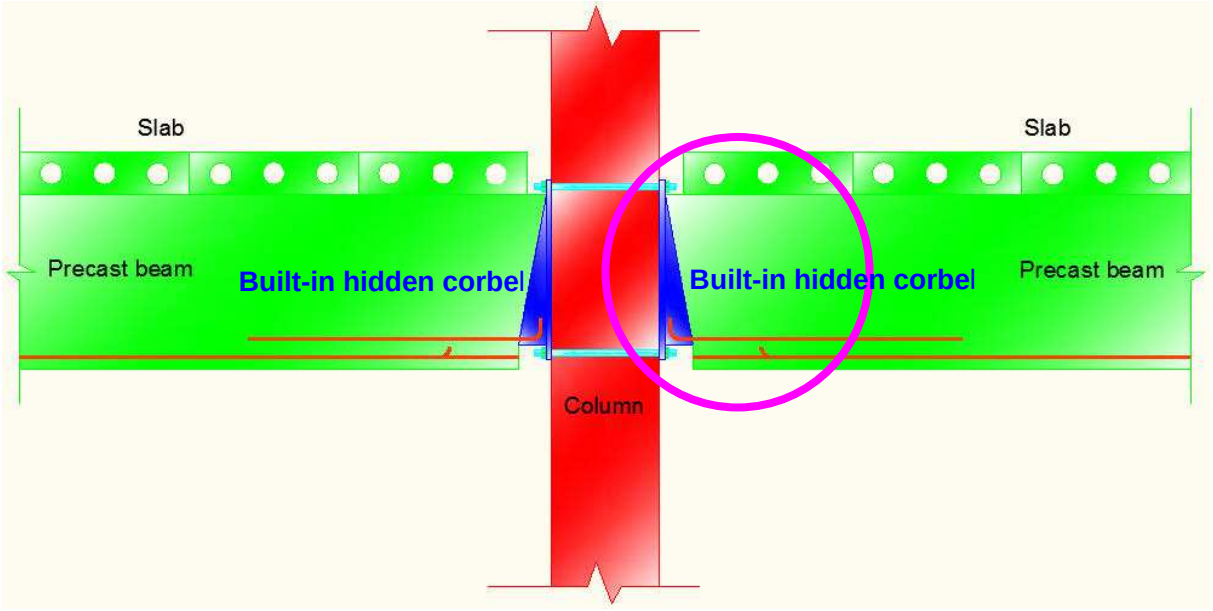

Figure 2.8: Sketch for the modified HCC.

This research focuses on the connection zone as indicated in Figure 2.8. The circled area in Figure 2.8 is enlarged to identify the mechanisms in the connection zone as shown numbered in Figure 2.9.

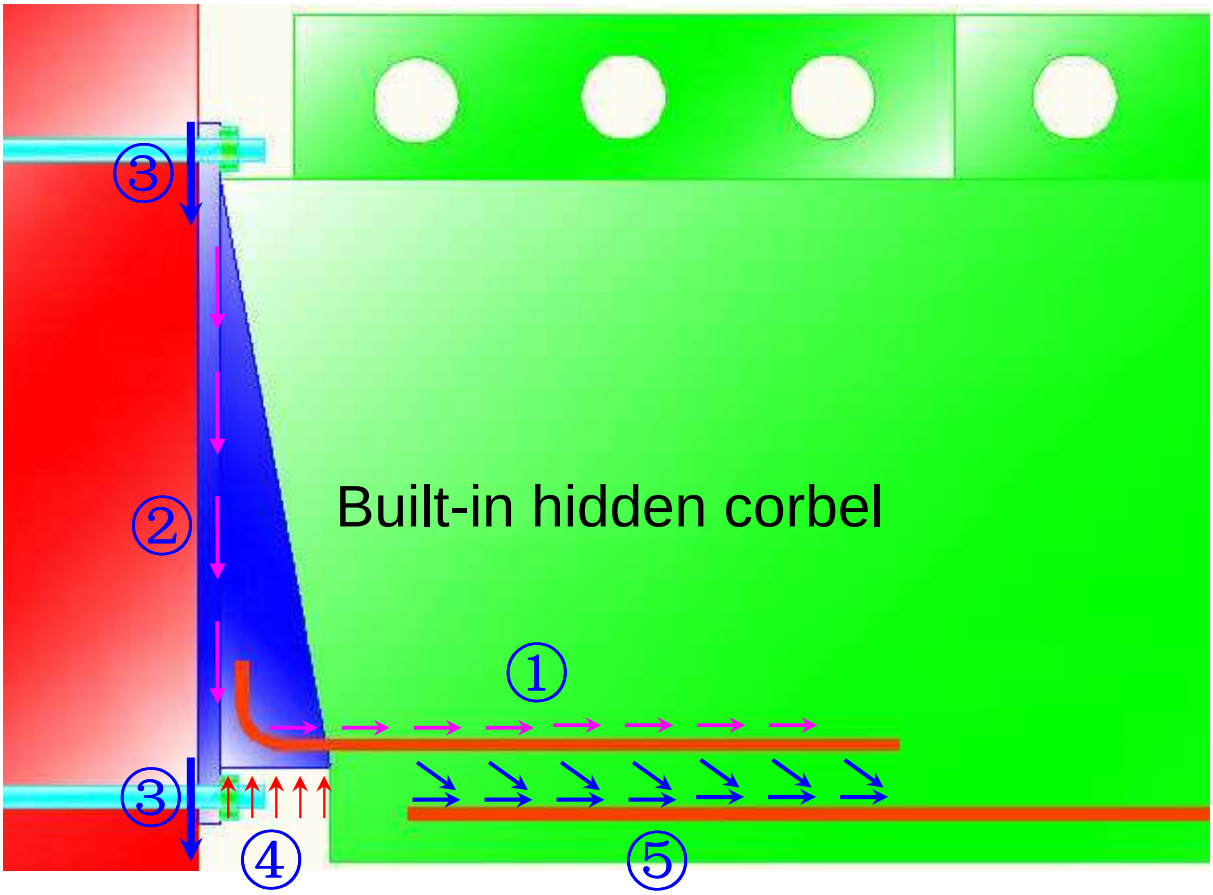

Figure 2.9: Sketch for mechanisms in connection zone.

As indicated in Figure 2.9, there are five types of mechanisms in the connection zone of the modified hidden corbel to be considered:

- Mechanism 1: tensile force from the tension reinforcement;
- Mechanism 2: shear force that is taken up by the welding between the triangular plate and vertical rectangle plate;
- Mechanism 3: shear force between the pre-cast beam and the pre-cast column, which is resisted by high strength bolts;
- Mechanism 4: bearing force onto the bottom plate;
- Mechanism 5: force transfer by a lap splice between different layers of bottom reinforcement.

After identifying these five types of mechanisms in the connection zone, they will be introduced in detail in the following sections.

2.4.1 Mechanism 1: Tensile force from reinforcement in the connection zone

The main purpose of the tension reinforcement is to resist bending moments and part of the shear force. These tensile forces will then be transferred to pre-cast concrete beam through bond between reinforcement and the concrete. In the connection zone, a suitable anchorage length is needed to prevent the tension reinforcement from pulling out of the concrete. Hence, most design codes specify either a certain length of anchorage or introduce methods to calculate the end anchorage length.

2.4.1.1 Comparison of the end anchorage length between different design codes

SABS 0100-1 (2000) specifies the end anchorage length for a simply supported beam to be twelve diameters of reinforcements beyond the centre of the support. Correspondingly, fifty percent of the main mid-span reinforcement should extend to the support for simply supported beams.

The British design code BS 8110 (1997) is similar to SABS 0100-1 (2000) on this specification.

Eurocode 2 (EN 1992-1, 2004) gives another way to determine the end anchorage length. Clause 9.2.1.4 from Eurocode 2 (2004) specifies the tensile force to be anchored from the bottom tensile reinforcement at end supports according to the following formula, which equation 2.1 is a special case of equation 2.5.

$$F_E = \left|V_{Ed}\right| \cdot \alpha_l / z \qquad (2.1)$$

Where:

F_E : Tensile force to be anchored.

V_{Ed} : Design value of the applied shear force.

z : Lever arm of internal forces.

$$\alpha_l = z(\cot\theta - \cot\alpha)/2 \qquad (2.2)$$

θ: The angle between the concrete compression strut and the beam axis perpendicular to the shear force.

α: The angle between shear reinforcement and the beam axis perpendicular to the shear force.

The angles of alpha and theta are shown in Figure 2.10.

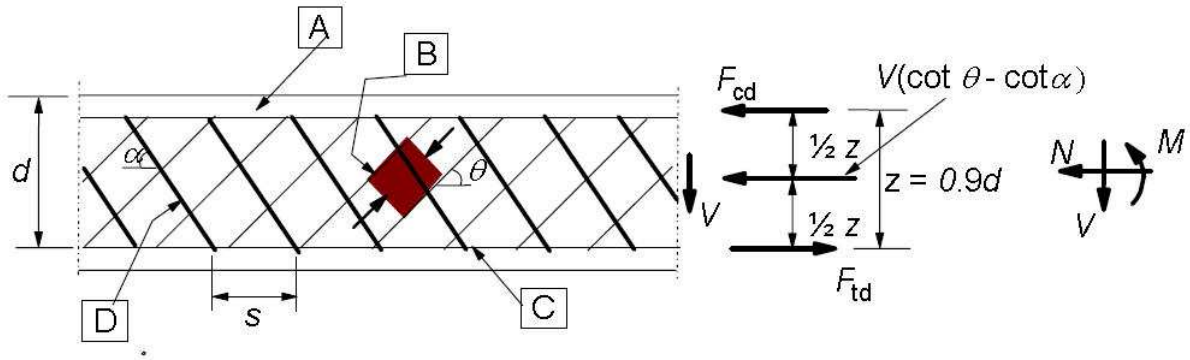

A - compression chord, B - struts, C - tensile chord, D - shear reinforcement

Figure 2.10: Sketch of truss model (Eurocode 2, 2004).

In case vertical stirrups are used near the support to resist shear force instead of bent-up bars, alpha equals ninety degrees. In South Africa, designers only use vertical stirrups to resist shear. Formula 2.2 will then change to:

$$\alpha_l = z\cot\theta/2 \qquad (2.3)$$

By substituting formula 2.3 into formula 2.1, we obtain:

$$F_E = |V_{Ed}|/2\cdot\cot\theta \qquad (2.4)$$

Where:

V_{Ed} : Design value of the applied shear force.

Eurocode2 also gives another formula to calculate tensile force in the tension reinforcement:

$$F = \frac{M}{0.9d} + \frac{V}{2}\cot\theta \qquad (2.5)$$

Where:

F : Tensile force in the tension reinforcement.

M : Ultimate limit state bending moment.

d : Effective depth of a cross-section

V : Ultimate limit state shear force.

Equation 2.5 can also be derived from Figure 2.10 when the design uses only vertical stirrups for shear reinforcement.

Comparing equation 2.4 and 2.5, it can be seen that equation 2.4 is a special case of equation 2.5 when the bending moment at support equals zero. Eurocode 2 (2004) is based on *The Variable Strut Inclination Methods* to determine the end anchorage length because equation 2.5 is based on this method.

The exact reason for the specifications in SABS 0100-1 (2000) and BS 8110 (1997) for the anchorage length for simply supported beam is unknown.

The tensile force for anchorage can be calculated according to Eurocode 2 (2004). However, Eurocode 2 (2004) limits the angle of θ in equation 2.5 to between twenty-two degrees and forty-five degrees. Concentrated loads will cause a stress concentration. For simply supported beams with uniformly distributed loads, a stress

concentration will occur in the support area as caused by the bearing force. The linear material theory near the support area is not valid in case of stress concentrations. In order to calculate tensile force near the support area, a non-linear material FE model is used to analyses how the stress is distributed near the support.

Although different design codes have different values for the bond stress, the principles for calculating the anchorage length are the same. The equation is shown below:

$$l_{anchorage} = \frac{F_s}{\pi \cdot \phi \cdot f_b} \tag{2.6}$$

Where:

$l_{anchorage}$: Anchorage length

F_s: Anchorage force

ϕ: Diameter of reinforcement

f_b: Bond stress

From equation 2.6, it can be seen that bond stress, anchorage force, bar diameter and anchorage length are interrelated. For structural design, anchorage length is one of the key criteria to check the strength of the structural member in the connection zone. Bond stress will directly affect the required anchorage length and is discussed in the next section.

2.4.1.2 Factors that affect bond stress

Bond stress interacts between the reinforcement and the adjacent concrete. Kong and Evans (1987: 221) state that adhesion, friction and bearing affect bond stress. Generally speaking, the reinforcement is quite similar across the world. The concrete

mix depends a lot on the water to cement ratio, aggregate size and type of sands. These components of concrete mix will influence the magnitude of bond stress.

Yasojima and Kanakubo (2004: 1) indicated that the maximum local bond stress increases proportional to the confinement force. Robins and Standish (1982: 129) also mentioned that a lateral pressure can significantly increase the bond strength, such as support region at beam to column connections and in deep beams. An increase in pull-out load of approximately 200% on the value for no lateral stress was obtained by applying a value of lateral stress close to the cube strength of the concrete (Robins and Standish, 1982: 133).

Eurocode 2 (2004) gives the value of bond stress under good or poor bond conditions. The bottom reinforcement subject to tension is considered to be good bond conditions. Eurocode 2 (2004) specifies the design value of bond stress according to different concrete cylinder strengths.

BS 8110 (1997) uses a formula to calculate the ultimate bond stress, which is given in equation 2.7 below:

$$f_{bu} = \beta\sqrt{f_{cu}} \qquad (2.7)$$

Where:

f_{bu} : Ultimate anchorage bond stress

β : Bond coefficient

f_{cu} : Characteristic cube strength of concrete

From BS 8110 (1997), it can be see that concrete strength will affect the ultimate bond stress. SABS 0100-1 (2000) does not give any equation for bond stress but defines the value of bond stress for different characteristic concrete cube strengths.

In order to compare the bond stress values between different design codes, the bond stress values from SABS 0100-1 (2000), BS 8110 (1997) and Eurocode 2 (2004) are presented in Figure 2.11 as a function of concrete cube strength.

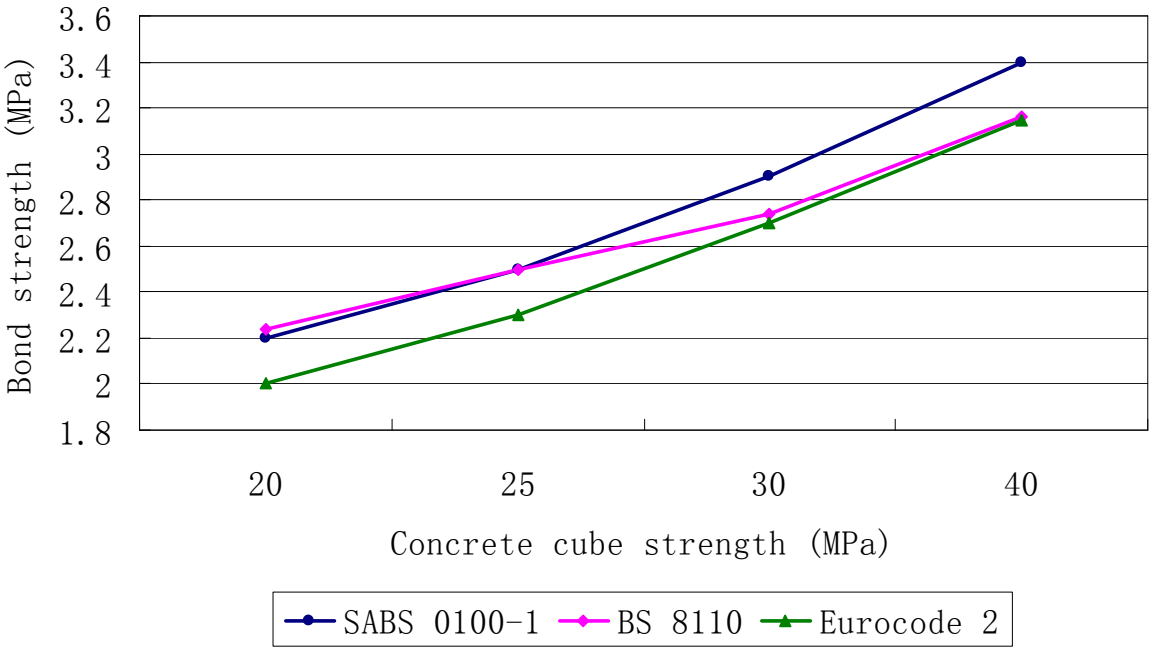

Figure 2.11: Bond stress between different design codes.

From Figure 2.11, it can be seen that Eurocode 2 (2004) has the lowest value of bond stress compared to the other two design codes. The bond stress values of SABS 0100-1 (2000) and BS 8110 (1997) are similar for lower concrete strength, but the slope for SABS 0100-1 (2000) is steeper than that of BS 8110 (1997).

The constituents of concrete mix such as aggregate (size), cement and sand will affect the bond stress. There are varieties in concrete mixes and the bond stresses for different concrete mixes are not the same. This investigation will only focus on reasons related to the transfer mechanism, which cause the changing in anchorage length, rather than material properties.

2.4.1.3 Factors that affect required anchorage length

Eurocode 2 (2004) defines that several factors influence the required anchorage length. These factors are:

- α1: The shape of bars.
- α2: Concrete cover to the reinforcement.
- α3: Confinement of transverse reinforcement not welded to the main reinforcement.
- α4: Confinement of transverse reinforcement welded to the main reinforcement.
- α5: Confinement by transverse pressure.

From the above factors, the confinement of transverse reinforcement will increase the bond stress. In addition, the transverse pressure will also increase the bond stress which in turn will reduce the required anchorage length. These effects can be applied to the modified hidden corbel connection.

Fib (2000:9) states that the stress state in the concrete surrounding the reinforcement has a significant effect on bond action. A transverse compressive force will increase bond stress and active confinement is always in favour of bond action.

As mentioned in 2.4.1.2, bearing affects bond stress. Bearing stress in the support will produce high pressure around the tension reinforcement, which extends into the support region. However, most design codes do not give any special consideration of how the bond will increase in the support areas.

The triangular side plate of the hidden corbel will provide transverse confinement to the concrete due to the effect of the Poison's ratio. This confinement will be in favour of the bond action. If it can be shown that the pressure from bearing forces and lateral

confinement can increase the bond, the end anchorage length can be reduced correspondingly.

2.4.2 Mechanism 2: Shear resistance of the hidden corbel

As shown in Figure 2.4, the triangular side plates, bottom plate and back plate are welded together to form a shoe and act as a hidden corbel. Shear is mainly taken by the welding between the triangular side plate and back plate through either full penetration welds or fillet welds. Clause 13.13.2 of SANS 10162-1: 2005 gives the formula on how to calculate the shear resistance of welds. The welding of plates belongs to the normal design procedure and has standard procedure in the manufacturing factory. Therefore, Mechanism 2 does not need further attention in this investigation.

2.4.3 Mechanism 3: Shear resistance of high strength bolts

High strength bolts are already standardised in South Africa. Clause 13.12 of SANS 10162-1: 2005 gives the formula to calculate the shear resistance of bolts. In addition, South African Steel Construction Handbook (SASCH) gives shear and tension resistance values for different types of bolts. Therefore, Mechanism 3 also does not need further attention in this investigation.

2.4.4 Mechanism 4: Bearing resistance of HCC

The bearing resistance refers to the resistance of the concrete on the corbel. Clause 6.2.4.4.4 of SABS 0100-1 (2000) specifies the ultimate bearing stress to be equal to 0.4 times characteristic concrete cube strength on condition of dry bearing on concrete. For other conditions, the ultimate bearing strength can be higher than this value. Therefore, 0.4 times characteristic concrete cube strength is used for a conservative design. The bearing resistance of HCC is used to determine the size of

the bottom plate of HCC. The plate needs to be large enough to prevent concrete from crushing. Therefore, Mechanism 4 also does not need further attention in this investigation.

2.4.5 Mechanism 5: Force transfer by a lap splice between different layers of bottom reinforcement

Clause 4.11.6.6 of SABS 0100-1 (2000) specifies that the lap length should be larger than the design tension anchorage length. The mechanism for lap splice is the same as that of anchorage. Because there is enough space for the development of lap splice, mechanism 5 also does not need further attention in this investigation.

From the above evaluation, it can be seen that the tensile force from reinforcement and its anchorage in connection zone, needs to be investigated further. Therefore, the way in which the stress is distributed in the connection zone is a key factor in understanding the anchorage length in the support. A non-linear material FE model is then used for the analysis of stress distribution in the connection zone.

Formulae can only express the relationship between parameters in that equation. The exact dimensions of a structure are needed before a FEA can be performed. Therefore, a skeletal frame model is used for the FE model and to provide reference data for the subsequent evaluation. The following paragraphs determine the dimensions of structural members for a FE analysis.

2.5 Selecting a skeletal frame model for analyzing mechanisms in the connection zone

In normal concrete buildings, the span-to-depth ratio of beams needs to be limited to meet the serviceability requirement. Table 10 of SABS 0100-1 (2000) specifies basic span to depth ratios for rectangular beams up to 10 metres. The exercise of the typical

structure was chosen to have a span length at 10 m. This is considered quite a long span which will result in rather high shear forces at member ends. By demonstrating that the HCC can be used in such cases, it will also be feasible for shorter spans.

The British National Pre-cast Concrete Association (2005:28) indicates that pre-cast beams can be designed with high span-to-depth ratios. Higher span to depth ratios result in longer beam spans and reduce the number of columns and supports.

In this study, a 10 meter span was selected. The beam dimensions were chosen so that the serviceability limit state will be satisfied from the specification of SABS 0100-1 (2000). The width and the length of a typical slab bay in the skeletal frames were chosen to be 2:1. A column layout of 5×10 m was chosen. A simplified sketch of the layout is shown in Figure 2.12.

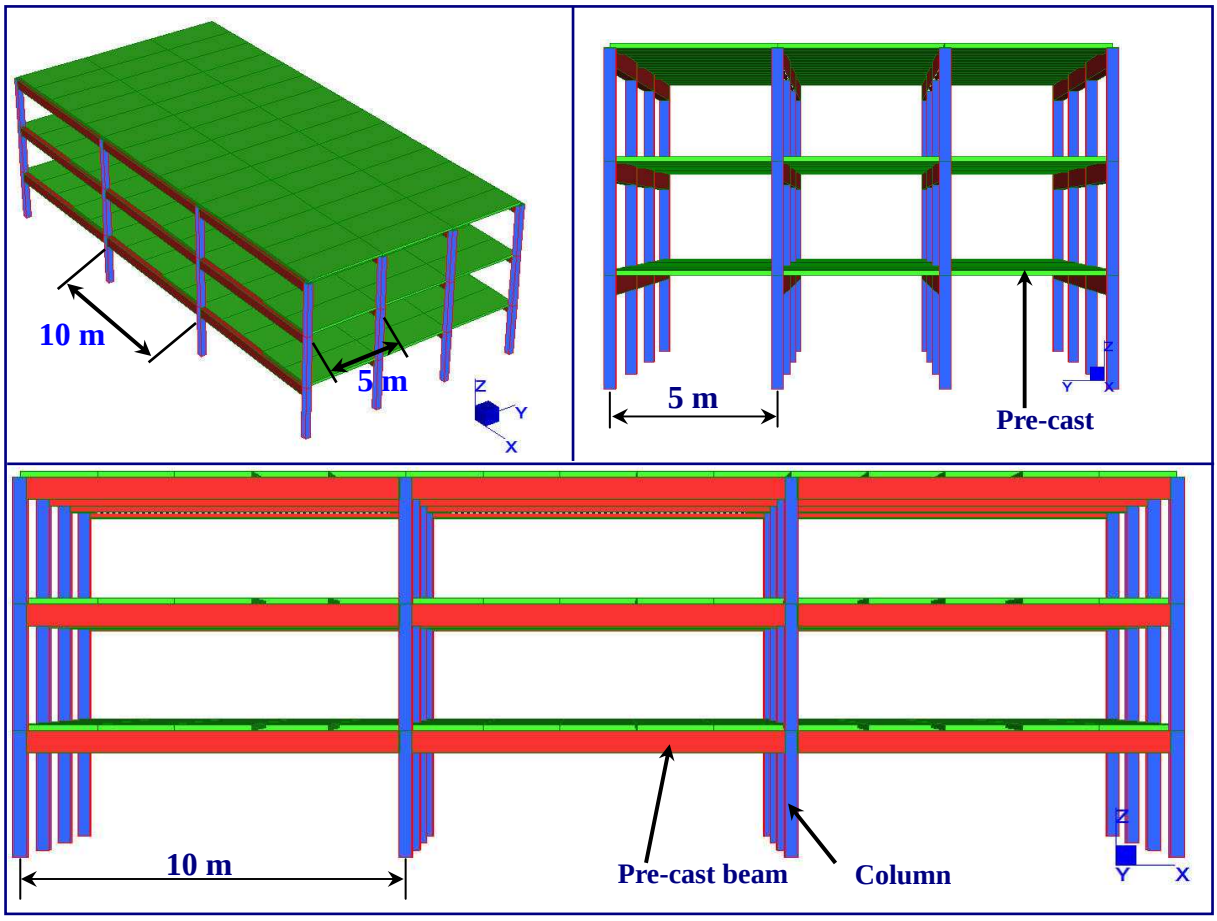

Figure 2.12: Sketch for the selected model.

The top left picture shows the isometric view of the skeletal frame model. The top right picture shows the transverse cross-section of the skeletal frame model and the bottom picture describes the longitudinal cross-section of the skeletal model.

It can be seen from Figure 2.12 that the pre-cast beams are fixed into the columns. The pre-cast slabs are then connected on top of the pre-cast beams to form the skeletal frames. For the modified HCC, if the bolts at the bottom part of the shoe can resist the shear force caused by self weight of pre-cast beams, then the pre-cast beams can lie directly on top of the bolts which can save temporary supports on site. After fixing the bottom bolts, the top bolts are fixed to guarantee enough shear capacity for the ultimate loads. This can greatly reduce the construction time and simplify the construction procedure. Hence, the modified HCC can make the design and construction easy and economical, which will have great potential for applications in South Africa.

2.6 Detailed information for the connection zone from the selected model

Based on the selected skeletal frame model, calculations on pre-cast beams are done and checked according to South Africa design codes. The detailed calculations are presented in Appendix A. The following sections introduce some important information based on the calculations of the skeletal frame model.

2.6.1 Description of design procedure

For pre-cast buildings, the pre-cast members are connected on site. The modified HCC enables the construction of skeletal frames to be more economical and practical. Because 10 metre is quite a long span, normally the beams are designed as a continuous beam for economical reasons. Two stages of installation are chosen based on the construction procedure.

Stage Ⅰ is the installation stage. This stage includes fixing of the pre-cast beams to pre-cast columns and then placing the pre-cast slabs on the pre-cast beams. Grout is used to fill the gap in the connection area to provide the fire resistance, to make the pre-cast building aesthetically pleasing, and to accommodate construction tolerances. Before a topping is placed over pre-cast slabs, the precast beam will support the slab load and wet topping concrete. Therefore, the pre-cast beam can be considered as a simply supported beam in this stage. A simple sketch of the beam configuration is

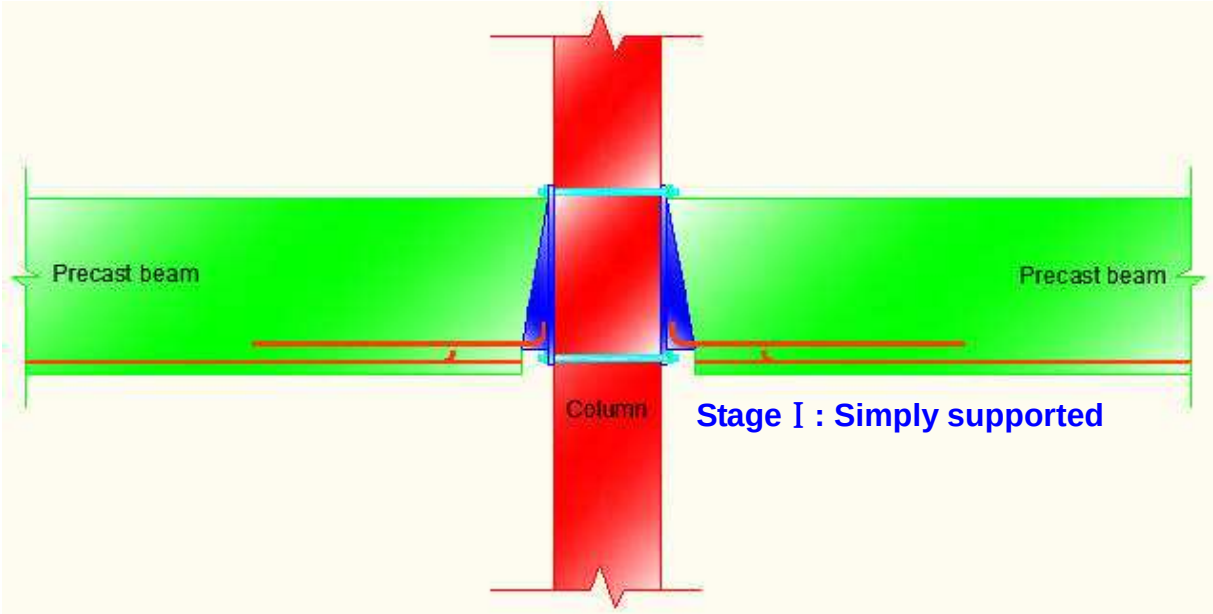

Figure 2.13: Sketch of beam type for Stage Ⅰ.

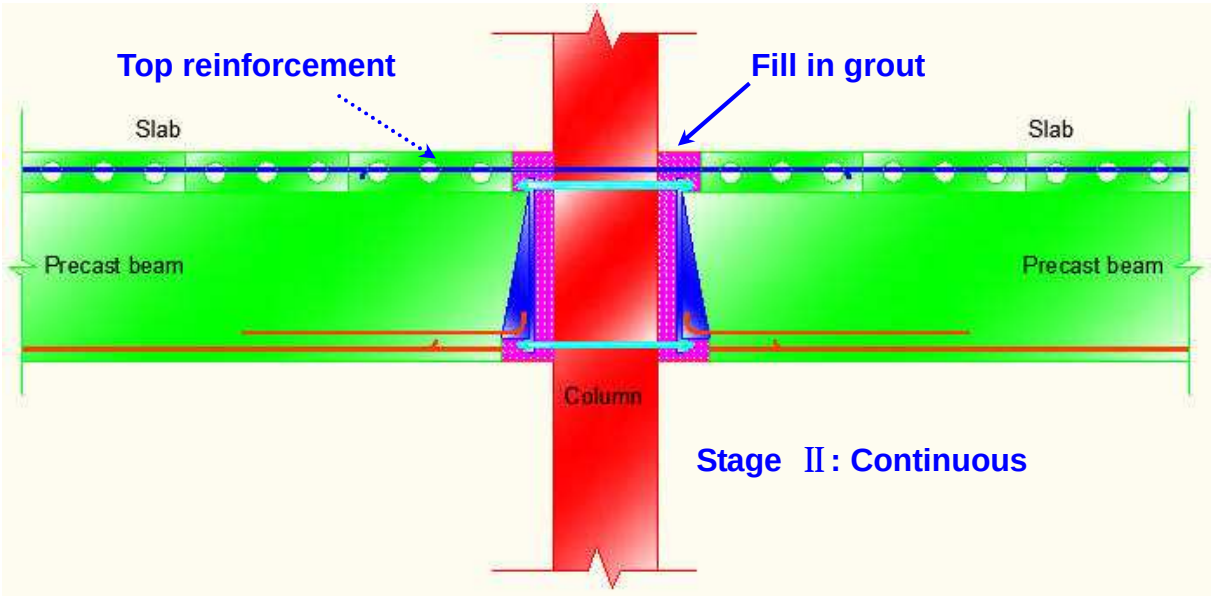

Figure 2.14: Sketch of beam type for Stage Ⅱ.

Stage Ⅱ is the final stage (Figure 2.14). All the components of the building structure have been completed and can be used as structural members. In this stage, the connection zone will resist the ultimate load from all load cases that are applied to the building. The top reinforcement in the structural slab is located either in a slot between the pre-cast slabs, or in a structural topping. It is now functional and can resist the negative bending moment in the support area. Therefore, the pre-cast beam will be regarded as a continuous beam in Stage Ⅱ.

2.6.2 Maximum bending moment and shear force for Stage Ⅰ

The loads in Stage Ⅰ include self weight of the pre-cast beam and the pre-cast floor. The beam load is 5.36 kN/m and the slab load is 13.75 kN/m. Therefore, the factored uniformly distributed load is 22.9 kN/m. Based on this load, the maximum bending moment is 286.6 kNm and the maximum shear force is 114.6 kN.

2.6.3 Maximum bending moment and shear force for Stage Ⅱ

The loads in Stage Ⅱ include dead load and live load. Dead loads include the self-weight of the beam, slab, brick walls and partition. The live load is the imposed load from the design code. For dead loads, except the loads for Stage Ⅰ, the brick wall load is 2.7 kPa and the partition load is 1.5 kPa. For the live load, the nominal imposed floor load is 2.5 kPa. Therefore, the factored uniformly distributed load is 48 kN/m. Based on this load, the maximum positive bending moment is 526.67 kNm and the maximum shear force is 264.9 kN.

2.6.4 Dimensions of the pre-cast beam

Based on the ultimate bending moments from Stage Ⅱ, the dimensions of the precast rectangular beam can be calculated. A beam with 360 mm in width and 620 mm in height is chosen. The concrete cover is assumed to be 35 mm and 4-Y-32 rebar is

selected for the tension reinforcement as indicated in Appendix A, therefore, the effective depth is 569 mm.

Table 2.1: Compare whether the simply supported beam can be used under the selected dimension with regard to different spans.

Span (m)	Conditions
5	Simply supported beam can be used
7.5	Simply supported beam can be used
9	Simply supported beam can be used
10	Continuous beam is needed

Table 2.1 shows the types of beams that can be designed with the cross section of 620×360 mm for different span length under the ultimate load in Stage Ⅱ. When considering only the tension reinforcement is used to resist the ultimate bending moment, the cross section of 620×360 mm can be designed for a simply supported beam with the span length less than 10 m.

2.6.5 Dimension of the hidden corbel

The width of the beam is 360 mm. By assuming the concrete cover to be 35 mm on each side of the hidden corbel, the width of the hidden corbel is 290 mm. In order to provide enough bearing resistance, the length of the hidden corbel is taken as 100 mm as indicated in Appendix A. The height of the shoe is taken as 620 mm.

From the above calculations, the maximum shear force in stage Ⅰ is smaller than fifty percent of that of stage Ⅱ (Final stage). The steel bolts were designed to resist the full shear force in the stage Ⅱ. Therefore, no temporary supports are needed for the installation phase of the pre-cast beams.

With the selected dimension of the hidden corbel, the bearing resistance of the hidden corbel and shear resistance of the high strength bolts are met. All that is required is a verification of the anchorage length of tension reinforcement.

2.7 Summary and conclusions

This chapter introduces the types of pre-cast buildings and explains three typical HCC from previous research. By comparing the advantages and disadvantages of these HCC and considering the current level of the manufacturing industry in South Africa, a modified HCC is proposed.

After defining the modified HCC, the mechanisms in the connection zone are identified. By applying five types of mechanisms in the connection zone with the South African design code, it is identified that the reasons for the end anchorage length of bottom reinforcement for simply supported beams is not clear. Eurocode 2 (2004) is then used to calculate the tensile force from reinforcement in the connection zone. This force directly relates to the end anchorage length for the tensile reinforcement. However, stress concentration effects in the support area make it difficult to directly apply the specification from Eurocode 2 (2004). Therefore, tensile forces in the connection zone need further investigation.

The tensile force in the connection zone is caused by stress that is distributed in that area. In order to obtain the stress distribution in the connection zone, a non-linear material FE model is used and described in subsequent chapters.

In order to obtain a better understanding of the mechanisms in the connection zone, a typical skeletal frame is chosen with a 10 m$\times$5 m bay arrangement. Dimension of the beam with 620 millimetres in height and 360 millimetres in width is then selected for the FE model. This data will be used as referencing data for later comparison. The next chapter focuses on the research methodology.

CHAPTER 3

RESEARCH METHODOLOGY

3.1 Introduction

The preceding chapters presented the background and defined the non-linear material FE model for this investigation. Through the FE analysis (FEA) of the non-linear material model, the stress distribution in the connection zone will be determined.

In this chapter, the methodology of this investigation is presented. The following steps are presented in more detail in this chapter:

Step 1: The tensile force in the reinforcement at the support is obtained by analyzing the stress distribution in the connection zone using a 2D FE model. Based on the results from Appendix A, the data to set up the 2D model is presented for two stages using the STRAND7 finite element software. The method to verify the results of the 2D FE model is then introduced using hand calculations.

Step 2: The hidden corbel and stress distribution is obtained using a 3D FE model. The elements used for the 3D model is introduced and methods to determine the stress confinement are then presented.

Step 3: The FE results are verified by a laboratory test. Based on the analyses from the FE results and calculations from design codes, pre-cast beams were designed and tested to verify whether the end anchorage length of tension reinforcement for a simply supported beam can be reduced.

3.2 Research methodology

The main topic for this investigation is to determine if the end anchorage length of tension reinforcement in the support zone as required by design codes can be reduced. The current design codes do not give an efficient way for calculating the end anchorage length. In addition, the value of the end anchorage length for simply supported beams that is specified in SABS 0100-1 (2000) maybe too conservative. In order to see if the end anchorage length can be reduced, a non-linear material FE model was used to analyze the tensile force in the bottom reinforcement that occurs near the support.

By defining the modified stress-strain curve of the concrete, the stress distribution in the beam can be analyzed by running the non-linear material model. A better understanding of the layout of the reinforcement and stirrups will be achieved by applying the methodology that compressive stress is resisted by concrete and that tensile stress is resisted by the reinforcement or stirrups.

3.2.1 Determining the tensile force in the connection zone through 2D modelling

In order to know the tensile force in the connection zone, a 2D model is needed. The stress distribution in Stage I (Installation stage) and Stage II (Final stage) that is mentioned in section 2.6.1 will be analyzed separately in Chapter 5 by considering the true design procedure.

The quality of the results from the FEA depends on the FE mesh. Because the research is focused on the connection zone, the elements in that zone are smaller than the centre section of the beam, which is depicted in Figure 4.6.

3.2.1.1 Setting up the 2D model

Two separate models are setup for Stage I and Stage II because the load cases and the boundary conditions are different. The relevant parameters for the two models used in the two stages are the following:

Stage I (Installation stage) input data for the STRAND7 of FE model:

- Total beam length: 10 m
- Total beam height: 620 mm
- Plate thickness (beam width): 360 mm
- Edge pressure (applied uniformly distributed load): 0.064 MPa
- Concrete: Characteristic compressive cylinder strength f_c = 25 MPa
- Type of analysis: 2D plane stress
- Material of analysis: Isotropic
- Material Yield Criterion: Max Stress
- Number of load steps: 50

The edge pressure 0.064 MPa is derived from the distributed load on the beam, which is equal to 22.9 kN/m (Section 2.6.2).

Stage II (Final stage) input data for STRAND7:

- Total beam length: 10 m
- Total beam height: 770 mm
- Plate thickness (beam width): 360 mm
- Edge pressure (applied uniformly distributed load): 0.133 MPa
- Concrete: Characteristic compressive cylinder strength f_c = 25 MPa
- Type of analysis: 2D plane stress
- Material of analysis: Isotropic

- Material Yield Criterion: Max Stress
- Number of load steps: 50

The value of the edge pressure applied on top of the plate elements is calculated in the same way as for Stage I. Section 2.6.3 indicates the distributed load to be 48 kN/m for the final condition of the beam.

3.2.1.2 Analyzing the 2D model

The results of the analyses are evaluated in Chapter 5. Principal stress plots show the distribution inside the beam for the two stages. The results will be considered in three steps.

First, the distribution of compressive principal stress and tensile principal stress will be evaluated to see the distribution in the beam.

Second, from the principal stress in each plate element, the normal stress and shear stress is calculated for the horizontal and vertical directions. The results from the analysis are then checked to see whether they are close to the results from hand calculations.

Third, the results are applied to equation 2.5, which comes from Eurocode 2 (2004), but have no limitations on θ in equation 2.5. Also, the tensile force in the connection zone is calculated and compared with hand calculations. By assuming a certain value of bond stress from the design code, the end anchorage length can be determined.

3.2.2 Determining the effect of hidden corbel on bond stress through 3D modelling

As mentioned before, the confinement in the transverse direction by the hidden corbel

and the confinement in the vertical direction from bearing support help to improve the bond stress, which in turn reduce the required end anchorage length. The 2D model can only show the stress distribution in the plane of the beam. The 3D model is then introduced to give a clear representation of the lateral confinement from the triangular side plates.

3.2.2.1 Setting up the 3D model

In order to determine the effect of confinement, the 3D model focuses on the hidden corbel and on the concrete inside the hidden corbel. To simulate the elements in the 3D model with the same loading conditions as in the 2D model, the results from the 2D model are applied as loading conditions in the 3D model.

Only concrete elements located inside of the hidden corbel are modelled in the 3D model, together with the steel shoe elements. Refer to Figure 3.1 which shows the 3D model of the end zone.

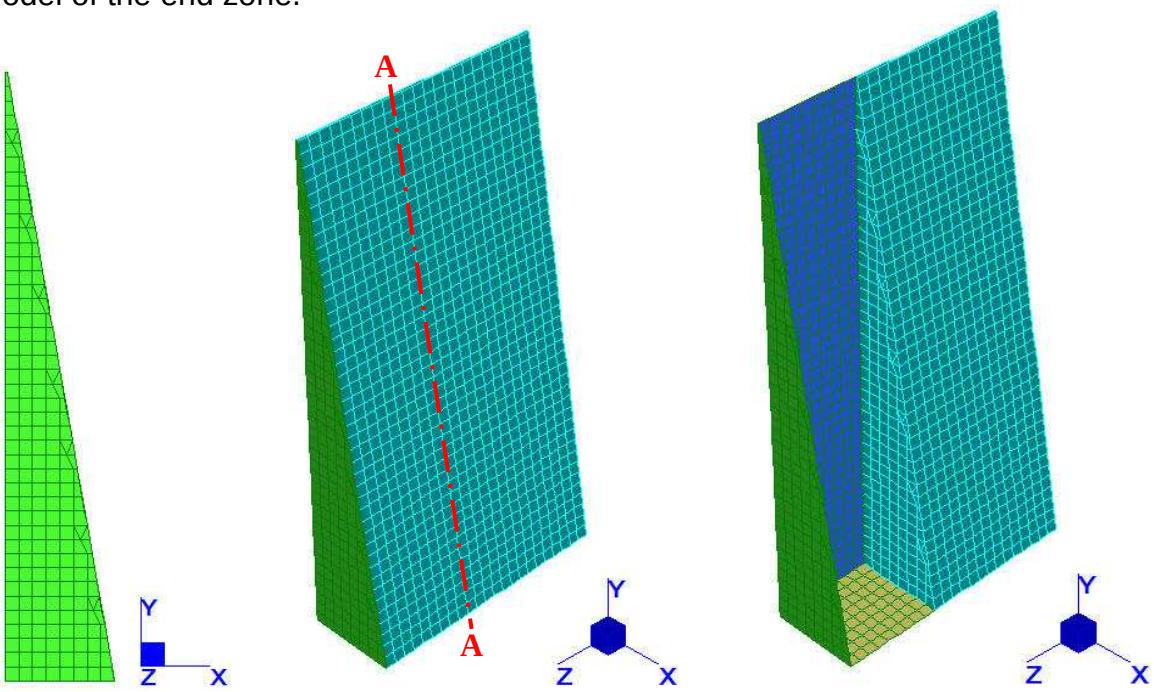

a) Side view b) Isotropic view c) Section cut out along A-A to show the shape of steel shoe

Figure 3.1: Layout of 3D model.

View (a) of Figure 3.1 shows the side view of the 3D model with concrete elements only within the zone enclosed by the steel plates. View (b) shows the isometric view of the 3D model and View (c) shows the isometric view of the brick elements in cross section area A-A (refer to View (b)).

The very top triangular section of the model was also removed for two reasons. The first is that the 3D model only focuses on the stress distribution near the bottom plate of the shoe and the second reason is that the angle of the triangular element is too small, which then affects accuracy of results.

3.2.2.2 Analyzing the 3D model

By varying the thickness of the triangular side plate in subsequent analyses, the confinement of the concrete can be compared. The stress distribution provides insight into the position inside the shoe which would have the best confinement to improve bond stress.

3.2.3 Verifying the end anchorage length through an experiment

In order to verify the effects of the results obtained by the 3D analyses, an experiment was conducted on actual end anchorage conditions.

A pre-cast beam was designed to be tested in the structural laboratory of Stellenbosch University. Four beam specimens were cast. These beams were designed to have the same layout of reinforcement and stirrups, but to have different anchorage conditions for tensile reinforcement which extends into the face of the support. The beams were tested after 7 days of curing to check whether the end anchorage length could be reduced.

A rough bond stress test was also executed directly after the concrete strength was

tested, which gave an indication of the magnitude of the bond stress. These consisted of pull out tests on embedded bars.

3.3 Summary and conclusions

This chapter introduced the methodology for this research. In order to determine whether the end anchorage length could be reduced, a non-linear material model was used in a FE analysis.

The purpose of setting up the 2D FE model was to obtain a better understanding of the stress distribution in a pre-cast beam. The results of the FE 2D model were then verified by hand calculations.

After the 2D model had been verified, a 3D model of the corbel was set up. By analyzing the stress distribution inside the corbel, the location of increased confined stress were identified which would in turn result in improved bond condition of the tensile reinforcement.

After the theoretical verification of the end anchorage length, an experimental verification was conducted. The experiment consisted of 4 pre-cast beams that had different end anchorage lengths, and was tested to verify end anchorage lengths.

The next chapter presents the 2D FE model and concrete confinement from the 3D model.

CHAPTER 4

NON-LINEAR MATERIAL MODELLING PROCEDURES

4.1 Introduction

Chapter 2 concluded that a non-linear material FE model is needed to obtain a better understanding of the mechanisms in the connection zone. The FE method (FEM) is then used as described in Chapter 5 to analyze the stress distribution in the connection zone.

Previously, the stress could only be done by hand calculation based on a mathematical model, which makes it difficult to apply for many fields. With the development of computer technology, FEM can now be applied in many industries. In civil engineering, especially in structural engineering, FEM is widely used for analysis of buildings, bridges, tunnels, etc. Non-linear material models have been integrated in many software packages, i.e. ABAQUS, ANSYS, DIANA, and STRAND7. Because many consulting companies in South Africa are using STRAND7 for the analysis of concrete structures, STRAND7 was selected as software package for this investigation. Also, it is available at the University of Stellenbosch.

Cook, Malkus, Plesha and Witt (2002: 22) introduce the formulation for the FEA force displacement relationship as follows:

$$[K]\{D\}=\{R\} \tag{4.1}$$

Where:

$[K]$: Conventional stiffness matrix of the structure.

$\{D\}$: Nodal degree of freedom of the structure and element respectively.

$\{R\}$: Total load on structural nodes.

From equation 4.1, the force is related to the displacements through the stiffness matrix. Different types of elements have their own specified stiffness matrix. Through the integration of each element in the model, detailed information such as stress, strain, etc. can be calculated by the FE software.

Cook, *et al*. (2002: 11) explained the methods for solving a problem by FEA. Figure 4.1 shows the procedure on FEA.

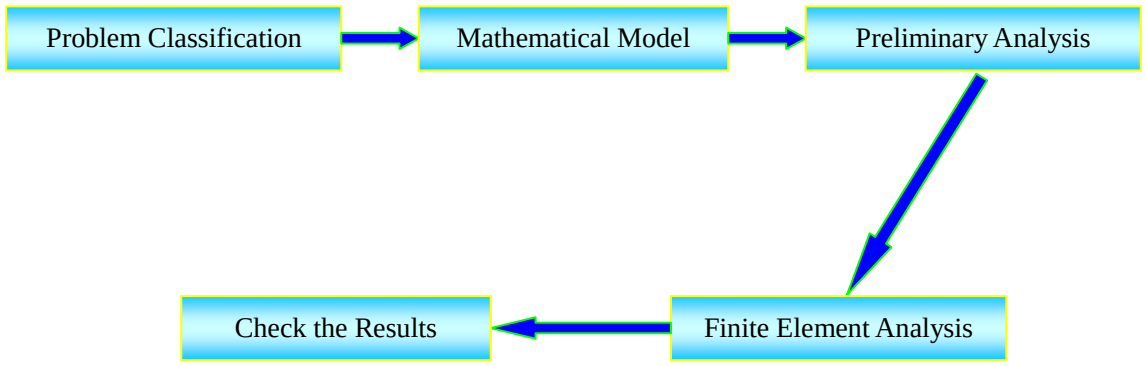

Figure 4.1: FEA procedures.

This chapter will classify the problem and build up a mathematical model. STRAND7 is the applied software for the FEA. The methodology for analyzing the problem will then be assumed. Subsequently, based on this methodology, element types are chosen for the model. After that, the method for analyzing the mathematical model is defined. The following section will discuss these matters step by step.

4.2 Classifying the problem of FEA

As mentioned before, the main purpose for using a FEA in this study is to find the

stress distribution near the support area. Due to the stress concentration near the support area, a non-linear material FE model needs to be set up.

Most design codes consider the bending moment and shear force in a certain plane. The bending moment and shear force are considered in the plane of the beam as indicated in figure 2.13. A 2D model has the advantage of illustrating the stress distribution more comprehensively in that plane. In order to analyze the stress distribution in the connection area, a 2D model was selected. For a pre-cast concrete beam, the materials included concrete and steel. The concrete can be simulated by 2D plate elements and reinforcement can be simulated by beam elements. By assuming a perfect bond, beam element can be connected to plate elements by sharing the same nodes.

However, the interaction forces between the concrete and reinforcements will cause stress redistribution. The stress redistribution, which is also a result of concrete cracking, makes it difficult to know the real condition of stresses distributed inside the concrete. The modelling of tension stiffening is a complex phenomena and not feasible with commercial software. In addition, the stress in the reinforcement depends on the reinforcement property and the diameter. For a certain beam under the same loading condition, the selection of reinforcement normally differs among different designers. Therefore, the variation of stress in reinforcement will effect the redistribution between the concrete and reinforcement. In order to proceed with the FEA, the properties of concrete were considered in the following section.

4.3 Proposed concrete stress-strain curve for non-linear analysis

Normal design codes disregard the tensile resistance of concrete for conservative design. However, concrete can resist a small tensile force. In order to simulate the actual concrete behaviour, a non-linear stress-strain curve is considered for the concrete both in compression and in tension.

4.3.1 Stress-strain curve in compression

Figure 1 of SABS 0100-1 (2000) gives a short term design stress-strain curve for the normal density concrete. However, it is stated that specialist literature should be consulted for non-linear analysis.

Desayi and Krishnan (1964) gave the following equation for calculating the stress-strain relationship for concrete.

$$f_c = \frac{E_c \varepsilon}{1 + \left(\frac{\varepsilon}{\varepsilon_0}\right)^2} \qquad (4.2)$$

Where:

f_c : Concrete cylinder strength.

E_c : Modulus of elasticity of concrete.

ε : Strain in concrete.

ε_0 : Strain corresponding to peak concrete stress. (f_c / E_c)

Many books and researchers use the same curve for non-linear analysis of concrete. Oehlers (1995: 44) recommends that the stress-strain curve from Desayi and Krishnan should be used for non-linear analysis of concrete. Kaewunruen and Remennikov (2006:325) used the same curve to model a railway pre-stressed concrete sleeper and obtained a good result.

Therefore, the stress-strain curve for non-linear concrete from Desayi and Krishnan is used in this investigation.

The 25 MPa concrete cylinder strength is equivalent to 30 MPa concrete cube strength, which is the concrete strength used in Appendix A. It is also used here for

the FE model. Table 1 of SABS 0100-1 (2000) shows that modulus of elasticity equals 28 GPa for concrete cube strength of 30 MPa. However, STRAND7 gives a more precise E_c value of 27460 MPa for concrete cylinder strength of 25 MPa. Based on these, the value of ε_0 was calculated by using 25 MPa divided by 27460 MPa.

After defining the values of E_c and ε_0, the stress-strain relationship was calculated from equation 4.2. The stress-strain curve was then plotted in figure 4.2.

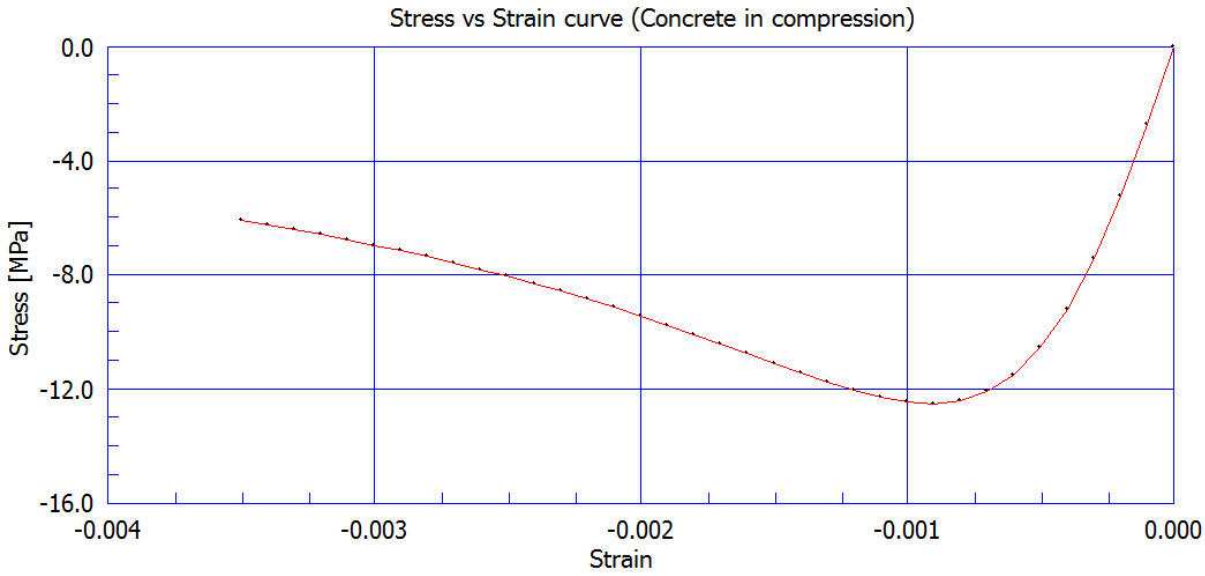

Figure 4.2: Non-linear stress-strain curve (concrete in compression).

In this investigation, the stress in the concrete in compression is defined as negative and the stress in the concrete in tension is defined as positive. The same principle is also applied for the strain. Therefore, the negative relationship is presented in Figure 4.2 and the peak stress value is 12.5 MPa of concrete in compression. This value is close to the concrete maximum design value as specified in table 1 from SABS 0100-1 (2000). The ultimate strain is taken as 0.0035 because this is the design ultimate strain for the concrete (SABS 0100-1 (2000)).

4.3.2 Stress-strain curve in tension

Table 3.1 of Eurocode 2 (2004) gives an expression for the tensile stress of concrete. The expression is as follows:

$$f_{ctm} = 0.3 \times f_{ck}^{2/3} \tag{4.3}$$

Where:

f_{ctm} : Mean value of axial tensile strength of concrete.

f_{ck} : Concrete cylinder strength.

Then, based on the following equation, the related ultimate tensile strain can be calculated.

$$\varepsilon = \frac{f_{ctm}}{E_c} \tag{4.4}$$

The stress-strain relationship for concrete in tension is shown in Figure 4.3.

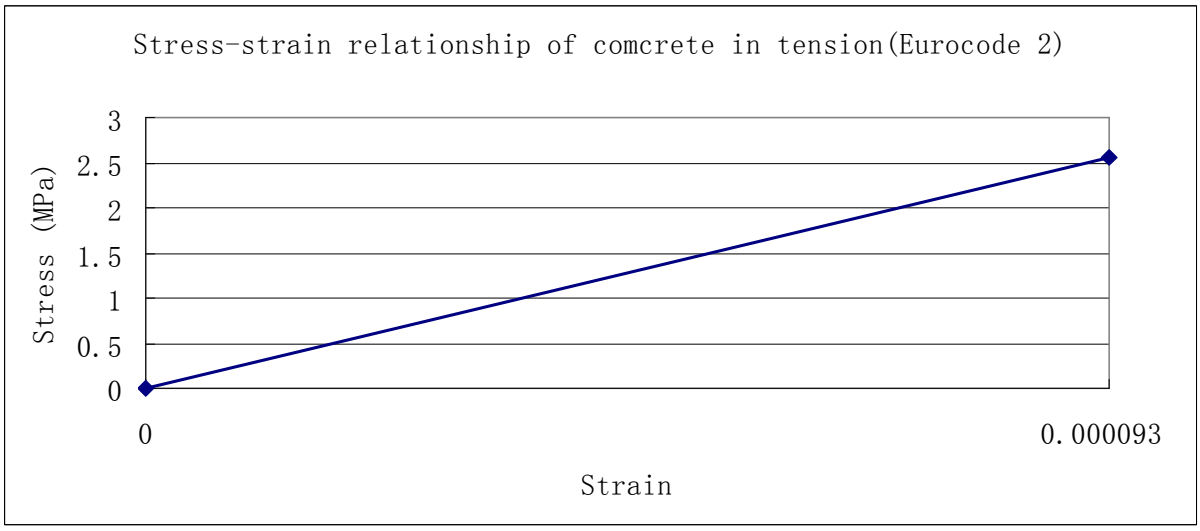

Figure 4.3: Stress-strain curve of concrete in tension based on Eurocode 2 (2004).

The corresponding strain caused by the tensile stress of concrete in Figure4.3 can be

used to model the crack. However, the stress and strain is so small and STRAND7 does not have a function to model the cracking and accompanying tension stiffening. In addition, this investigation focuses on the stress distribution and not on the development of cracking. Therefore, the tension field is allowed to develop in the stress-strain curve. The tensile stress is then used to calculate a tensile force by hand, which is considered as the tension force in the reinforcement. By allowing the tensile field, the linear elastic in the concrete, the plate elements are used to simulate both the concrete and reinforcement.

Kong and Evans (1987: 220) explain that bond stress corresponds to the change of stress in the reinforcement bar. For design purposes, the strain in the reinforcement is assumed to be equal to the adjacent concrete under the effective bond. Therefore, the tension field of the stress strain curve keeps the same gradient as shown in Figure 4.3 and assumes the ultimate tensile stress in the steel to be 200 MPa. The assumed stress-strain curve for the concrete in tension is shown in Figure 4.4.

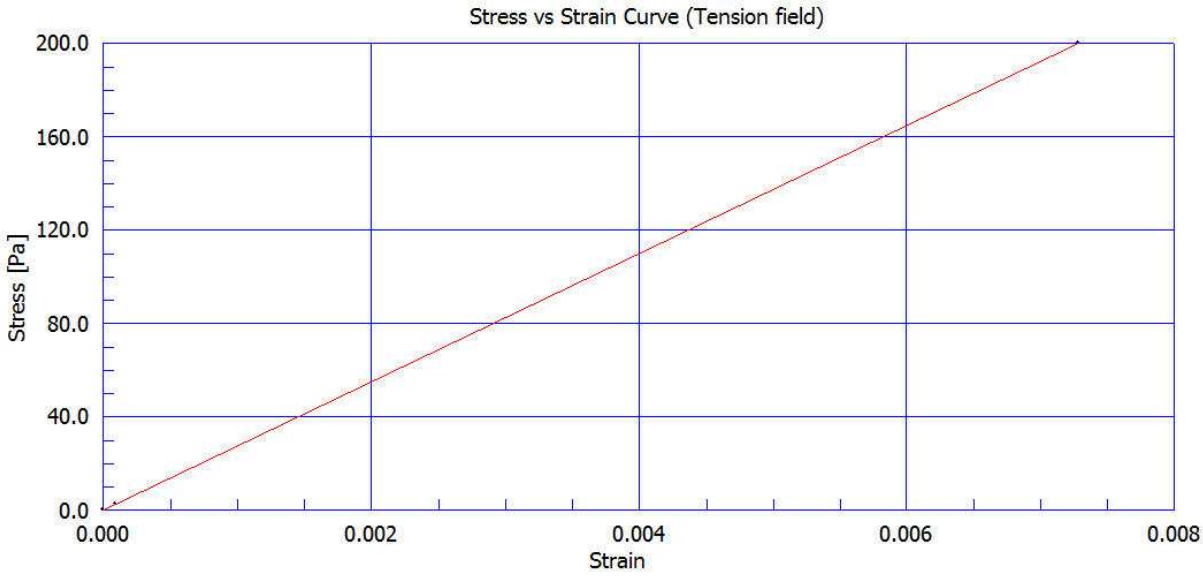

Figure 4.4: Modified stress-strain curve in the tension field.

4.4 Setting up a methodology for the FEA approach for material behaviour

The methodology of modelling was set up for this investigation. That is, the plate

element can take both compressive stress and tensile stress. The compressive stress is resisted by the concrete and the tensile stress will be converted to a tensile force (by hand), to be resisted by the reinforcement.

The advantage of the methodology for this investigation is that with the tensile field allowed, the stress distribution arises directly from the modelling. The layout of reinforcement and stirrups are based on the layout of the stress distribution, which makes the analyses more flexible. Otherwise, with different layouts of reinforcement and stirrups, the stress distribution differs and more analyses are needed. The method on how to apply the above stress-strain curves in the FEA is presented in the following section.

4.5 Non-linear FEA method

Among the methods for solving non-linear static problems, the Newton-Raphson (N-R) and modified N-R methods are widely used.

4.5.1 Comparison between original N-R method and modified N-R method

Cook, *et al*. (2002: 597) explain clearly how the N-R method and the modified N-R method are used in a non-linear analysis. Both are divided into several load steps according to the stress-strain curve or force displacement curve. For each load step, many iterative cycles are needed to achieve convergence. The difference is that the original N-R method achieves convergence by updating the tangent stiffness prior to each calculation, while the modified N-R method achieves convergence by using the same tangential stiffness.

The updated tangential stiffness of the original N-R method requires few iterative cycles to reach convergence. This characteristic makes hand calculations easier to solve simple problems. However, the modified N-R method needs many iterative

cycles to reach convergence, which is not suitable for hand calculation.

For a model with a large number of elements, the stiffness matrix is very large and it is difficult to solve the number of equations even with computer programmes. In this case, the modified N-R methods can save time because the tangent stiffness is the same for each load step. Therefore, most software packages apply the modified N-R method to solve non-linear problems. STRAND7 also uses the modified N-R method to solve non-linear problems.

4.5.2 Convergence Criteria for modified N-R method

By applying the modified N-R method, convergence is normally difficult to achieve when solving problems which includes many elements. The modified N-R method can reach the target of each load step infinitely closer by applying more iterative cycles, but in most cases, it will never reach the exact target. Therefore, convergence criteria are applied when the result is close enough to the target, which makes the calculation relatively quick and economical.

Cook, *et al*. (2002: 620) give two types of convergence, namely force and displacement convergence.

Force convergence: $$\|e_R\| < \varepsilon_R \|R\| \tag{4.5}$$

Where:

$\|e_R\|$: Norm of the residual force vector in the current iteration

$\|R\|$: Norm of the residual force vector at the first iteration of each load step.

ε_R : Force tolerance.

Displacement convergence: $\|\Delta D\| < \varepsilon_D \|\Delta D_0\|$ (4.6)

Where:

$\|\Delta D\|$: Norm of incremental displacement vector.

$\|\Delta D_0\|$: Norm of total displacement vector.

ε_D: Relative displacement tolerance.

STRAND7 uses convergence tolerances for non-linear analysis with a value of 0.001 for force tolerance and 0.0001 for displacement tolerance. It can be recognized that the smaller these values are, the more accurate results will be and the more difficulty the convergence criteria will be satisfied.

4.6 Modification of the stress-strain curve for non-linear analysis

The proposed stress-strain curve from Section 4.3 can be used to present the concrete behaviour. However, the N-R method and the modified N-R method can only reach convergence when the stress-strain curve has a positive gradient. From Figure 4.2, it can be seen that with an increase in strain, concrete stress soon reaches its peak value and then reduces gradually. Therefore, the proposed stress-strain curve can not be applied.

In order to solve this problem, some changes were made to the stress-strain curve. After the concrete reaches its peak stress value, it remains more or less the same until it reaches the ultimate concrete strain. The change to the material behaviour is justified by two reasons. The first reason is that this research is only focused on the stress distribution in the connection zone. Therefore, the correct modelling in areas away from the connection zone is of lesser importance. The second reason is that the strain is relatively small in the connection zone.

Another change is to reduce the number of points on the stress-strain curve used to define the stress-strain relationship. For non-linear analysis, the stress-strain curve should be as simple as possible to enable fast calculation (STRAND7, 2005). Therefore, the number of points located between the origin (point '0' in Figure 4.5) and the peak value (point '1' in Figure 4.5) are reduced, but the slope of the curve remains the same. This will guarantee fast and economical calculation and will only slightly affect the accuracy of the results.

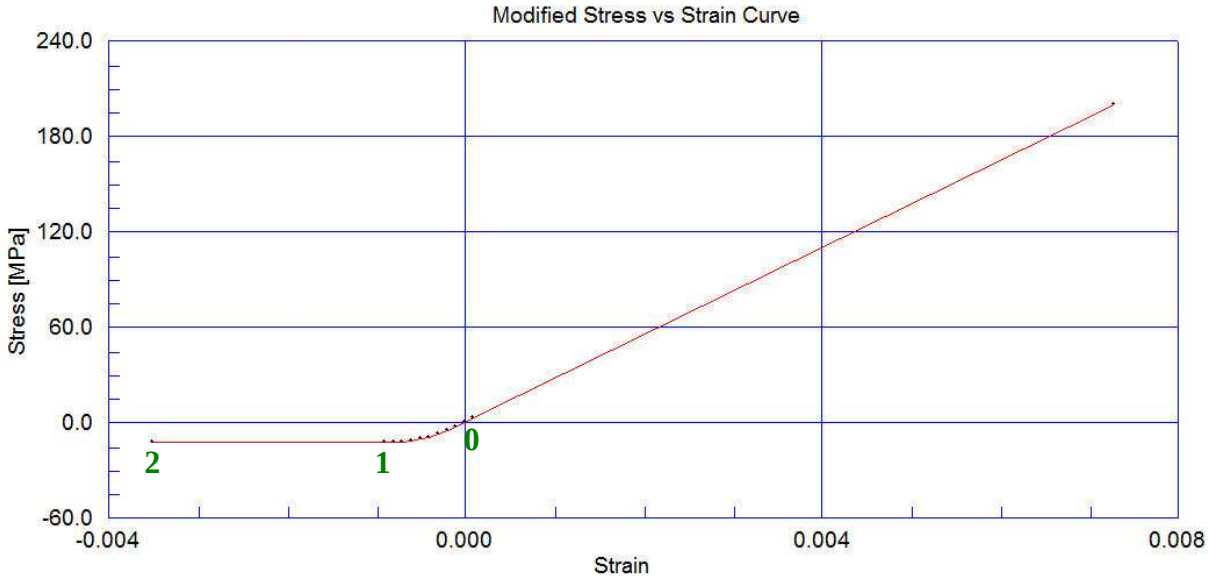

Figure 4.5: Modified stress-strain curve for model analysis.

From Figure 4.5, there is a small angle between the point of the original peak value as indicated by '1' and the ultimate point as indicated by '2'. The stress value increases from 12.49 MPa at '1' to 15 MPa at '2'. This enables the non-linear analysis to run properly.

The assumption of relatively small strain in the connection zone is justified by the results of the FE modelling. For the region next to the support and in the connection zone, the value of maximum strain is 0.00008 in both X and Y directions. For the region directly above the support, the value of maximum strain is 0.00014 in both X and Y directions.

4.7 Setting up the model for 2D analyses

After defining the dimensions of the system and understanding the principles for the non-linear analysis, the model was setup. As introduced in section 2.6.1, two stages are needed for the installation of the skeletal frames. The structural depth for Stage I consists only of the height of the beam (as shown in Figure 2.13). For Stage II, the structural depth also includes the additional height of slab (as shown in Figure 2.14). The following section will introduce the procedure for setting up the model.

4.7.1 Step 1: Choosing the plate element

The quadratic rectangle Q8 element of STRAND7 (2005) was selected for the analysis in stead of a bilinear rectangle Q4 element. Cook, *et al*. (2002: 98) explained that the Q4 element exhibits shear locking behaviour because it can not model pure bending. On the other hand, the Q8 element can display both its shear strain as well as the bending strain.

4.7.2 Step 2: Choosing the size of each plate element

In Section 2.5, a 10 metres span was chosen for the pre-cast beam and in Section 2.6.4, the cross section of the beam is chosen to be 620 mm×360 mm (Stage I).

Because the bottom plate of the hidden corbel in Figure 2.5 will take all the bearing force, the grout beneath the bottom plate does not resist any forces and is hence excluded from the model.

From the methodology that a tension field is allowed in the plate element (Section 3.4), the bottom plate of the hidden corbel is located 51 mm from the extreme bottom fibre of the pre-cast concrete beam, which is also the distance between the centroid of bottom reinforcements to the extreme bottom fibre of the pre-cast concrete beam.

This enables the tensile stress from outside the support to be directly transmitted into the support. Section 2.6.5 shows the length of the hidden corbel to be 100 mm. Based on these dimensions, the layout of the model for Stage I is shown in Figure 4.6.

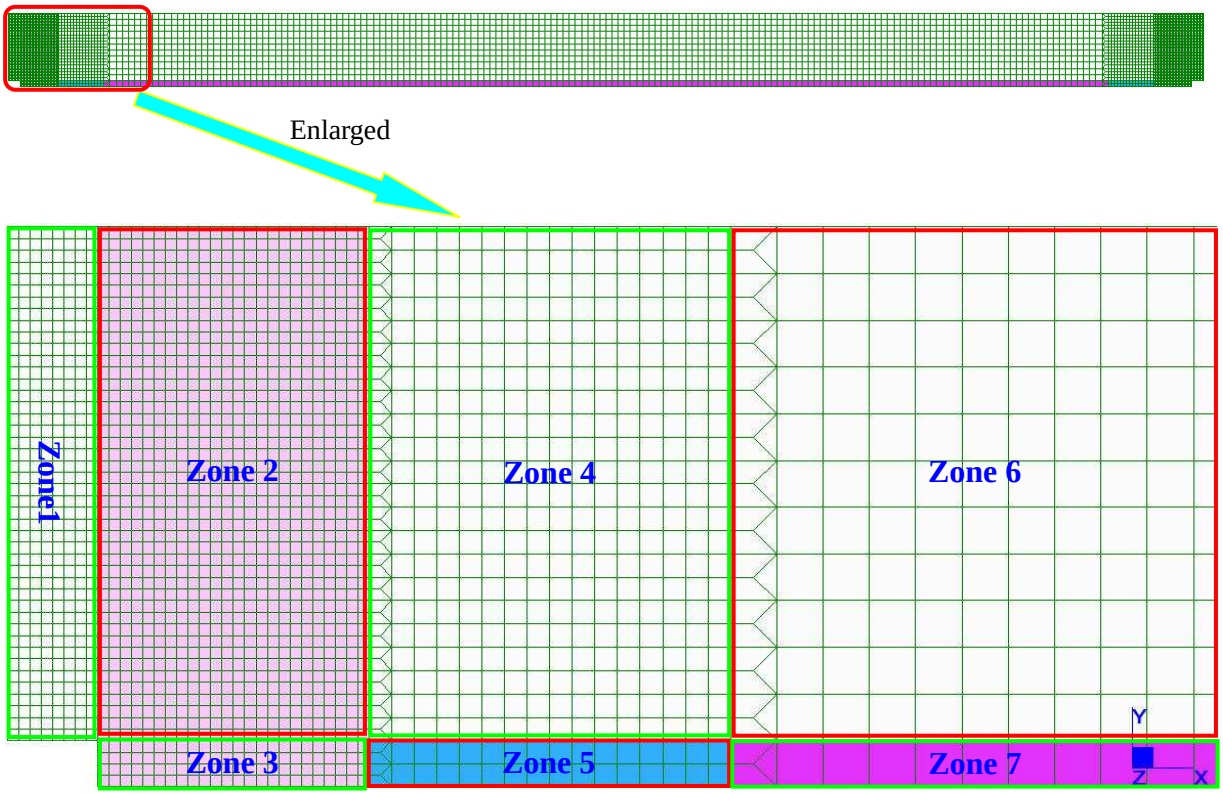

Figure 4.6: Layout of the model for 2D analysis.

In order to provide a good mesh, the length and the height of the elements are kept as similar as possible. Because of symmetry, the enlarged section of Figure 4.6 only shows the left side of the beam. Each zone is identified in the Figure as described below:

- Zone 1: The elements in the support area located above the support level.
- Zone 2: The elements next to the support area located above the support level.
- Zone 3: The elements next to the support area and located below the support level.
- Zone 4: The elements next to zone 3 and located above the support level.

- Zone 5: The elements next to zone 3 and located below the support level.
- Zone 6: The elements in the centre of the beam span and located above the support level.
- Zone 7: The elements in the centre of the beam span and located below the support level.

Each zone has a rectangular shape and the dimension for each plate element in that zone is the same. The dimensions of the zones and elements are listed in table 4.1. The meanings of symbols are indicated in Figure 4.7.

Table 4.1: Element and zone dimension for the model (Stage Ⅰ).

	H (mm)	L (mm)	Number of finite elements		Finite element size	
			Horizontal direction	Vertical direction	a (mm)	b (mm)
Zone 1	569	100	8	44	12.5	12.9
Zone 2	569	300	24	44	12.5	12.9
Zone 3	51	300	24	4	12.5	12.7
Zone 4	569	400	16	22	25	25.8
Zone 5	51	400	16	2	25	25.5
Zone 6	569	4200	82	11	51.2	51.7
Zone 7	51	4200	82	1	51.2	51

The height for construction Stage Ⅱ is increased because the top reinforcement has the function to resist the negative bending moment over the continuous support. The height for Stage Ⅱ includes the height of the beam (620 mm) and the height of the slab (150 mm), therefore the total structural height is 770 mm for Stage Ⅱ. Except for the elements in the slab, the remainder of the elements are the same as those in Stage Ⅰ. Only the numbering of elements for the slab for construction Stage Ⅱ is

shown in Figure 4.8 because the rest of the elements are the same as for Stage Ⅰ. The dimensions for these additional elements in Stage Ⅱ are listed in table 4.2.

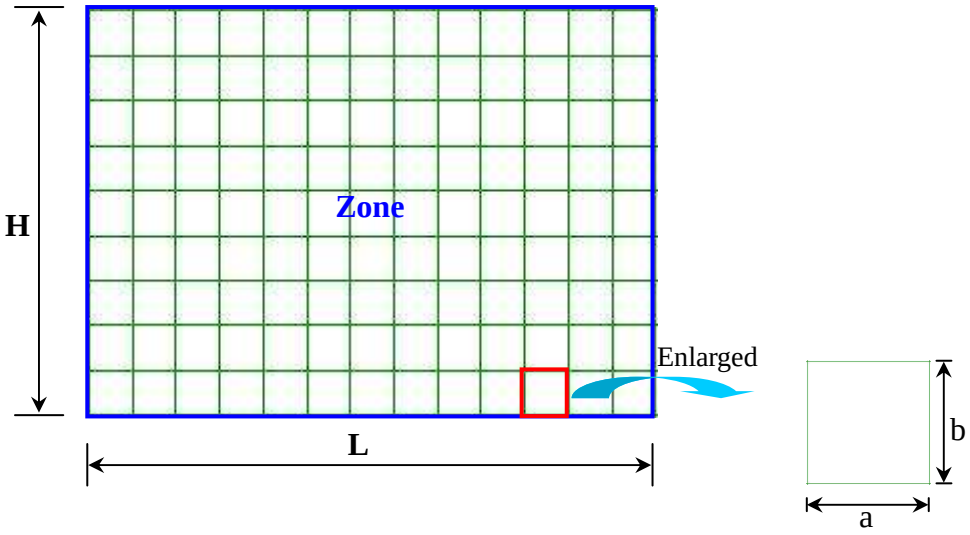

Figure 4.7: Definition of parameters in table 4.1.

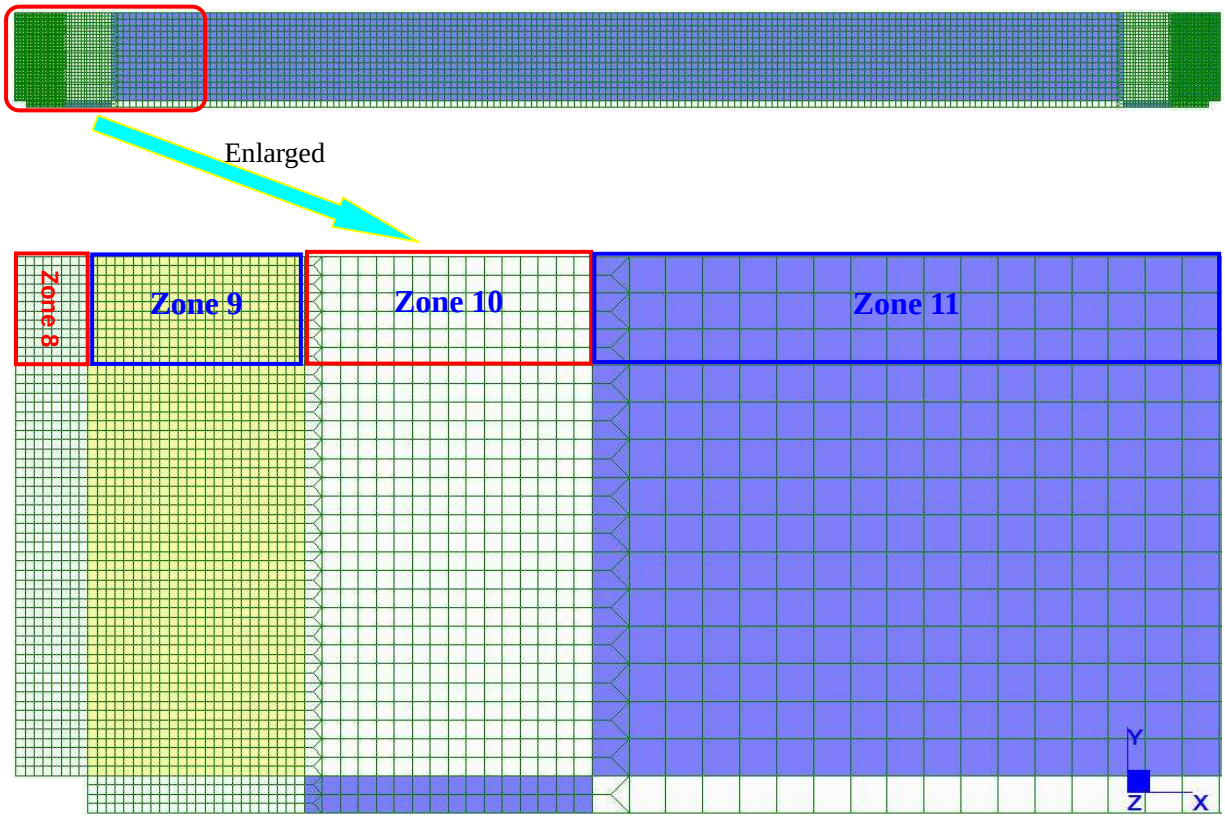

Figure 4.8: Layout of the 2D model for additional zones in construction Stage Ⅱ.

The additional zones are described below:

- Zone 8: The elements located directly above Zone 1.
- Zone 9: The elements located directly above Zone 2.
- Zone 10: The elements located directly above Zone 4.
- Zone 11: The elements located directly above Zone 6.

Table 4.2: Element and zone dimension for the model (Stage Ⅱ, additional zones).

	H (mm)	L (mm)	Number of finite elements		Finite element size	
			Horizontal direction	Vertical direction	a (mm)	b (mm)
Zone 8	150	300	24	12	12.5	12.5
Zone 9	150	300	24	12	12.5	12.5
Zone 10	150	400	16	6	25	25
Zone 11	150	4200	82	3	51.22	50

4.7.3 Step 3: Defining the input data for the model

The following basic input data was selected for the model:

- Concrete: Compressive cylinder strength f_c = 25 MPa
- Analysis type: 2D plane stress
- Material characteristic: Isotropic
- Yield Criterion: Max stress

In the STRAND7 software package, if the tension and compression behaviour of the material is different, a stress strain curve can be defined for both positive and negative strains, which can only be analyzed with a Max Stress criterion in a non-linear elastic

material analysis.

4.7.4 Step 4: Boundary conditions

According to section 2.6.1, the beam can be regarded as a simply supported beam for Stage Ⅰ (installation stage) and as a continuous beam for Stage Ⅱ (final stage). The boundary conditions are shown in Figure 4.9 for Stage Ⅰ and 4.10 for Stage Ⅱ.

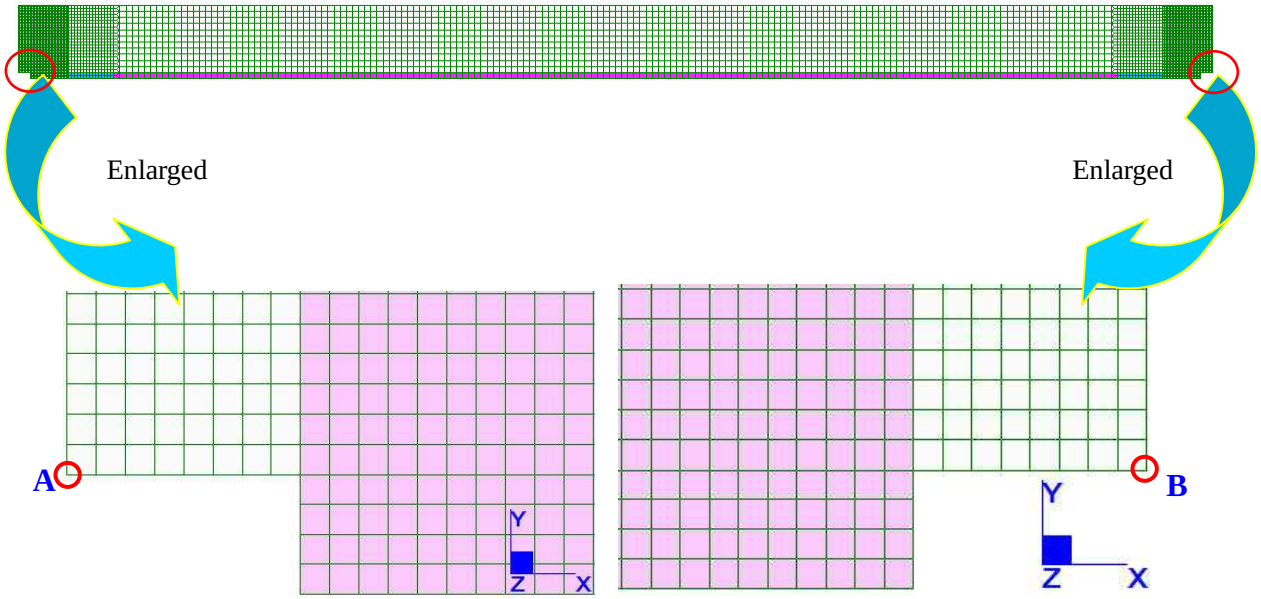

Figure 4.9: Boundary conditions for Stage Ⅰ.

In Figure 4.9, point A is confined in translation in both X and Y directions and point B is confined in translation in the Y direction. Because the analyze type is 2D plane stress, no confinement on rotation is needed.

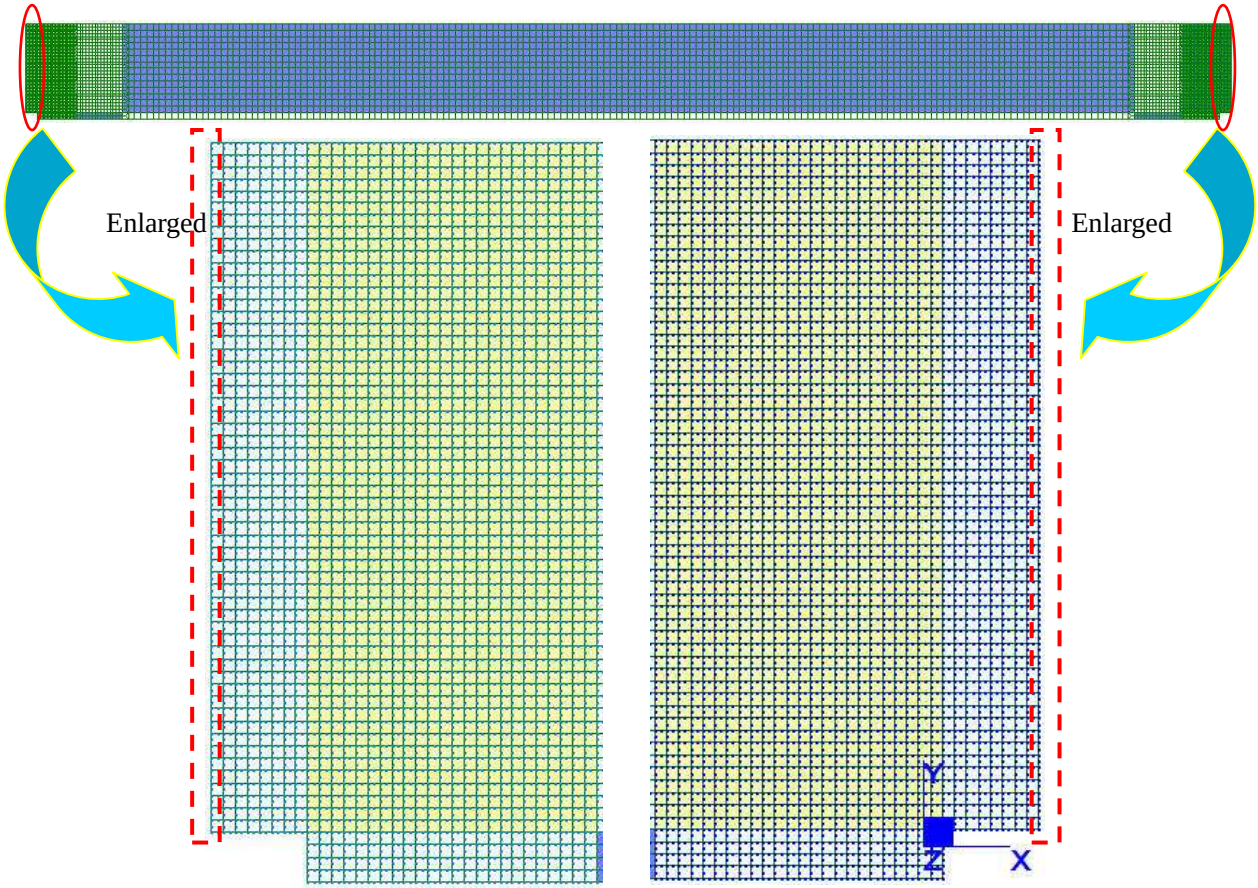

Figure 4.10: Boundary conditions for Stage Ⅱ.

The boundary conditions for Stage Ⅱ are shown in Figure 4.10, the edge nodes in the dashed rectangular blocks (Bottom picture of Figure 4.10) are confined in translation in both X and Y directions.

The bottom plate of the corbel provides the vertical seat for the concrete beam. In the finite element model this plate is modelled by the provision of restraint conditions for the nodes at this location. If the bottom plate of the corbel is too stiff, then there is no deformation in the corbel, which will result in the beam lifting at the end. This is addressed later in Chapter 5 and is shown in Figure 5.1. If the corbel is too soft, then the corbel does not function as vertical support at all. Therefore, the stiffness of the corbel will affect the modelling results. Detailed information on modelling the corbel will be presented in Chapter 5.

4.7.5 Step 5: Loading cases and load steps

As introduced in Section 2.6.2, the loading case in Stage I include self weight of the pre-cast beam and the pre-cast floor and gave the factored distributed load for Stage I. Section 2.6.3 introduced the loading case in Stage II includes dead load and live load and gives the factored distributed load for Stage II. Therefore, the uniformly distributed loads can be directly applied to the model.

For the non-linear analysis of the model, it is difficult to meet the convergence criteria. Therefore, 50 equal loading steps were selected for the non-linear analysis until the load reaches the ultimate value. An automatic load stepping is also selected so that if the solution does not converge at one of the steps, STRAND7 will restart the solution from the last converged solution with a smaller load increment.

4.8 Setting up the model for a 3D analysis

Confinement in the support zone will reduce the required anchorage length of the tension reinforcement at the support region. In order to know the stress distribution in the concrete in the corbel area, a 3D model is needed. The 3D model includes the hidden corbel and the concrete inside the shoe.

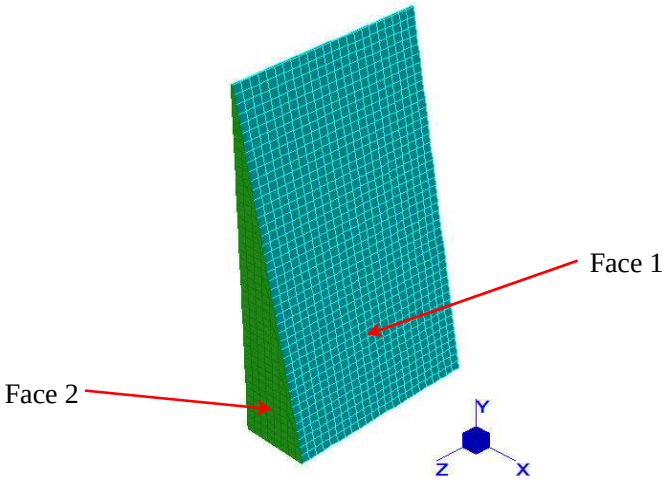

Figure 4.11: Layout of 3D model.

As shown in Figure 4.11, the loads are applied on face 1 of the 3D model, which are obtained from the internal forces in the elements from the 2D model. By applying the loads resulting from the 2D model, the stress inside the corbel can be obtained from the 3D model. The 3D model can show the effect of the confinement from the triangular side plates.

A 3D model combining brick elements of the concrete and shell elements of the steel plates is then compiled. There are two types of brick element, one is an 8-noded hexahedron brick element and the other is a 20-noded hexahedron brick element. The 8-noded hexahedron brick element like the Q4 plate element has the defect of shear locking (Cook, *et al*., 2002: 217). Like the Q8 plate element, the 20-noded hexahedron brick element can both display its shear strain as well as the bending strain in 3D and was therefore selected. The nodes of shell elements modelling the hidden corbel were connected to the nodes of the brick elements so that they could deform correspondingly.

The principles of a 3D analysis are the same as those of a 2D analysis and the detailed analysis will be discussed in Chapter 5.

4.9 Summary and conclusions

This chapter classified the problem and set up the methodology for the non-linear material modelling. The theory on how to proceed with a non-linear model was then introduced. In order to start the modelling, the non-linear stress-strain curve was discussed. After that, the method on how the STRAND7 software was used to analyze non-linear material modelling was explained. Based on the modified N-R methods and the methodology for non-linear modelling, a modified stress-strain curve was compiled for the analysis.

The analyses include a 2D model and a 3D model. The 2D model is used to analyze

the stress distribution in the connection zone. These stresses will also be used in Chapter 5 to calculate tensile force in that region. The 3D model is used to obtain the stress distribution in the hidden corbel. The compressive stress in the transverse direction shows a better confinement caused by the triangular side plates and the compressive stress in the vertical direction indicates a better confinement results from the bearing support.

The basic procedure is introduced and the exact dimensions for elements are then defined for 2D and 3D modelling. The detailed analysis will be presented in Chapter 5. The next Chapter will present the detailed methodology, which is based on the dimensions as mentioned above.

CHAPTER 5

COMPARISON BETWEEN NUMERICAL RESULTS AND THEORETICAL CALCULATION

5.1 Introduction

Chapter 2 presented the modified Hidden Corbel Connection (HCC) and further defined the dimensions for the skeletal frames considered in this study. In order to analyze the stress distribution under the effect of stress concentration, a non-linear material model was set up. Chapter 3 described the methodology of how the data was analyzed in this study and how it was then verified. Chapter 4 then introduced the basic principle on how the non-linear static solver works in STRAND 7 and defined the types of elements to be used for the model.

The main purpose of this chapter is to determine if the end anchorage of the tension reinforcement can be reduced. For the non-linear 2D model, the following steps are considered in this chapter. Firstly, the non-linear FE material model was analyzed as introduced in previous chapters and the data collected from the analysis was analyzed. Secondly, the stress distribution in the beam was analyzed for two separate stages: Stage Ⅰ and Stage Ⅱ as mentioned in Section 2.6.1 and a comparison is then made between them. Thirdly, the stresses on each element were calculated based on the results from STRAND7 and by using the theory of *Mohr's circle*. Finally, the data was verified through theoretical calculations.

After the verification of the data, the stress distribution will then be used to analyze the lay out of reinforcement and stirrups. The tensile force for end anchorage was then calculated through the results of the model.

For the 3D model, the following steps were taken. Firstly, the loads calculated from the 2D model were applied to a 3D model and a linear static analysis was performed. Secondly, the stress distributions were obtained for alternative possible loading conditions. Thirdly, the effect of confinement in the concrete by different thicknesses of side plates was compared. Lastly, the bond stress was predicted for the above conditions.

5.2 The non-linear material 2D model

In Chapter 4, it was described that the stiffness of the hidden corbel will affect the stress distribution in the end zone. In practice, it is often custom to place a rubber pad in the contact area between the end of a pre-cast beam and the support to avoid crushing of the concrete.

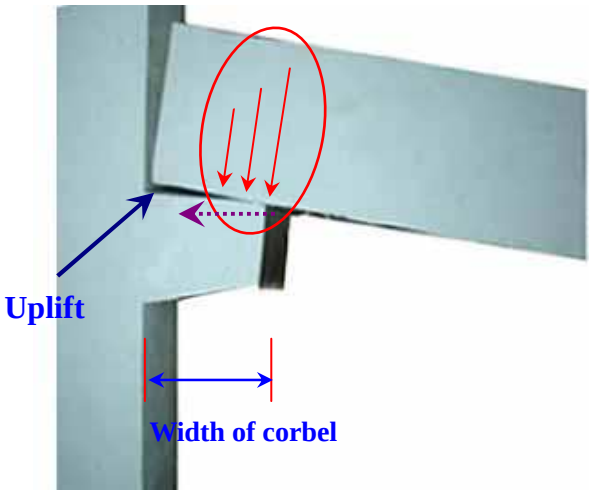

Figure 5.1: Performance of beam under loads.

In this study, a spring stiffness is used to simulate the support conditions based on the following reasons:

- In practice, a uniformly allocated bearing pressure of 0.4 times characteristic concrete cube strength is assumed to perform the design.

- In an elastic analysis, the beam performs as in Figure 5.1. The end of the beam lifts up and results in high stresses gather in the circled area, which will result in local crushing.
- The local crushing will distribute along the length of the support (dotted arrow in Figure 5.1) until the full width is used.
- This phenomenon was modelled in this study by the provision of spring at the support to obtain a stress distribution as shown in Figure 5.2.

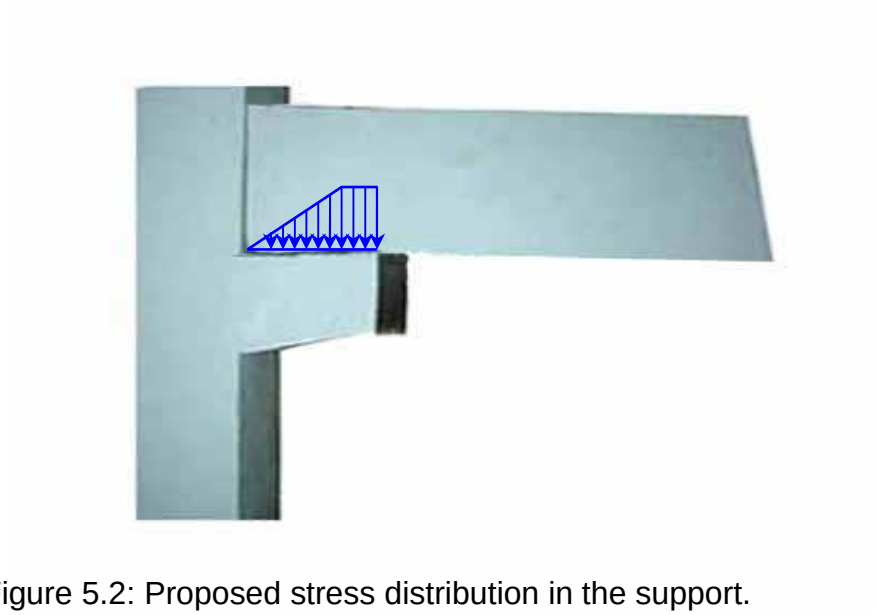

Figure 5.2: Proposed stress distribution in the support.

5.2.1 Determining suitable support conditions

In order to determine the stiffness of the rubber pad, trial and error methods were used. The assumption was made that the spring stiffness should guarantee that the end of the beam located inside the support area remains in compression. The modified HCC, however, was assumed to have a bearing area that would meet the bearing requirements from the design code.

5.2.1.1 Simulating the stiffness of the spring support

In this study, a truss element is used to simulate the spring support and is then connected to the Q8 plate element.

5.2.1.1.1 Determining the stiffness of the truss element

In order to simulate the stiffness of the support, the standard uni-axial force deformation equations were used (Craig and Roy, 2000).

$$k = \frac{F}{\Delta L} \tag{5.1}$$

$$k = \frac{E \cdot A_s}{L} \tag{5.2}$$

Where:

k : Stiffness of spring

F : Axial force on the truss element

ΔL : Change of the length in L

E : Modulus of elasticity

A_s : Cross section area of the truss element

L : The length of the truss element

5.2.1.1.2 Applying the truss element to the model

The truss elements were connected to the Q8 plate element inside the corbel area as indicated in Figure 5.3.

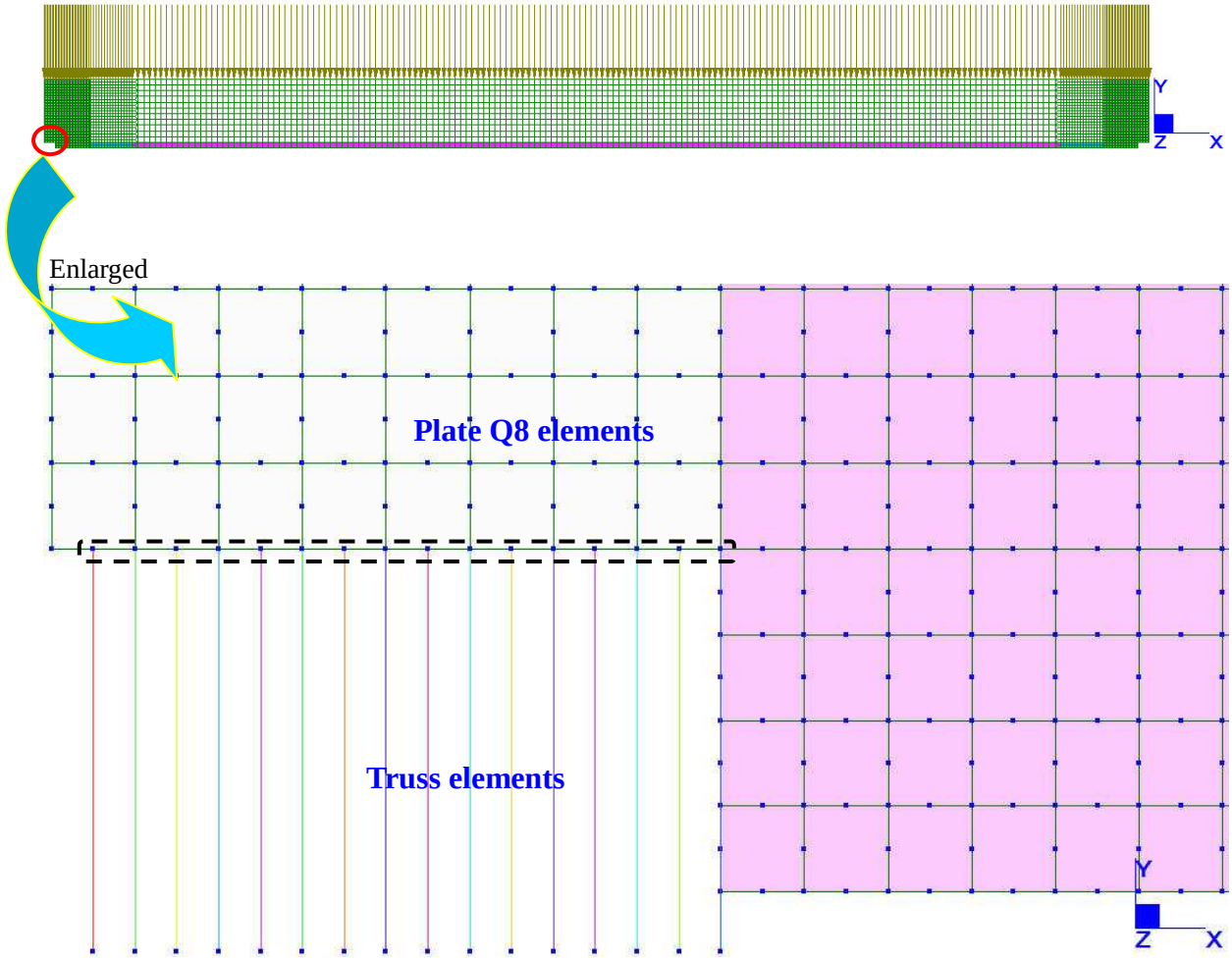

Figure 5.3: Extract from 2D-STRAND7 model: Truss elements connected to plate elements.

In order to provide a suitable stiffness for the truss elements, an assumption was made that the interface between the plate elements and the truss elements remains plane under deflection. This assumption was based on two reasons. The first reason is that if the plane interface remains plane, a good bearing resistance will be provided. The second reason is that the assumption could guarantee the stress distribution as that indicated in Figure 5.2.

Cook, *et al*. (2002: 353) suggested that care should be taken when simulating a uniform elastic foundation because the distribution of consistent nodal load is not the same for each node of the plate element. STRAND7 indicates that '*A more accurate representation of a distributed load can be obtained by using a consistent approach*

when transferring the load'. Therefore, the consistent nodal load distribution of the Q8 plate element was considered before simulating the spring stiffness. The consistent nodal load is given by STRAND7 and shown in Figure 5.4.

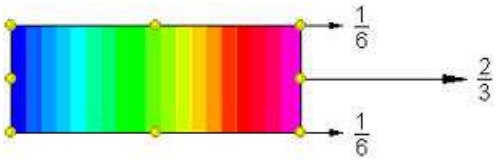

Figure 5.4: Consistent nodal load for 2D elements (STRAND7, 2009).

In order to guarantee the plane interface remains plane during deformation, the following procedure was followed with reference to Figure 5.5:

Step 1: Assume that the hidden corbel deforms under applied load as indicated by the dotted line in Figure 5.5. Because the contact surface remains plane, the absolute deformation for each node is proportionate.

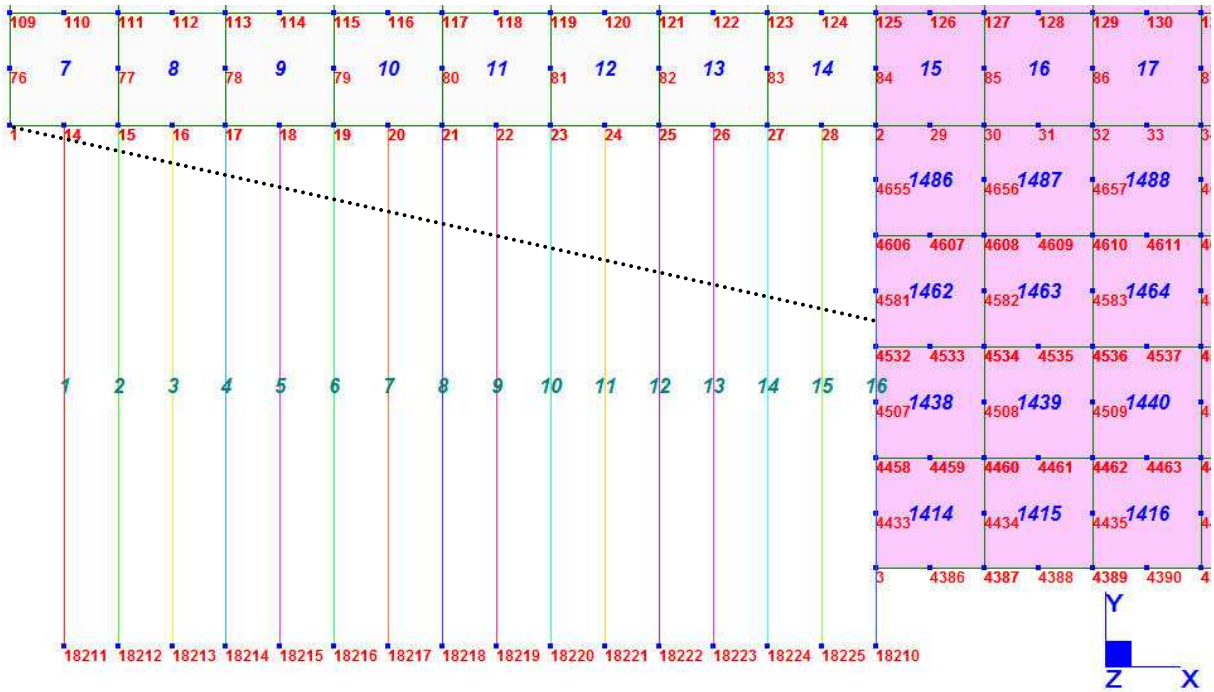

Figure 5.5: Sketch for nodes and elements.

When the beam deforms, the truss elements shorten. According to equation 5.1, the

stiffness of the truss element can be calculated, which is also proportionate. For the first stage, the exact deflection and stiffness are not known yet, hence, an initial value is assumed as indicated in table 5.1.

Table 5.1: Stiffness for Q8 plate elements in Figure 5.5.

Plate Q8 element	The distance between node 1 to each Q8 plate element L (mm)	Spring stiffness k (kN/mm)
Element 7	12.5 (node 1 to node 15)	12531.8
Element 8	25 (node 1 to node 17)	6265.9
Element 9	37.5 (node 1 to node 19)	4177.2
Element 10	50 (node 1 to node 21)	3132.9
Element 11	62.5 (node 1 to node 23)	2506.3
Element 12	75 (node 1 to node 25)	2088.6
Element 13	87.5 (node 1 to node 27)	1790.2
Element 14	100 (node 1 to node 2)	1566.4

Step 2: The spring stiffness corresponding to the consistent nodal load was distributed from each Q8 plate element to its nodes. In order to do this, the modulus of elasticity was assumed to be 200,000 MPa and the length of each truss element was taken as 60 mm. The stiffness on each node was then calculated based on the rule that is depicted in Figure 5.4 and equation 5.2.

Table 5.2: Distributing the stiffness from plate elements to truss elements.

Truss element	Stiffness (kN/mm)	Belonging to plate Q8 element		Belonging to truss element	Corresponding area (mm^2)	Corresponding diameter (mm)
Node 14	8354.5	7		Element 1	2506.4	56.4
Node 15	3132.9		8	Element 2	939.8	34.5
Node 16	4177.2			Element 3	1253.2	39.9
Node 17	1566.4	9		Element 4	469.9	24.4
Node 18	2784.8			Element 5	835.4	32.6
Node 19	1218.3		10	Element 6	365.5	21.5
Node 20	2088.6			Element 7	626.5	28.2
Node 21	939.8	11		Element 8	281.9	18.9
Node 22	1670.9			Element 9	501.2	25.2
Node 23	765.8		12	Element 10	229.7	17.1
Node 24	1392.4			Element 11	417.7	23.0
Node 25	646.4	13		Element 12	193.9	15.7
Node 26	1193.5			Element 13	358.0	21.3
Node 27	559.4		14	Element 14	167.8	14.6
Node 28	1044.3			Element 15	313.3	19.9
Node 2	261.0			Element 16	78.3	9.9

Table 5.2 gives the detailed calculation on the stiffness for each node and the corresponding area and diameter of bar size.

Step 3: The length and the diameter of the truss element is calculated in step 1 and step 2. The exact stiffness can be calculated through changing the modulus of elasticity E according to equation 5.6. Therefore, a trial and error method was used to find a critical E value. A value of E equals to 4600 MPa was found to meet the requirement, which allows the end of the beam, that is located inside the support area, to remain in compression.

5.2.2 Stress distribution during Stage I

A specific material stress-strain curve was applied for each zone in the 2D model. The zones for Stage I was defined in Section 4.6.2 and depicted in Figure 4.5. A

non-linear static analysis was then performed after defining the spring stiffness and the material stress-strain curves.

5.2.2.1 Selecting the stress-strain curve for each zone

The material stress-strain curve has already been defined in Section 4.5. However, zone 1 is in the bearing zone, where elements should not experience much tensile force. Therefore, a slight change was made to the stress-strain curve in zone 1 so that only a small tensile force was allowed. No horizontal reinforcement is needed in that zone, and therefore the tensile stress limit is equal to the tensile force of the concrete itself. The stress-strain curve for zone 1 is shown in Figure 5.6. The remainder of the zones are modelled with the stress-strain curve indicated in Figure 4.5.

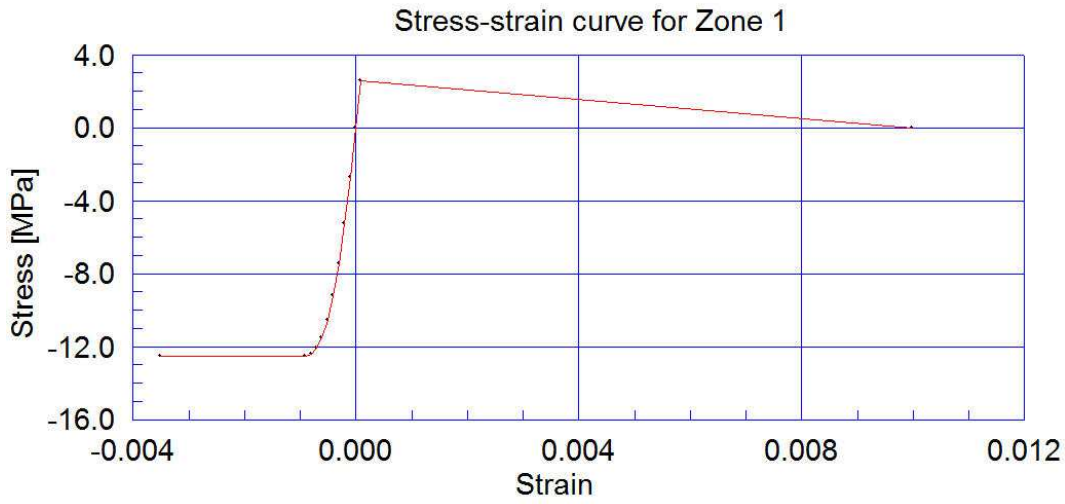

Figure 5.6: Stress-strain curve for zone 1.

The tensile stress in Figure 5.6 reduces gradually after the concrete reaches its maximum tensile stress.

5.2.2.2 Non-linear static analyses and analyzing distribution of the principal stresses

The principal stress is defined as V11 and V22 for each Q8 plate element. Left

Sections 1 and 2 in Figure 5.7 is enlarged to show the distribution of principal stresses for each stage.

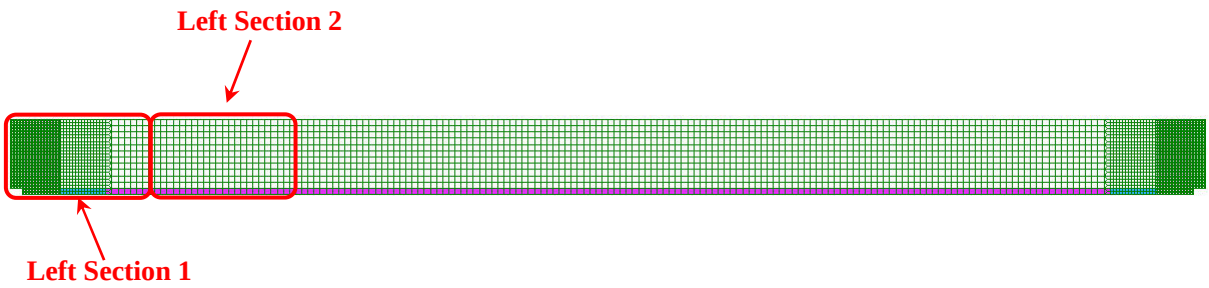

Figure 5.7: Defining sections to show stress distribution.

5.2.2.2.1 Distribution of principal stress V11 for Stage Ⅰ (tensile)

Figure 5.8 shows the distribution of principal stress V11 from zone 1 towards zones 6 and 7. The direction of principal stress V11 in the bottom section of zone 2 and the middle section of zone 4 are approximately equal to 45 degrees with the horizontal. Because the methodology of the non-linear material modelling is that the tensile stress should be resisted by the reinforcement and stirrups, the required reinforcement should be placed at 45 degree, such as bent-up bars. However, it is custom to rather use horizontal reinforcement and vertical stirrups to take the place of bent-up bars. The principal stress V11 (tensile) directions demonstrate why the shear crack near the end support is approximately 45 degrees under uniformly distributed loads.

The angle of the principal stress V11 reduces from the support towards zone 7. While the magnitude of tensile stress (V11) increases from left to right, the vertical component of V11 decreases. This is because the shear force reduces from the end support region towards the centre of a simply supported beam.

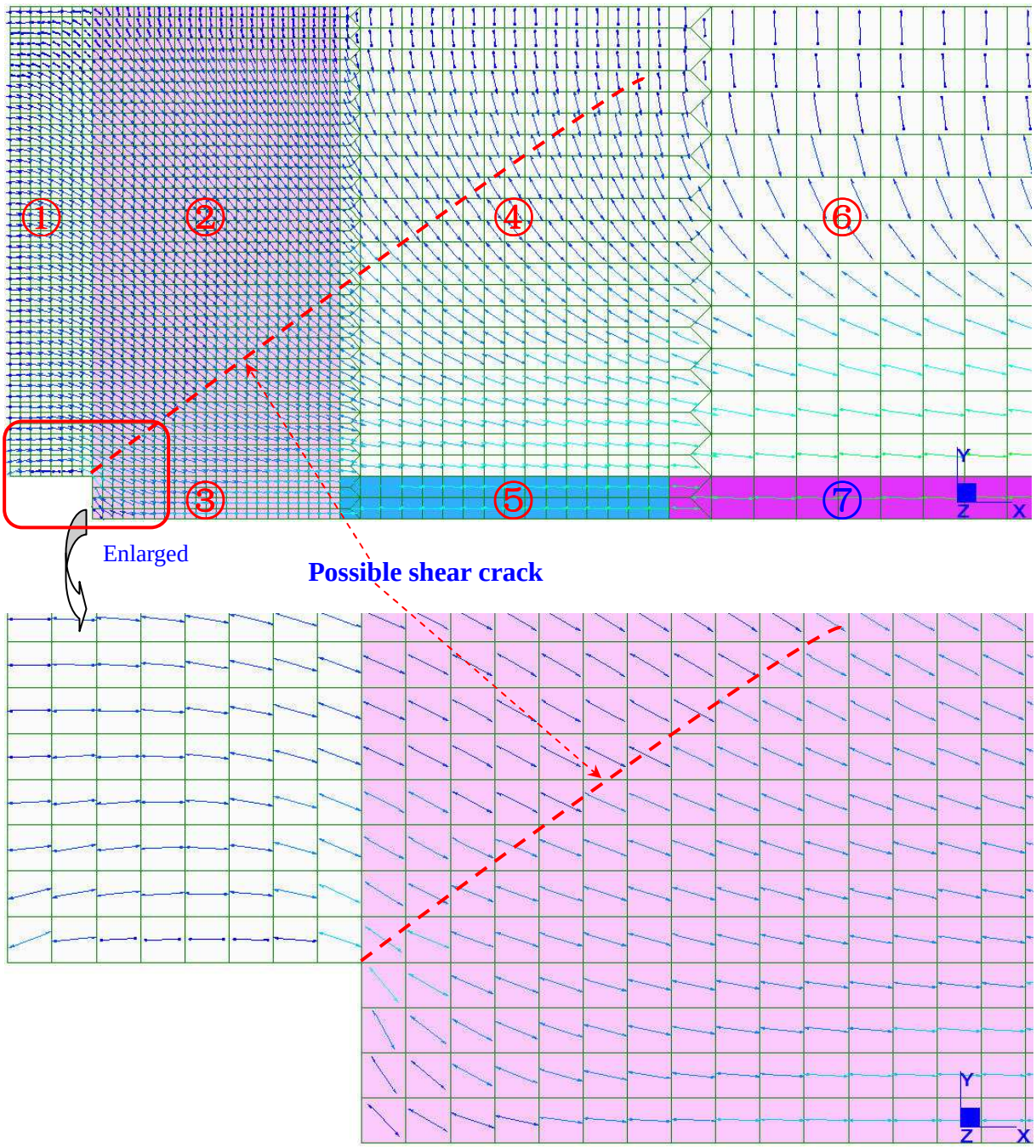

Figure 5.8: Principal stress distribution V11 (tension) for Stage Ⅰ (Left Section 1).

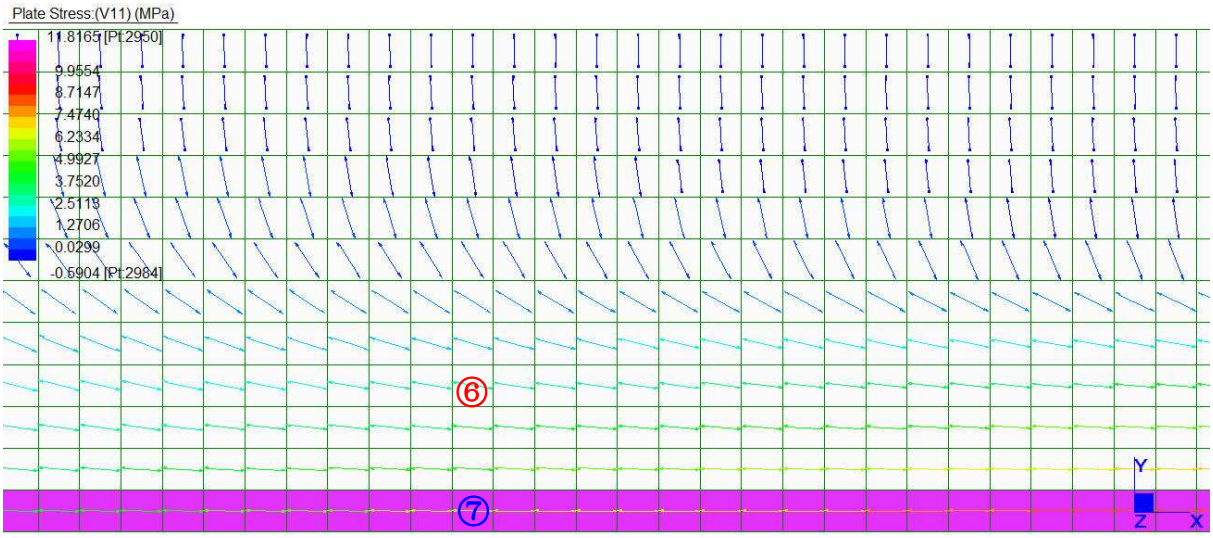

Figure 5.9: Principal stress distribution V11 for Stage Ⅰ (Left Section 2) (Refer to Figure 5.7).

Figure 5.9 depicts the principal stress V11 in Left Section 2 in which zones 6 and 7 are located. Because this section is close to the middle of the beam, the bending moment is dominant and the tensile stress at the bottom increases from the left side to the right in Figure 5.9.

5.2.2.2.2 Distribution of principal stress V22 for Stage Ⅰ (compression)

Figure 5.10 shows the distribution of principal stress V22 (compression) from zone 1 towards zones 6 and 7. The direction of the principal stress V22 in zone 1 is almost vertical, which means the hidden corbel resists the reaction force and propagates the force to bearing in zone 1. The direction of the principal stress V22 near the bottom section of zone 2 and zone 4 are approximately equal to 45 degree, which is perpendicular to V11 in the same elements. The direction of the principal stress V22 in zones 3 and 5 is nearly vertical and horizontal in the top of zones 2 and 4. The typical arch action of compressive stress from the support towards the beam center can also be seen from Figure 5.10.

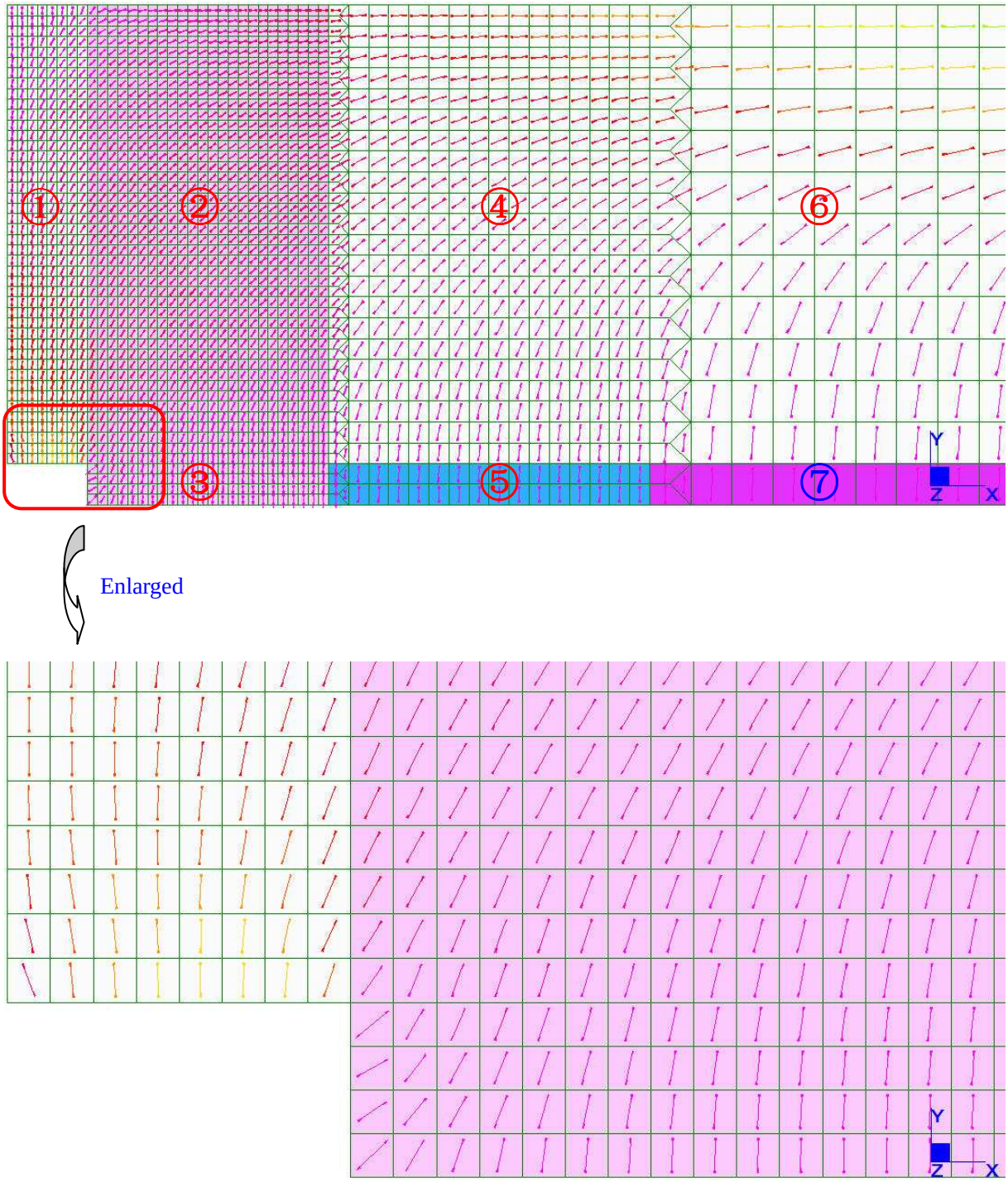

Figure 5.10: Principal stress distribution V22 (Compression) for Stage Ⅰ (Left Section 1).

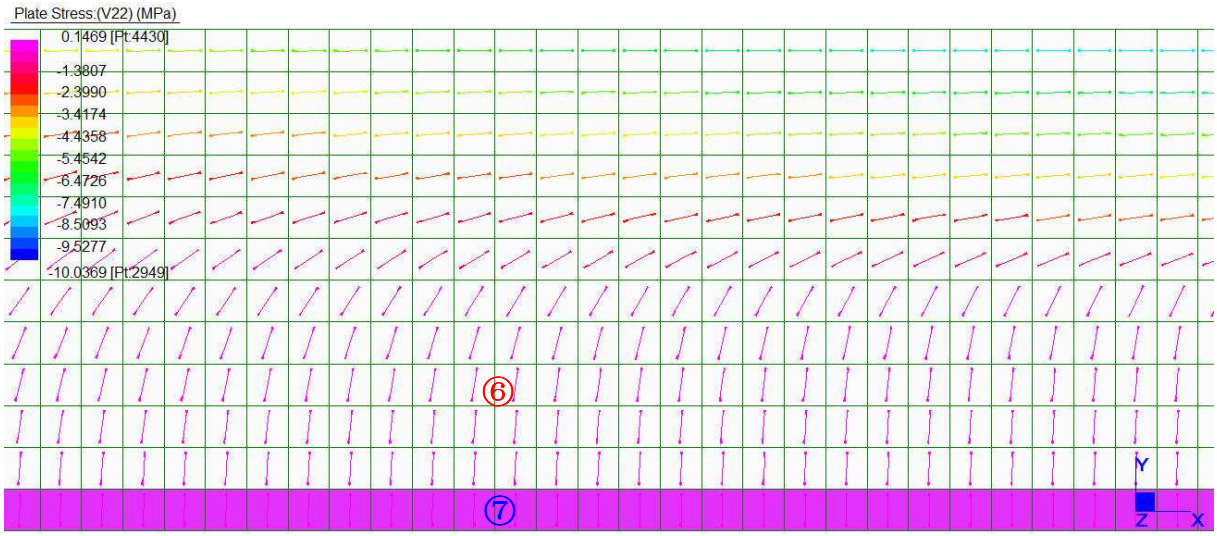

Figure 5.11: Principal stress distribution V22 for Stage Ⅰ (Left Section 2) (Refer to Figure 5.7).

Figure 5.11 shows the principal stress V22 (compression) in Left Section 2 in which zones 6 and 7 are located. The top part of zone 6 is in compression due to the increasing bending moment in this area.

5.2.3 Stress distribution during Stage Ⅱ

For construction Stage Ⅱ, the applied distributed loads are almost double those of Stage Ⅰ. In order to perform a non-linear static analysis for Stage Ⅱ, the stress-strain behaviour for each zone was defined. The zones for Stage Ⅱ were defined in Section 4.7.2 and depicted in Figures 4.6 and 4.8.The non-linear static analysis was then performed and the distribution of principal stress was evaluated.

5.2.3.1 Selecting the material stress-strain curve for each zone

The boundary conditions for Stage Ⅱ represent the conditions of the continuous beam. Because of the high negative bending moment in zone 8, there should be a high tensile stress in zone 8 and at the top of zone 1. Therefore, a stress-strain curve as indicated in Figure 4.5 applied to all zones.

5.2.3.2 Performing a non-linear static analysis and evaluating the principal stress distribution

The principal stress is also defined as V11 (tension) and V22 (compression) for each plate Q8 element.

5.2.2.3.1 Distribution of principal stress V11 for Stage Ⅱ (tension)

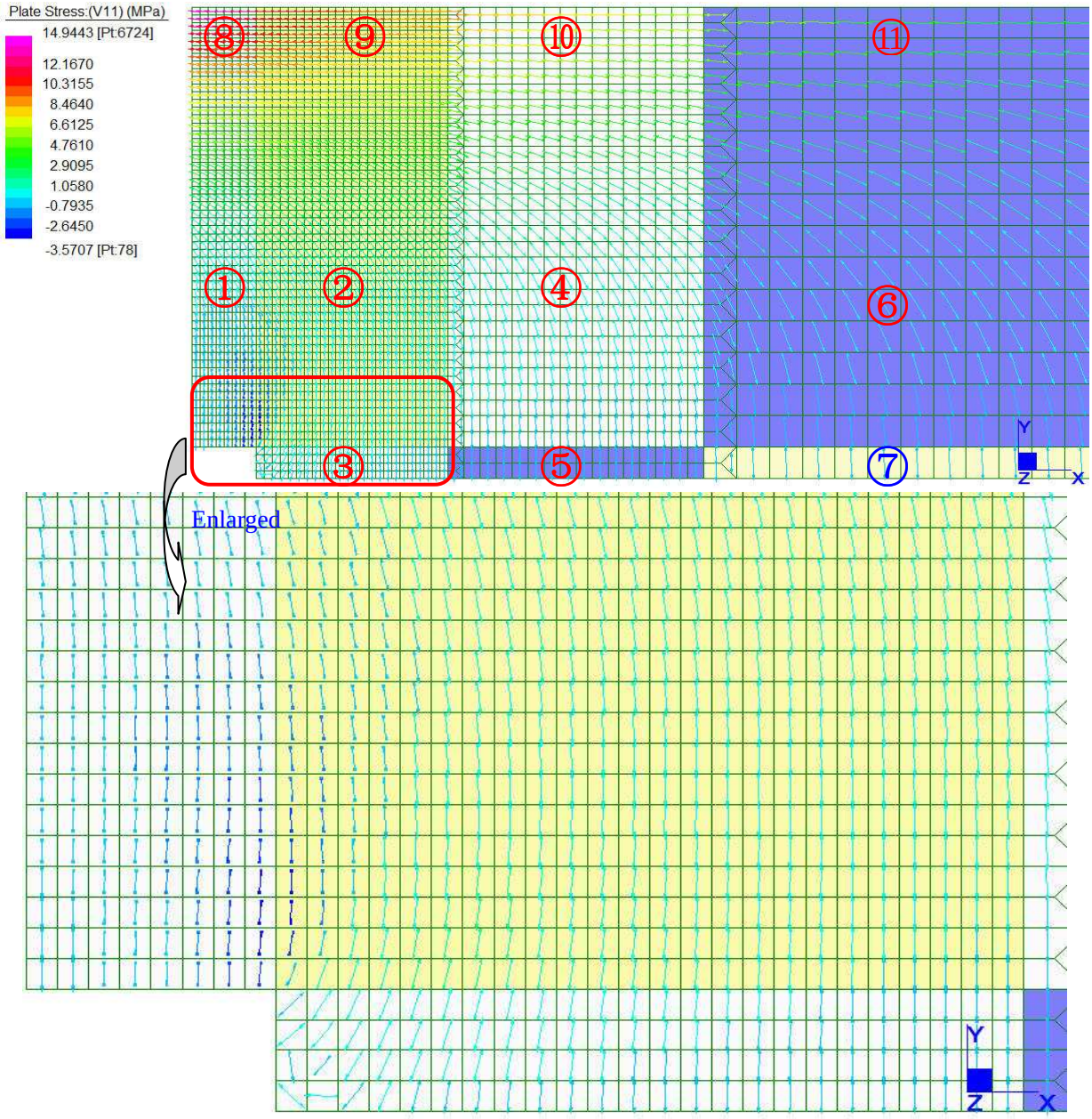

Figure 5.12: Principal stress distribution V11 for Stage Ⅱ (Left Section 1) (Refer to Figure 5.7).

The stress distributions in zones 1, 2, 3, 4, 8,9,10 and part of zone 6, 7, 11 are shown in Figure 5.12. The direction of the principal stress V11 is almost horizontal and the value of stress decreases from zone 8 to part of zone 11. The direction of tensile stresses V11 at the top (horizontal direction) changes to a vertical direction at the bottom further away from the support. It can be seen how the direction of the principal stress V11 (tension) changes from the top left corner to the bottom right corner in Figure 5.12.

The compressive stress occurs in the bottom parts of zone 1 and zone 2 and in the left part of zone 3. Therefore, the bottom reinforcement is not in tension in this zone and tension anchorage is not an issue.

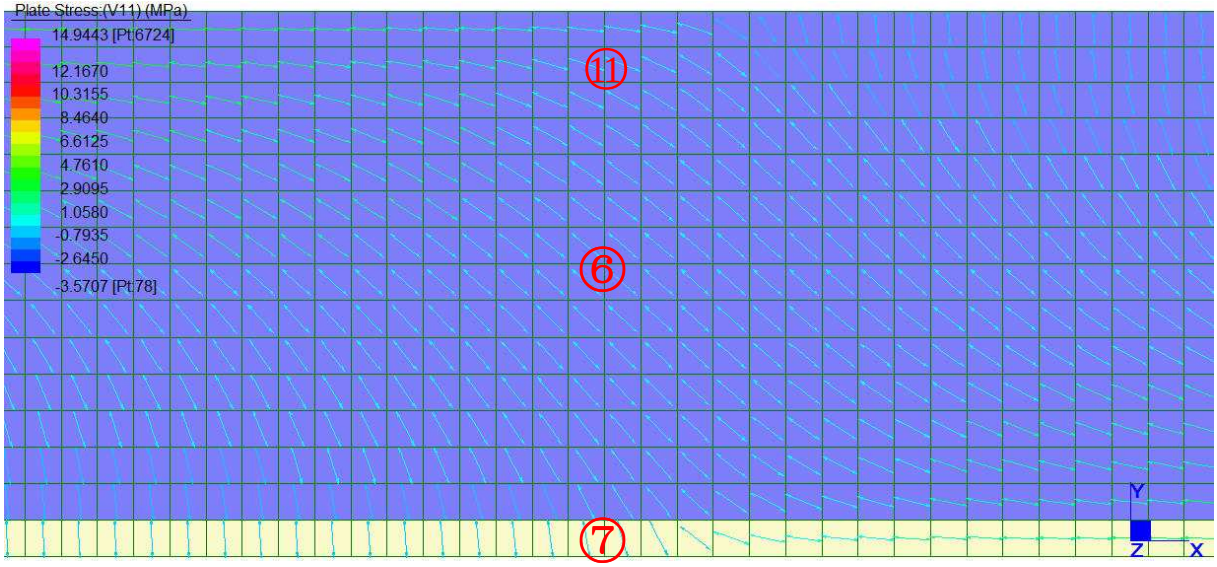

Figure 5.13: Principal stress distribution V11 for Stage Ⅱ (Left Section 2) (Refer to Figure 5.7).

Figure 5.13 indicates the principal stress V11 in Left Section 2, which is adjacent to Left Section 1, and includes zones 6, 7 and 11. The change in direction of the tensile stress from top to bottom and from the left to the right side of the picture can clearly be seen. The direction of the tension field from the top to the bottom right shows the shifting of bending moment from the negative to positive.

5.2.2.3.2 Distribution of principal stress V22 for Stage Ⅱ (compression)

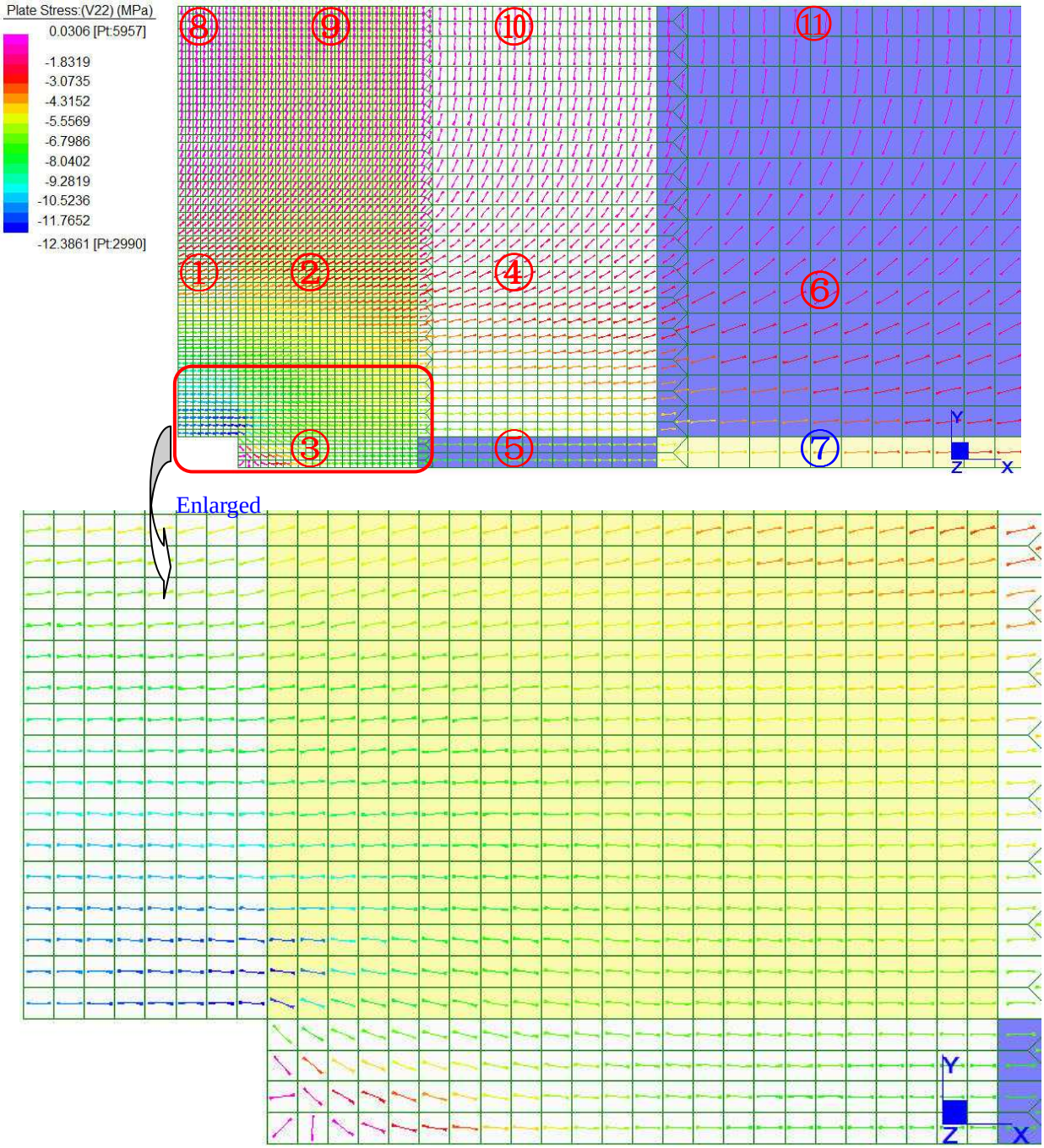

Figure 5.14: Principal stress distribution V22 for Stage Ⅱ (left section 1) (Refer to Figure 5.7).

Figure 5.14 gives the stress distribution in zones 1, 2, 3, 4, 8,9,10 and part of zone 6, 7, 11. The maximum compressive stress occurs in the joint area of zones 1, 2 and 3. The maximum compressive stress propagates towards the right top side of the picture.

The direction of principal stress in the middle parts of zones 4 and 6 is approximately equal to 45 degrees, which acts as a transition section.

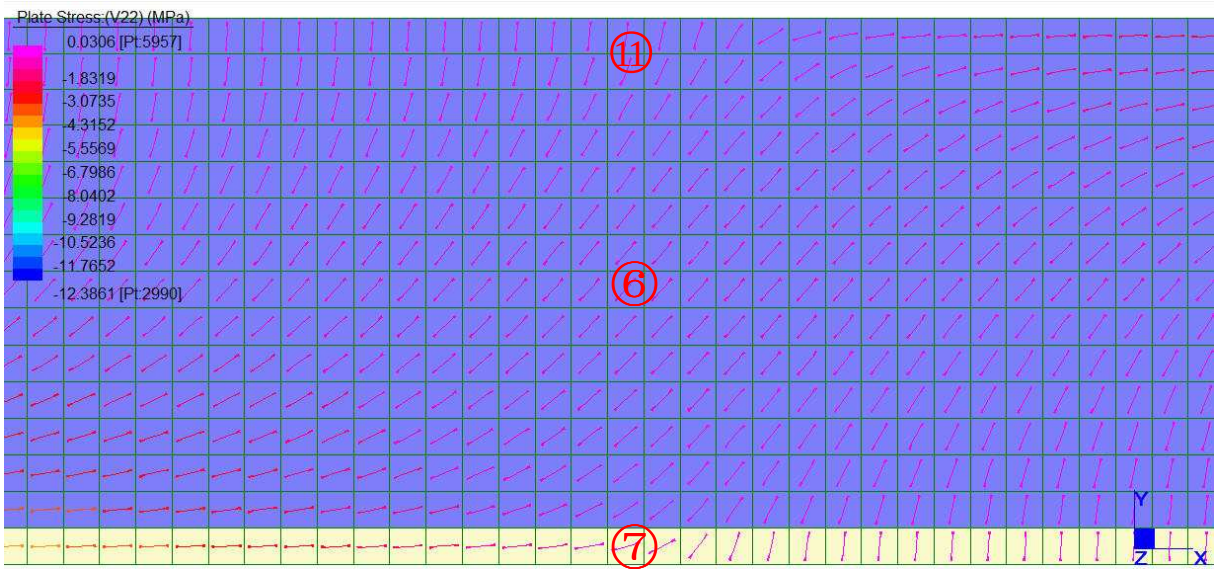

Figure 5.15: Principal stress V22 for Stage Ⅱ (left section 2) (Refer to Figure 5.7).

Figure 5.15 shows the principal stress V22 in Left Section 2, which is adjacent to Left Section 1, and which belongs to zones 6, 7 and 11. The compressive stress distribution is as expected.

5.2.4 Comparing the principal distribution of stresses between Stage Ⅰ and Stage Ⅱ

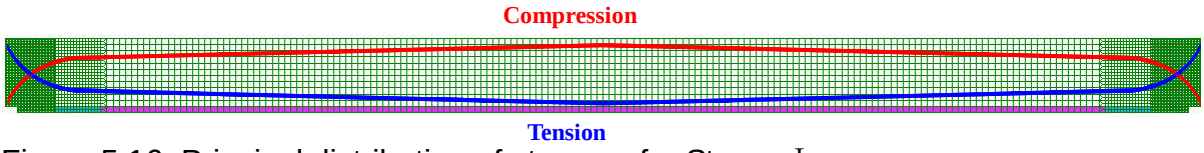

Figure 5.16: Principal distribution of stresses for Stage Ⅰ.

The distribution of principal compressive and tensile stresses is shown in Figure 5.16. The compressive stress zone centreline is in the form of an arch and that of the tensile stress in the form of a suspended chain.

For the compressive stress, unlike a deep beam, the arch action at the end of the beam develops quickly and turns gently after approximately one effective depth from

the face of the support.

For the tensile stress, the suspended chain reduces quickly at the end support and turns gently when it is nearing the middle section of the beam. The tensile force at the bottom, which needs to be anchored for reinforcement bars along the beam, is a combination of principal stress V11 and V22.

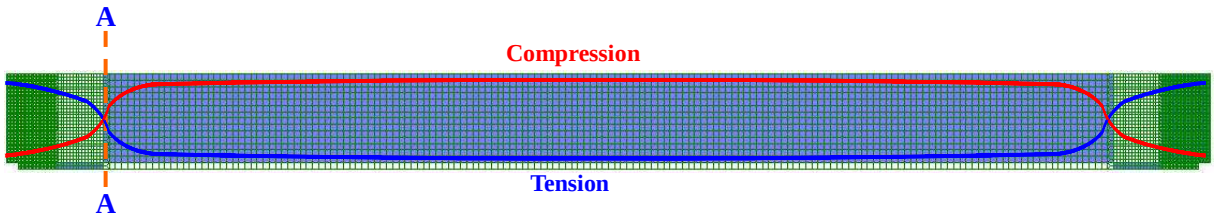

Figure 5.17: Distribution of principal stresses for Stage Ⅱ.

For Stage Ⅱ, the compressive stress starts from the bottom of the end support and is then converted to the top after a certain distance from the support. By comparing it with Stage Ⅰ, the start of the compressive stress does not appear to have the arch action. After a certain distance, the distribution of compressive stress is nearly the same as that of Stage Ⅰ.

The tensile stress starts from the top of the end support and reduces gradually, the centreline of which does not appear to be a suspended chain. After a certain distance, the distribution of tensile stress does form a suspended chain, which is nearly the same distribution as that of Stage Ⅰ.

In Figure 5.17, the location of cross section marked A-A is located where the absolute value of the horizon components of principal stress V11 and V22 are equal. The horizontal internal force at section A-A is thus balanced and there are no horizontal compressive and tensile stresses at that cross section. Therefore, the cross section A-A does not have a bending moment and acts as the critical section for the beam where the value of bending moment changes from negative to positive.

Based on the above analysis, the anchorage for tension reinforcement at the support regions needs to be ensured for Stage Ⅰ. As for Stage Ⅱ, there is not a similar problem of bond failure in tension. Therefore, the investigation focuses on Stage Ⅰ. The following paragraphs will verify the FE model for Stage Ⅰ through supportive calculations.

5.2.5 Verifying the FE analyses

By comparison of the two construction stages, it was shown that bar anchorage in the end zone needs to be further investigation for construction Stage Ⅰ. Results for the verification consisted of Q8 plate elements in zone 2 and zone 3, which were used to verify the validity of the FE model.

In order to do so, some hand calculations were done to verify the FE model. The verification consisted of checking the shear force for each cross section in the connection zone. In addition, the methods introduced in Eurocode 2 (2004) with no limit of theta were used to estimate the stresses for comparison with the FE model.

5.2.5.1 Verifying the FE results by shear forces

Before the HCC calculation started, a simple FE model was set up and it was discovered that the principal stress in the centroid of plate elements gives the most accurate results. The stress values on the nodes of plate element, however, has a sizeable error, which are also indicated as ‘error bars’ when they are plotted by STRAND7. Therefore, the verification of the shear force was calculated based on principal stress in the centroid of the plate element.

The detailed principal stress results were obtained from the STRAND7 results file, which provides detailed information for each element. The non-linear 2D model for Stage Ⅰ has a total of 5888 Q8 plate elements. An example on how to calculate the shear force and the detailed results are listed in Appendix B.

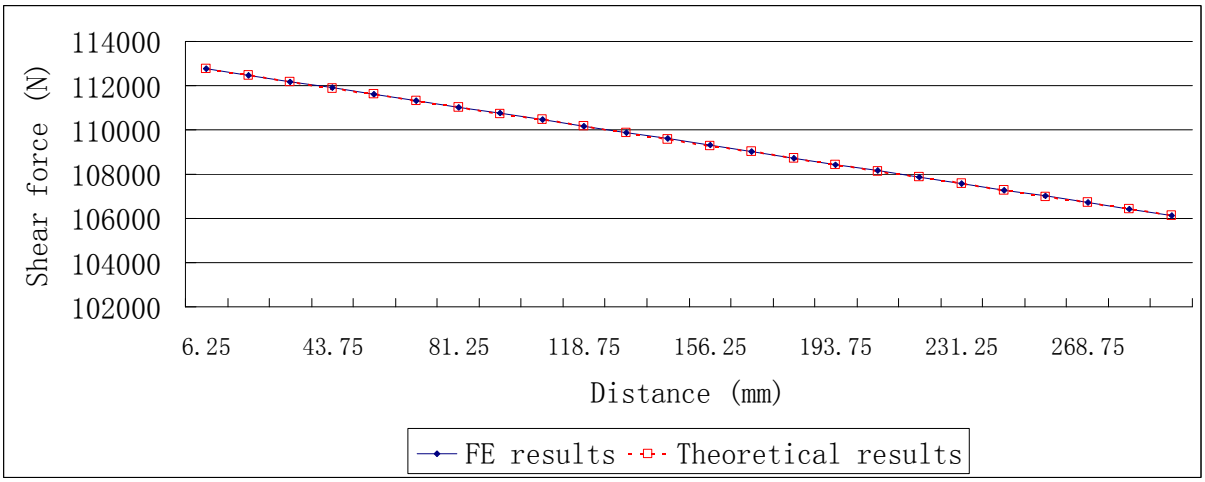

Figure 5.18: Comparison of shear force (FE results vs. theoretical results).

From Figure 5.18, it can be seen that the dashed line overlaps with the real line, which appears as a single plot. This means that the values calculated from the model are almost identical to those based on the theoretical calculation. The shear forces obtained from the FE model perfectly represent the actual shear force. The FE mesh in the connection zone is thus fine enough to obtain suitably accurate results.

5.2.5.2 Verifying the FE model analyses from theoretical calculations

Besides verifying the shear force, the combination effect of bending moment and shear force, which contribute to the bottom tensile force from equation 2.5, were also calculated. Because the true angles of truss analogy in the zone of stress concentration is unknown, the angles calculated from equation 2.5 were used to estimate the accuracy of the results.

The angle θ was calculated based on equation 2.5 and then used to compare with the theoretical angle in that area to verify the data. The theoretical angle is introduced for comparison as follows:

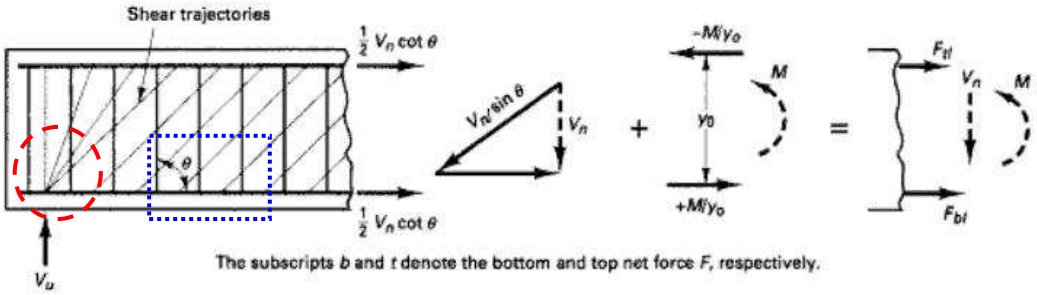

Figure 5.19: Steel planar truss analogies (Nawy, 2009).

Nawy (2009: 169) shows the steel planar truss analogy in Figure 5.19. The dashed circled block indicates the angle for shear trajectories. However, in the dotted rectangular block, the shear trajectories are almost parallel with each other, which mean the angle is identical. The shear trajectories between the dashed circle block and the dotted rectangular block should have some integrated shear trajectories. Huber (2005:30) indicates the truss analogies of reinforcement as indicated in Figure 5.20.

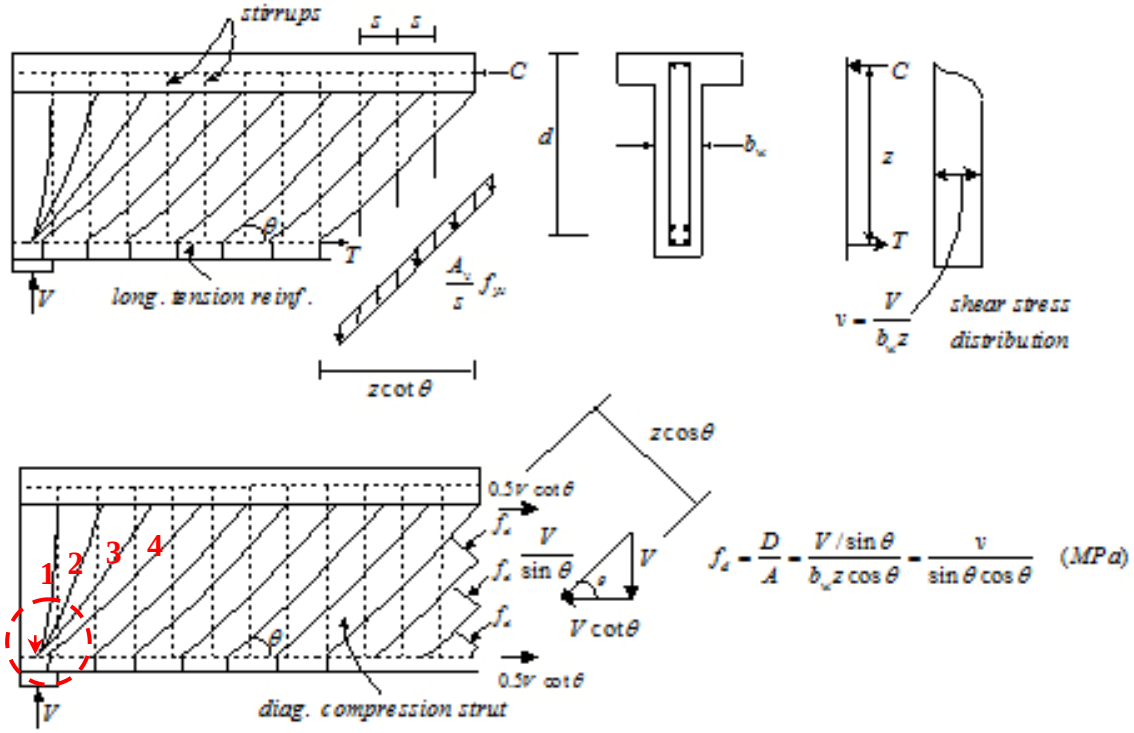

Figure 5.20: Truss analogies of reinforce concrete (Huber, 2005).

In Figure 5.20, it can be seen that the bottom part of shear trajectory ‘4’ shifts slightly to the right side as indicated in the dashed circled block. Theoretically, the angle for

shear trajectories can be calculated for each cross section when they are originating from the downward arrow in the dashed circled block (Figure 5.20). The distance of shifting of shear trajectory '4' at the bottom is unknown which gives a rough estimation of the shear trajectory angle. Therefore, the angle of shear trajectories calculated from FE results for each cross section in zone 2 and zone 3 should be larger than those of the theoretical calculations as indicated in Figure 5.21.

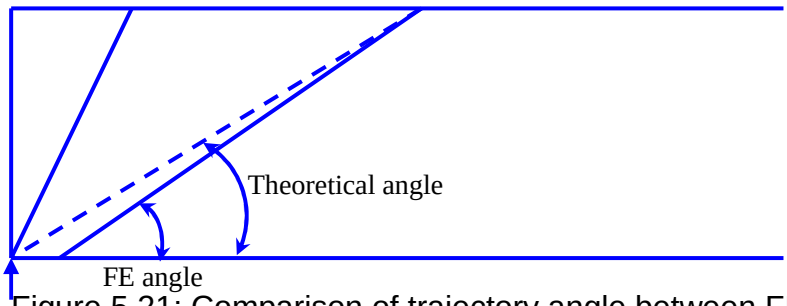

Figure 5.21: Comparison of trajectory angle between FE result and theoretical calculations.

Because there are so many Q8 plate elements in zone 2 and zone 3, an example showing the procedure on how to calculate the tensile force and the angle are presented in Appendix C. The detailed results are also listed in Appendix C.

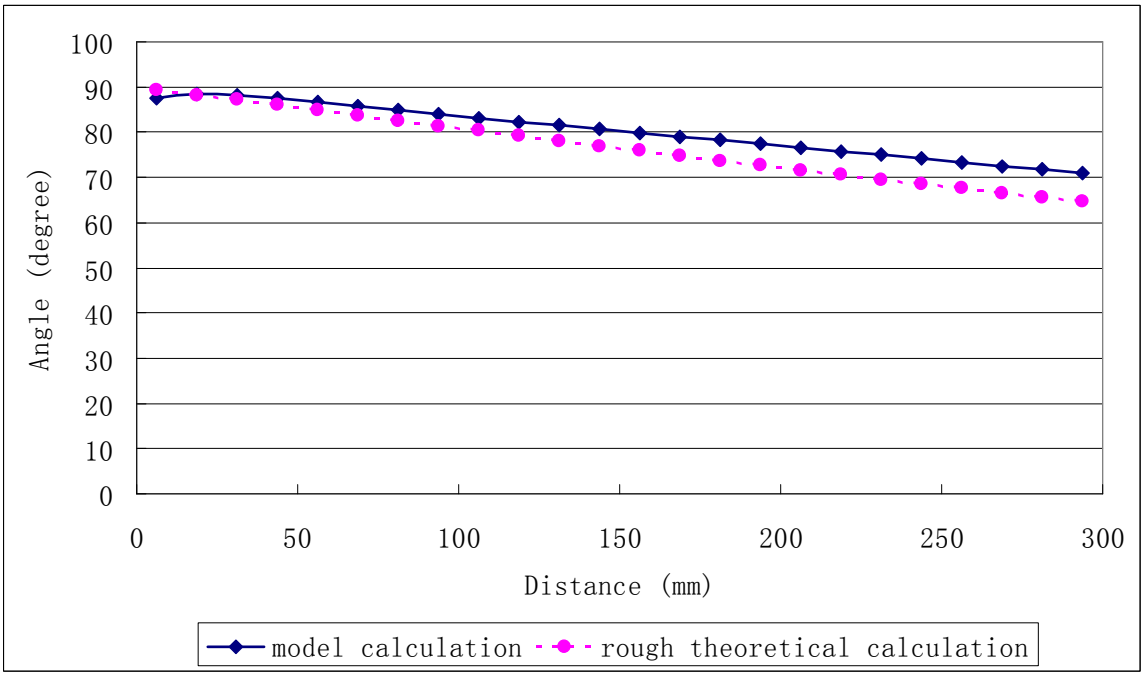

Figure 5.22: Comparison of angle between model calculation and rough theoretical calculation.

Figure 5.22 shows the comparison of the angle between the model calculation and rough theoretical hand calculation. It can be see that except for the first point from the left, the rest of the theoretical points have an angle which is smaller than those calculated from the FE results. The reason for the first point for which the angle of the FE results is smaller than theoretical calculation is that the calculation is based on the Q8 plate elements and each stress is calculated from the model has a slight error. The errors were included with the summing of all the forces that are contributing to the shear force.

However, the distribution of principal stress in Figure 5.10 appears to have a similar shear trajectory as that in Figure 5.20, which explains a slightly changing of angles. Therefore, the 2D FE model represents the stress distribution in the beam quite well and these results were then used as input for a 3D analysis.

5.3 The 3D model

The purpose of the 3D model is to determine lateral confinement in the concrete in the hidden corbel resulting from the triangular side plates. Before comparing the thickness of the triangular side plates, the loading conditions in the 3D model had to be defined. It should provide the same loading conditions as in the 2D model. Because the 3D model includes a large number of elements and degree of freedom, only a linear static analysis was performed.

5.3.1 Applying loads on 3D model

In order to simulate the elements in the 3D model with the same loading conditions as in the 2D model, the principal stress from the 2D model on those elements, which were crossed by the line as indicated in Figure 5.23, were calculated and then applied as loading conditions in the 3D model.

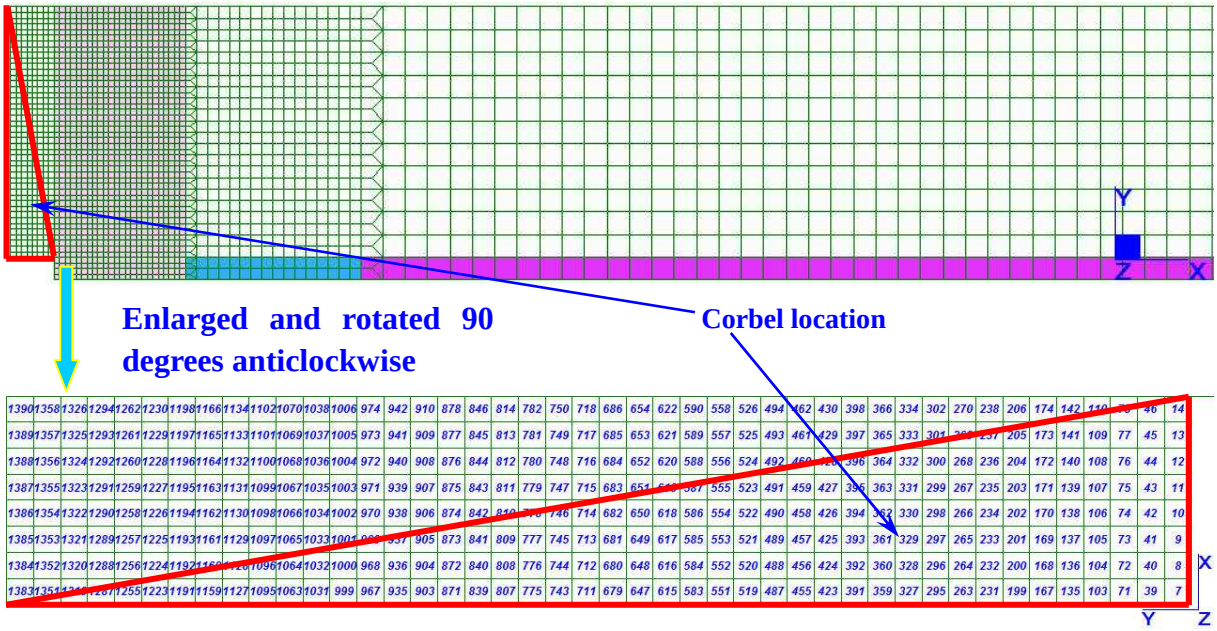

Figure 5.23: 3D model surface elements.

STRAND7 provides several ways for applying the stress to a surface of a 3D brick element. The normal stress σ_n and shear stress τ in Figure 5.24 were calculated and applied to the 'face 1' (Figure 4.11) of the 3D model.

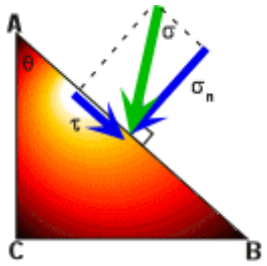

Figure 5.24: Normal and shear stress on a certain face.

5.3.2 Comparing confinement under the different thicknesses of triangular side plates

After the stresses were applied to the 3D model, three thicknesses of triangular side plate were set up in the model for the comparison of confinement stresses (Stress in

ZZ direction of the FE model). In order to compare the confinement in the concrete in the hidden corbel, the thicknesses of triangular side plates are assumed to be 4.5, 10 and 20 mm.

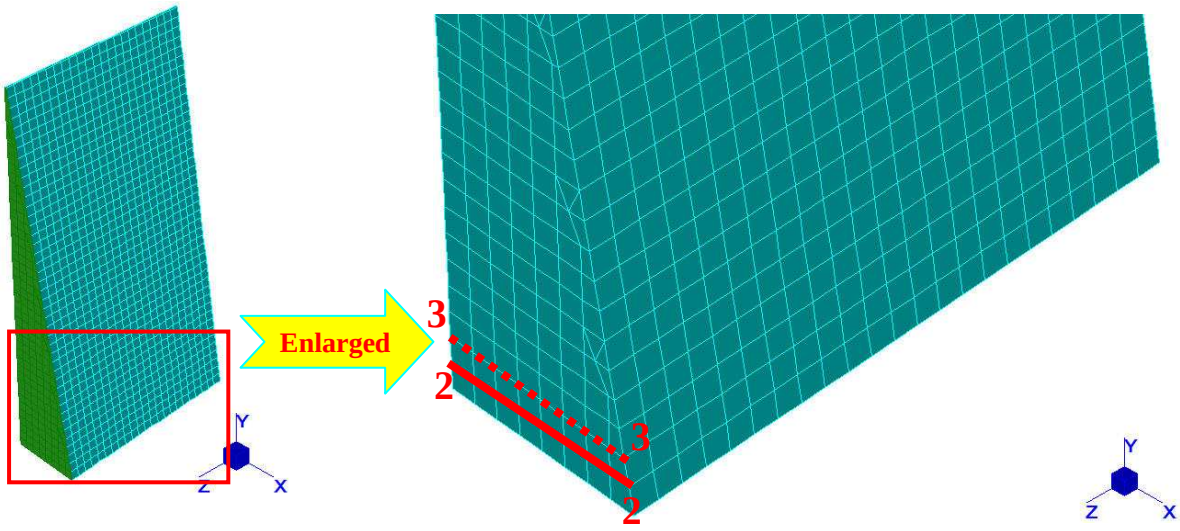

Figure 5.25: Location of bottom lines 2-2 and 3-3.

In order to obtain a direct value of confinement, bottom lines 2-2 and 3-3 are defined in Figure 5.25. The full line is called bottom line 2-2 and the dotted line is called bottom line 3-3. The stress in the ZZ direction shown by contour and those nodes in bottom lines 2-2 and 3-3 are indicated in the Figures 5.26 to 5.28. The figures provide stress for side plates between 4.5, 10 and 20mm.

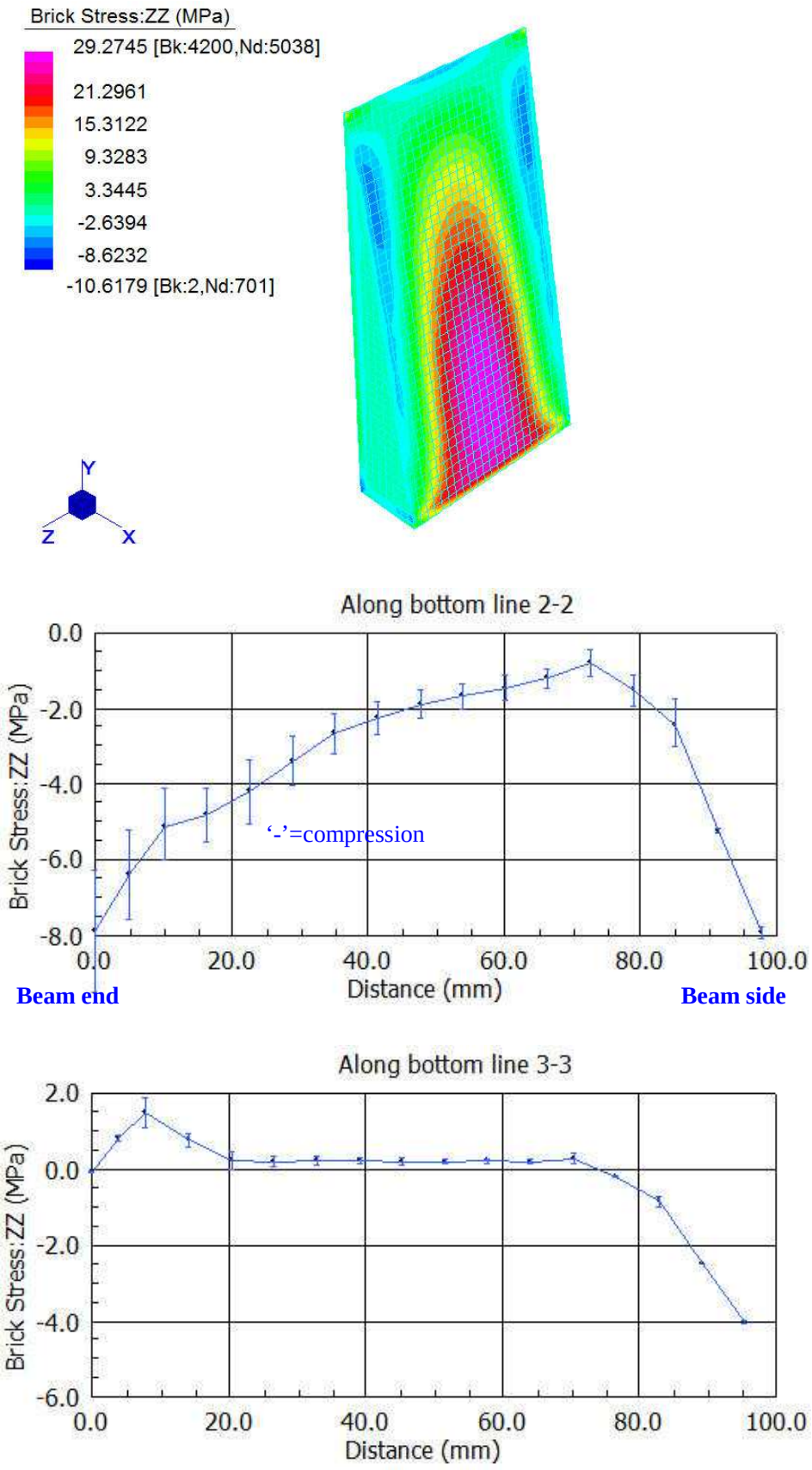

Figure 5.26: Stress distribution in ZZ direction for 4.5 mm thick triangular plate.

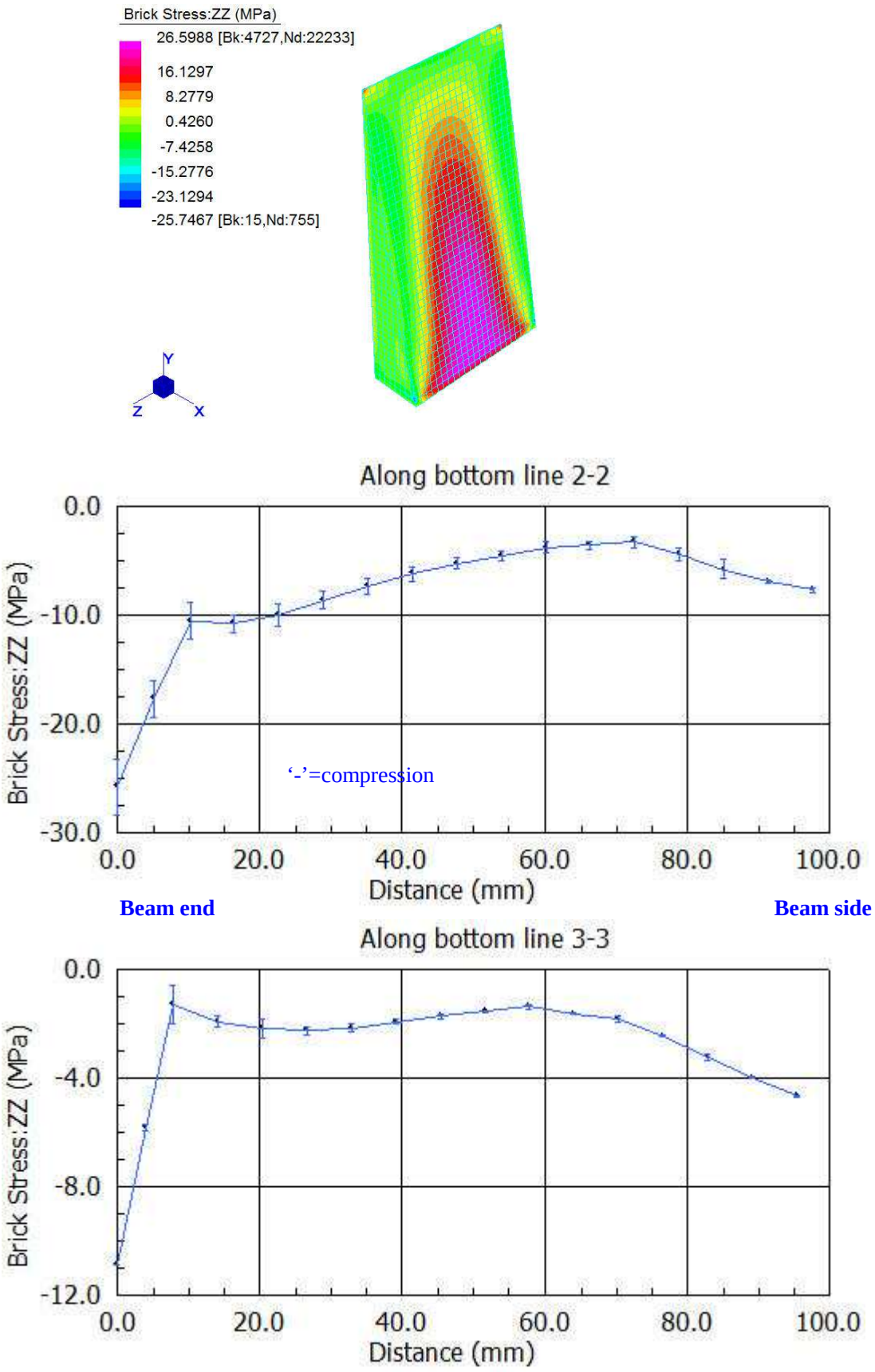

Figure 5.27: Stress distribution in ZZ direction for 10 mm thick triangular plate.

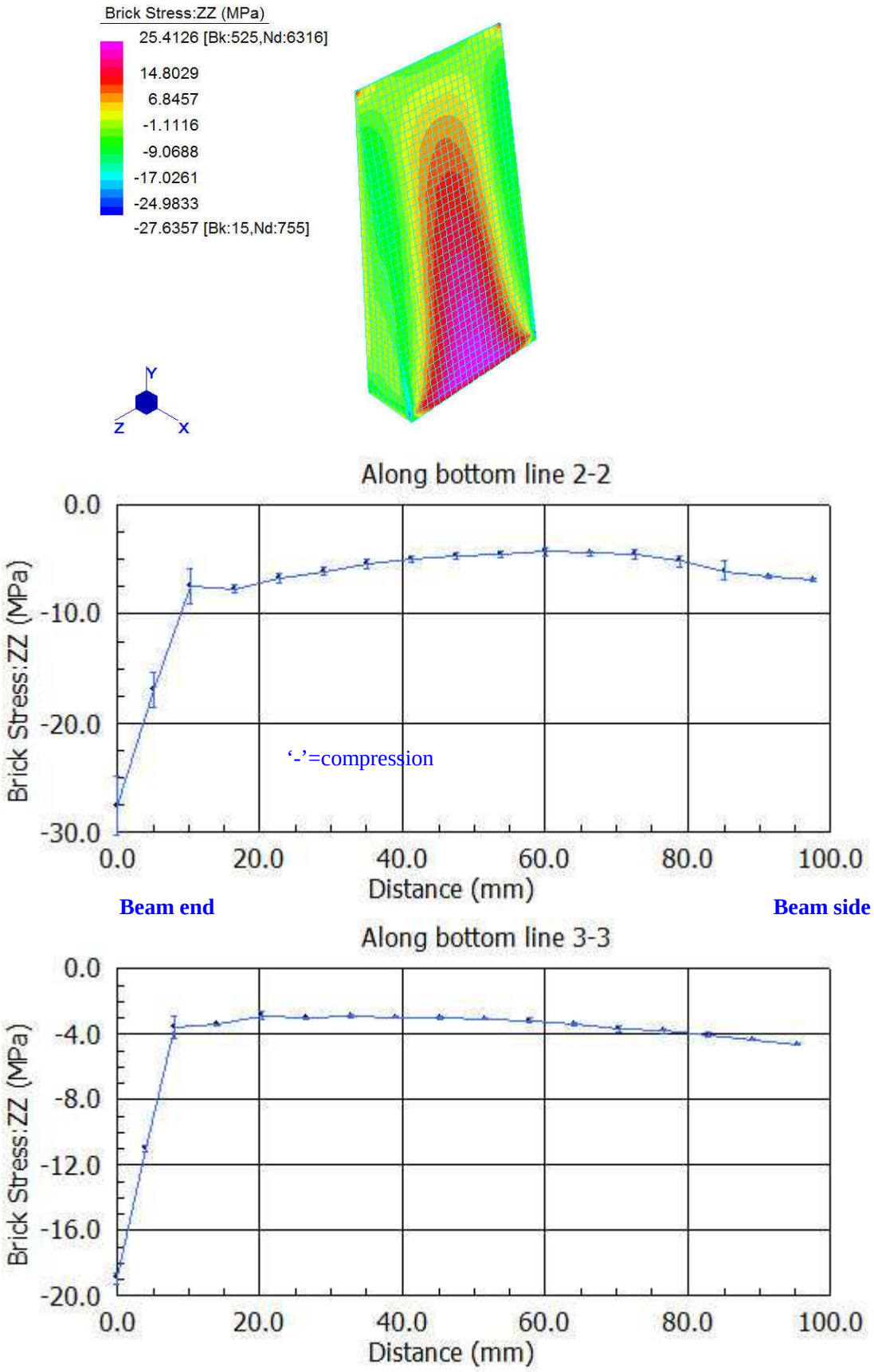

Figure 5.28: Stress distribution in ZZ direction for 20 mm thick triangular plate.

The stress in the Z direction read from the contour does not differ much between Figures 5.26 to 5.28. However, it does differ when reading the stress values as plotted along bottom lines 2-2 and 3-3, shown in figures 5.26 to 5.28.The bottom line 2-2 from Figures 5.25 to 5.27 shows that the compressive stress in Z direction with 10 mm plate is similar to that of 20 mm and better than that of 4.5 mm. From bottom line 3-3, it can be seen that there is nearly no compressive stress in the Z direction for a 4.5 mm thick plate, while the 10 mm and 20 mm thick plate still do show some compressive stress. Therefore, the confinement by the 10 mm and 20 mm plates are similar and better than that of a 4.5 mm plate.

5.3.3 Alternative tensile stress transfer modelling options with stress distributions results

With the same loading conditions as that of the 2D model, the elements in the 3D model also represent the compression zone at the top of the beam and the tension zone at the bottom of the beam. The tensile force at the bottom of the beam is resisted by the tension reinforcement. The increase of confinement stresses will increase the bond stress, which in turn can transfer more tensile stress to the tension reinforcement. The loads are applied gradually on the beam after fixing certain structural members or applying certain live loads. Because the increase of reaction force will lead to the increase of bond stress, the exact tensile force that the bond stress can resist between reinforcement and concrete is unknown. This result in the uncertainties on the magnitude of tensile force that could be transferred to the tension reinforcement

In order to compare the stress distribution in the hidden corbel, two options are made to evaluate the effects by transferring a certain tensile force to the tension reinforcement. For the 2D FE model, the top region of the beam is in compression and the bottom section of the beam is in tension. Only the Q8 plate elements in the tension zone contribute to the transfer of tensile stress to the tension reinforcement. The two

options are then focused on transferring the tensile force in the tension zone.

Option 1 is that the stress distribution in each Q8 plate elements is the same as that of the 2D model. Option 2 is that the normal stress in the X direction is converted to the tensile force in the tension reinforcement, the remainder of the stresses do not change. By comparing the stress distribution in the Y and Z directions separately, the location of better confinement in the hidden corbel can be represented.

For the reason that the thickness of the 10 and 20 mm triangular side plates do not have a significant influence on the confinement, the results of the 20 mm thick triangular side plate was used to compare the confinement in the concrete.

5.3.3.1 Identification of the Q8 plate elements in the tension field.

The tension field in the 2D FE model is the region that all the elements are in tension. In order to find the tension field of the beam, a cross section 'A-B' is cut as indicated in figure 5.29. The stress distribution on the centre nodes of elements in the X direction was obtained from the FE results and was plotted in figure 5.29.

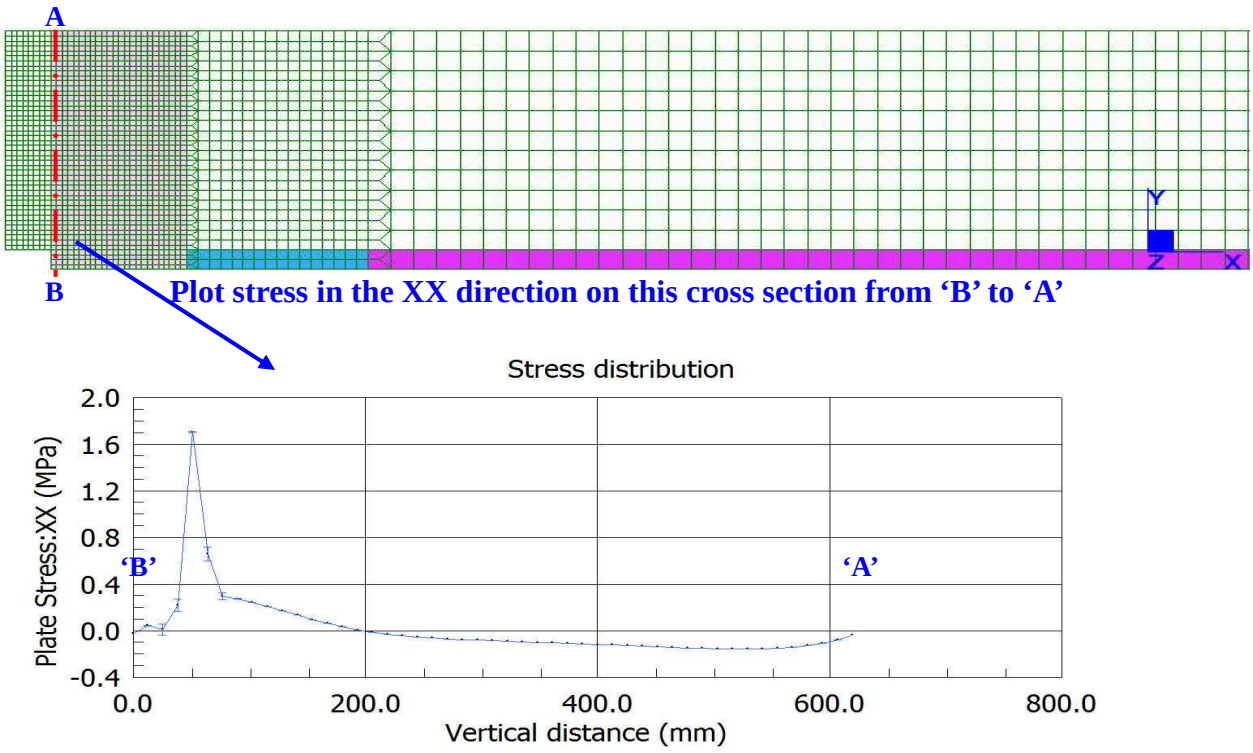

Figure 5.29: Stress distribution in the cross section next to the face of the support.

As indicated in Figure 5.29, a total height of 193.25 mm is in tension zone measured from the bottom extreme fibre of the beam. A total of fifteen Q8 plate elements are located in the tension zone. These fifteen elements were used to compare the confinement under two options. Option 1 is already used to compare the effect of confinement as indicated in Section 5.3.2. The transferring of tensile stress to the tension reinforcement for Option 2 is introduced as follows:

Option 2: The normal stress is transferred to the tension reinforcement.

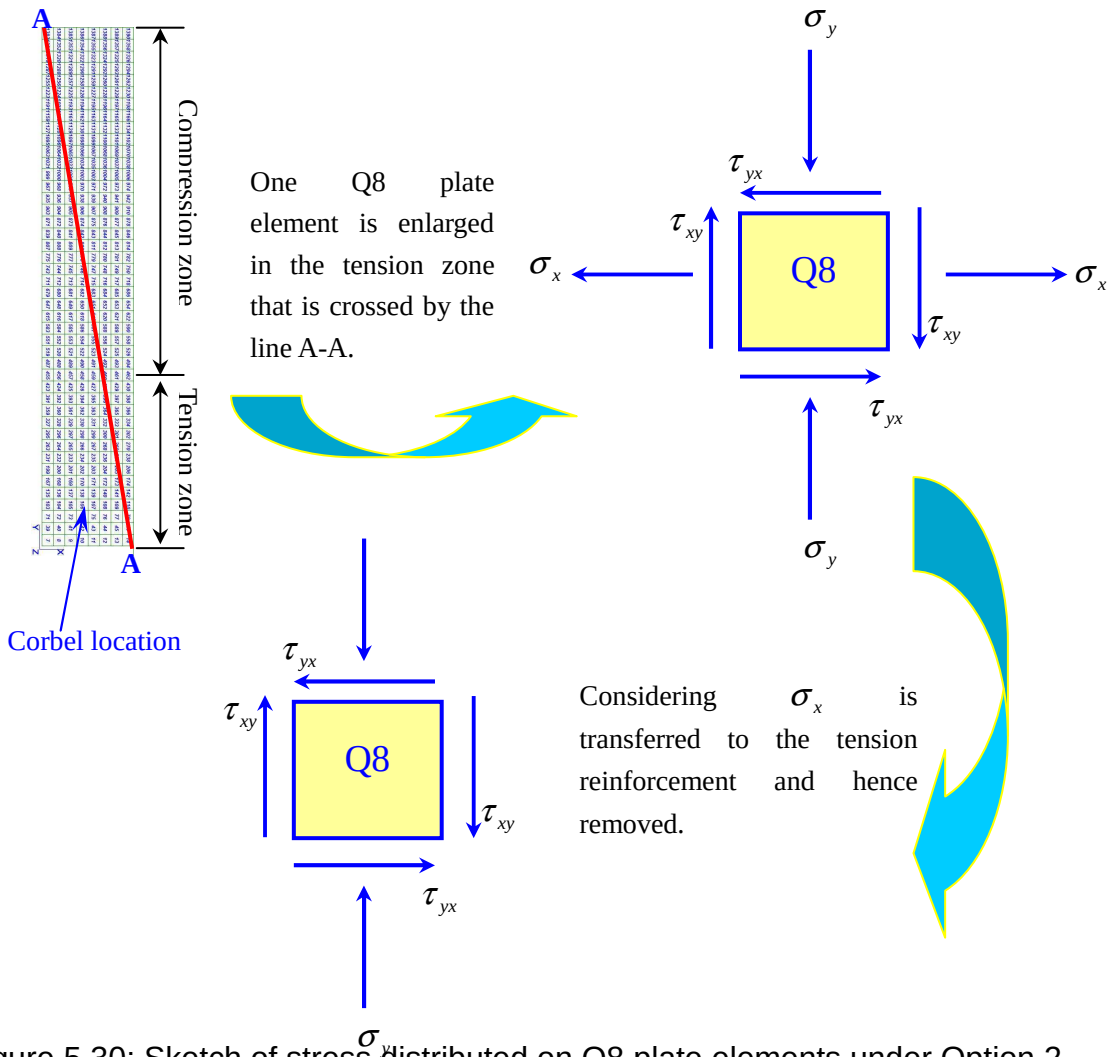

Figure 5.30: Sketch of stress distributed on Q8 plate elements under Option 2.

Figure 5.30 shows the stress conditions for Option 2. The normal stress σ_x is

removed and the normal stress σ_y and shear stress τ were used to calculate the stress allocated in the tension zone of 'face 1' (Figure 4.11). The equivalent tensile stress σ_x was then converted to a tensile force and applied to the tension zone of the 3D FE model as indicated in Figure 5.31.

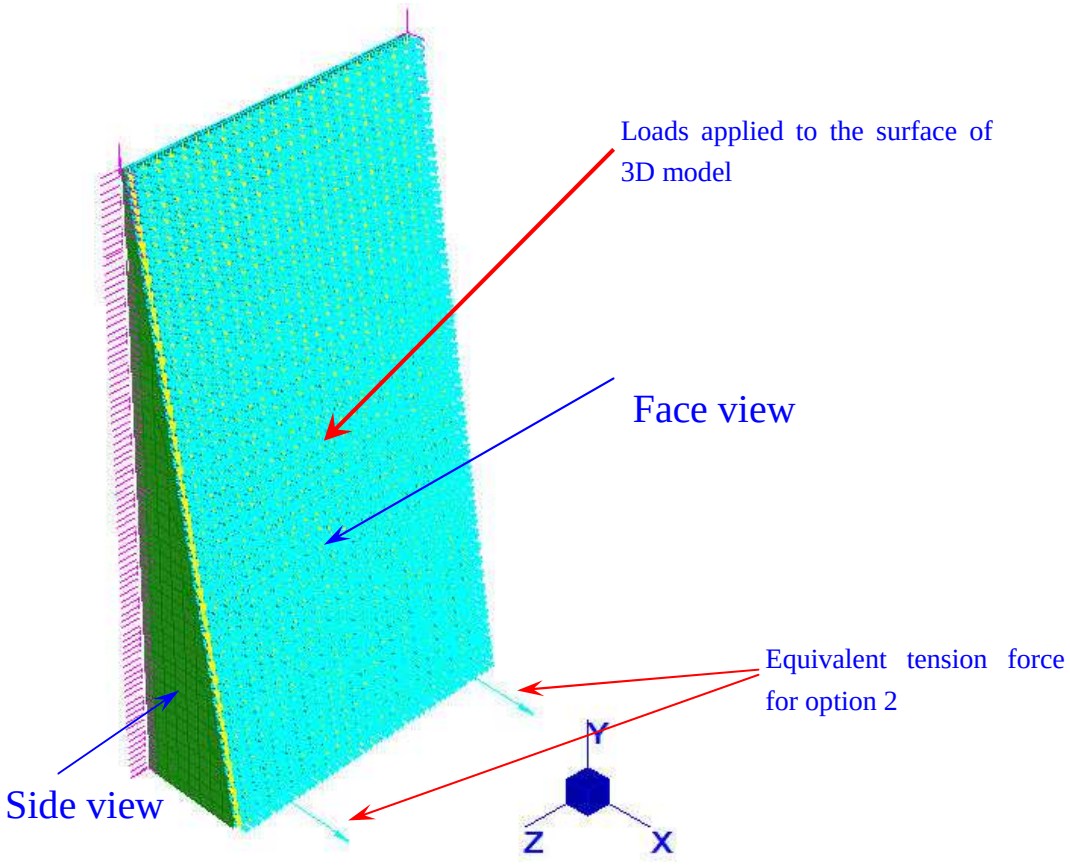

Figure 5.31: Isometric view of 3D FE model under Option 2.

5.3.3.2 Comparing the stress distribution under the two options

To evaluate the confinement by the triangular side plate, the stress in the Z direction of the two FE models should be compared. In the same way, the confinement by the bottom plate of the hidden corbel should also be compared in the Y direction between these two FE models.

5.3.3.2.1 Comparing the confinement in the Z direction under the two options

The confinement of the triangular side plate will affect the stress distribution in the Z direction. Figures 5.32 to 5.33 show the effect of confinement in the Z direction under the two options.

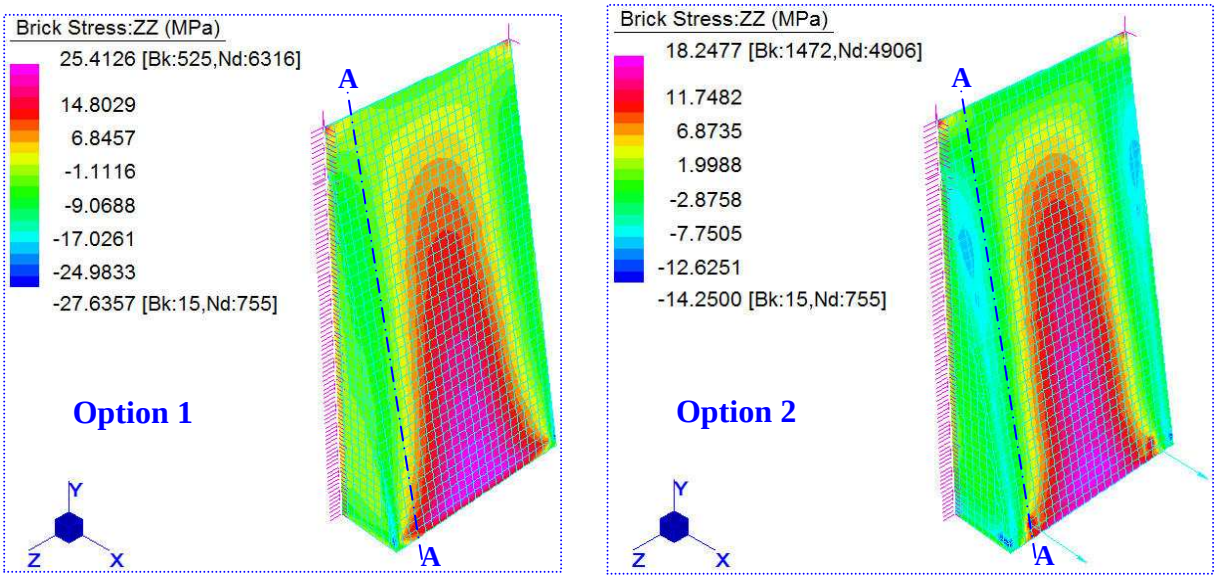

Figure 5.32: Comparison of the effect of confinement in the Z direction under the two options.

Figure 5.32 shows the stress distributed in the Z direction of the brick elements under the two options. The stresses that are distributed in the brick elements are quite similar under the two options. It can be seen from the side view that the compressive stress does not differ much along the surface. However, the stress in the Z direction reduces as one move further away from the triangular side plate as observed from the face view. The stress changes from a compressive stress near the triangular side plate to a tensile stress further away from the triangular side plate.

The equivalent tensile force in Option 2 contributes to the stress redistribution at the bottom of the hidden corbel (Figure 5.32). The face view of Option 2 indicates that the tensile stress in Z direction around the equivalent tensile force is larger compared to the elements close to the triangular side plate. From the face view, the magnitude of

stresses near the equivalent tensile force under Option 2 is approximately the same as those under Option 1. In order to observe the stress distribution along the equivalent forces, a section is cut out along A-A (Figure 5.32) to compare the confinement in the Z direction under the two options.

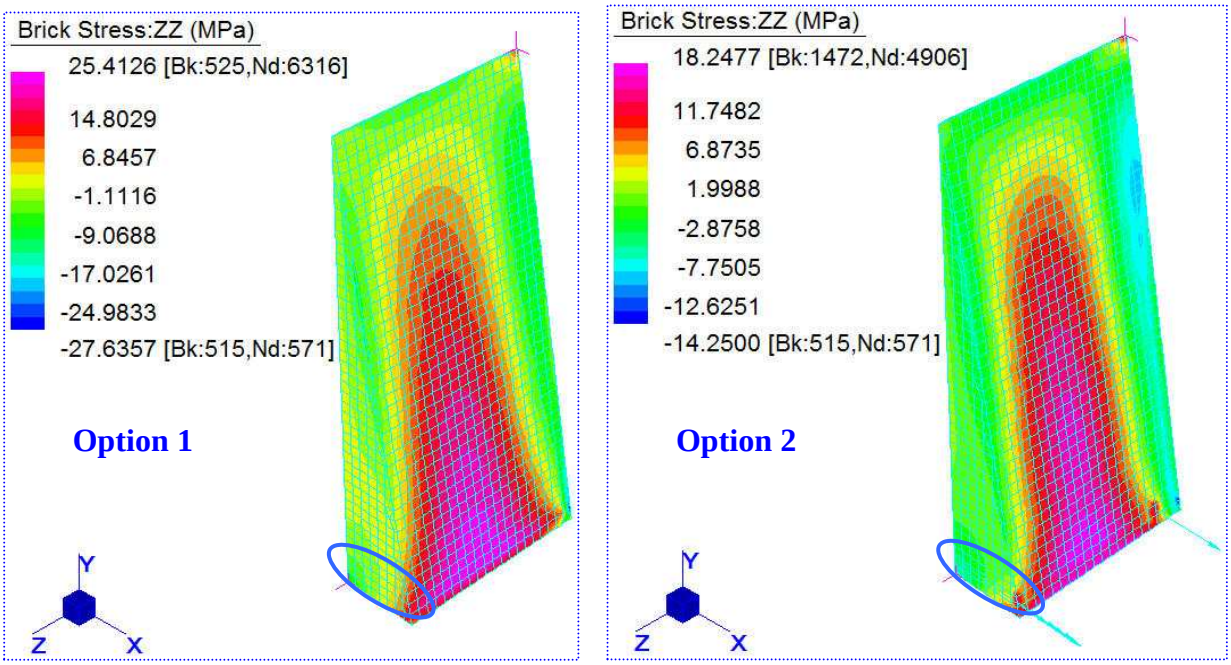

Figure 5.33: Comparison of the effect of confinement in the Z direction along Section A-A for the two options.

It can be seen from Figure 5.33 that the compressive stress in the Z direction in the circled block under Option 2 is larger than that under Option 1. As indicated in the circled block, the compressive stress in the Z direction is larger especially for those elements which are located close to the back plate of the hidden corbel.

By comparing the stress distribution from Figures 5.32 to 5.33, it is seen that the confinement stresses in the Z direction under Option 2 is better than those under Option 1. Based on the stress distribution under the two options, it can be concluded that the confinement is better closer to the triangular side plate than in the centre of the corbel. In addition, the confinement is better when the tensile stresses are transferred to concrete via tension reinforcement.

5.3.3.2.2 Comparing the confinement in the Y direction under the two options

Section 5.3.3.2.1 compared the confinement in the Z direction under the two options. Besides the Z direction, the confinement in the Y direction also assists to improve the bond stress. In order to compare the confinement caused by the bearing of the hidden corbel, the stress distribution in the Y direction is compared in Figures 5.34 to 5.35 under the two options.

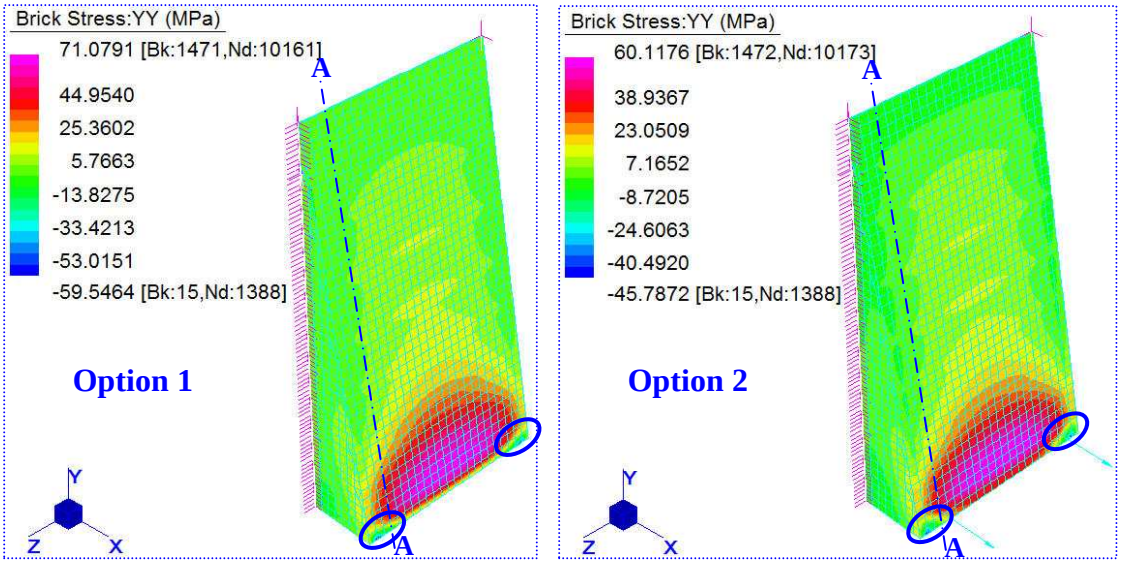

Figure 5.34: Comparison of the effect of confinement in the Y direction under the two options.

Figure 5.34 illustrates the stress distributed in the Y direction of the brick elements under the two options. It can be seen from the face view that the compressive stress in the circled blocks area under the two options is similar, but the magnitude of compressive stress under Option 2 is slightly larger than that of Option 1. The stresses in the circled blocks are in compression while the stresses in the middle zone of the bottom elements are in tension. From the face view, the area of compressive stress is relatively narrow and the stress reduces when it is further away from the circled blocks (Figure 5.34). From the side view, the stresses in the Y direction are nearly identical for those brick elements near the bottom of the hidden corbel. Similar to the confinement in the Z direction, a section that is cut out along A-A (Figure 5.34)

is used to compare the stress distribution in the Y direction along the equivalent forces.

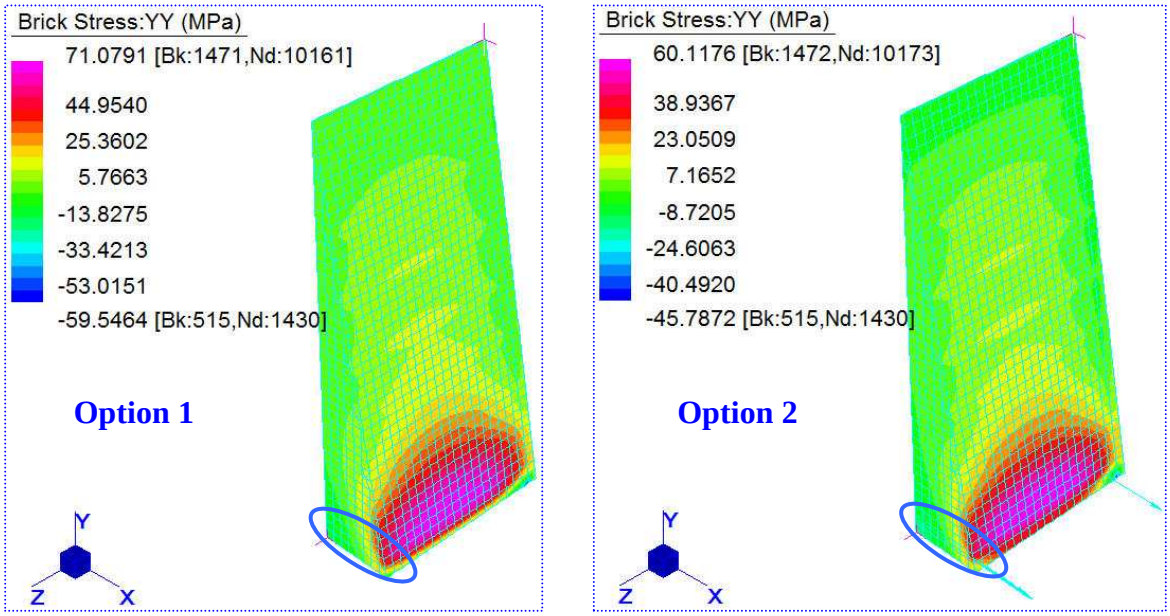

Figure 5.35: Comparison of the effect of confinement in the Y direction along Section A-A for the two options.

Unlike the stress distribution in the Z direction, the compressive stresses in the Y direction in the circled blocks under the two options are nearly identical (Figure 5.35). However, similar to the stress distribution in the Z direction, the compressive stresses in the Y direction are larger for those elements that are located nearer to the back plate of the hidden corbel.

By comparing the stress distribution from Figures 5.34 to 5.35, it is demonstrated that the confinement stresses in the Y direction under the two options are similar. Based on the stress distribution under the two options, it can be concluded that the confinement is better in the region close to the intersection between the triangular side plate and the bottom plate as indicated in the circled block in Figure 5.34.

5.3.3.3 Stress distribution inside the hidden corbel under the two options

Section 5.3.3.2 compared the stress distribution under the two options on the edge surface of the hidden corbel. In order to better understand how the tension zone develops inside the hidden corbel, four cross sections were cut to show the stress distribution in YY and ZZ directions. The locations of the sections are shown in Figure 5.36.

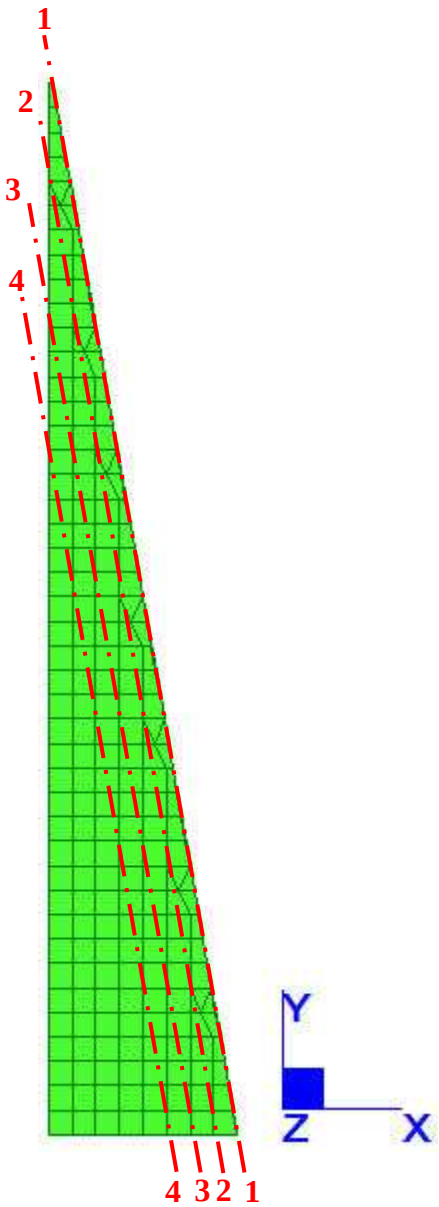

Figure 5.36: Defining layers from the side view of the 3D model.

The side view of the 3D model is shown in Figure 5.36. Layers 1-1 to 4-4 are parallel to each other with an equal distance of 12.5 mm for the adjacent layers. These layers are used to compare the effect of confinement for each layer.

5.3.3.3.1 Comparing the confinement in the Z direction for four layers under Option 1

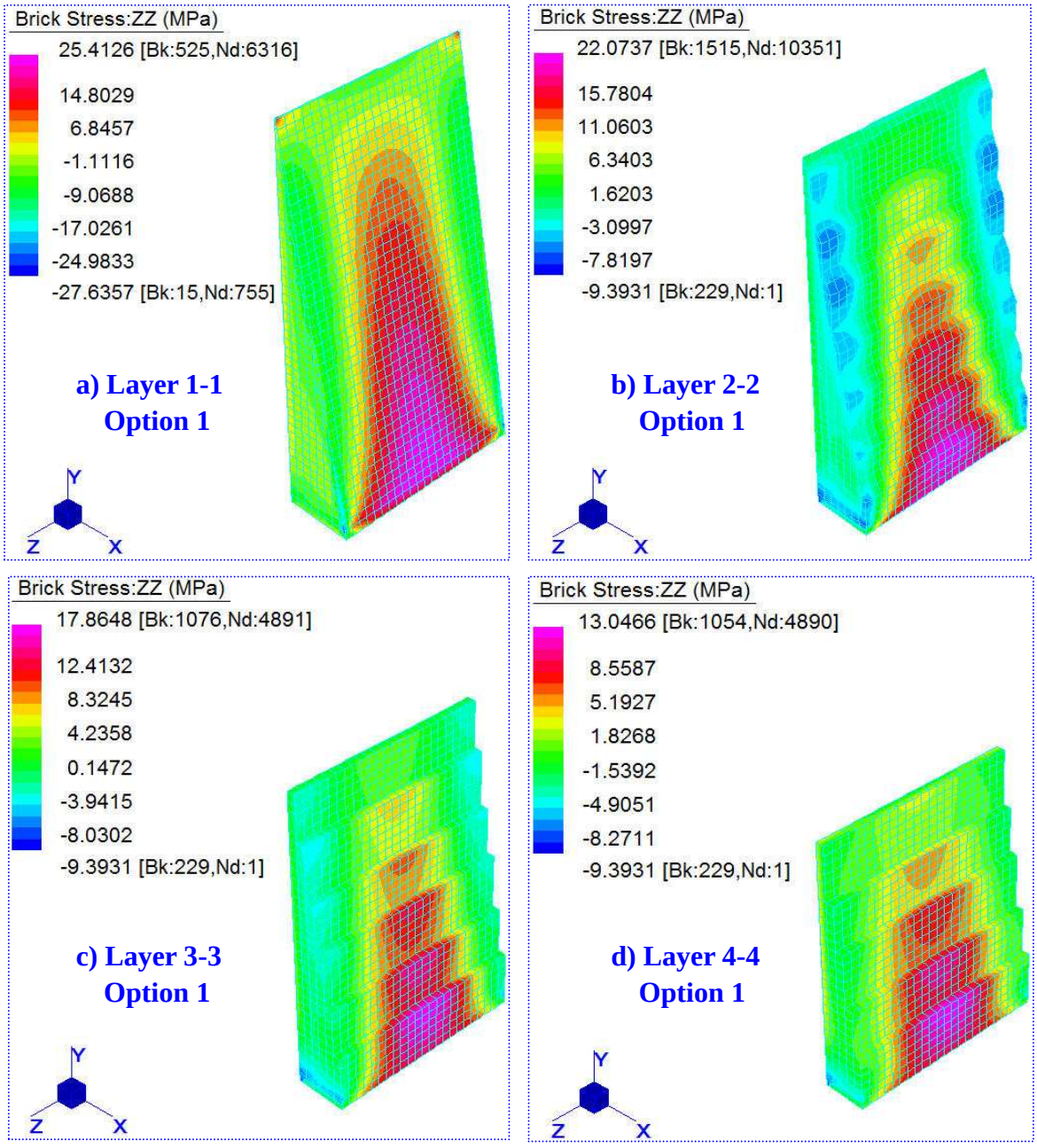

Figure 5.37: Isometric view of stress distribution in the Z direction for four layers under Option 1 (compression is (-)).

Figure 5.37 shows the isometric view of stress distribution in the Z direction under Option 1. It can be seen that the distribution of stresses in the Z direction are quite similar to each other from figures a) to d). The magnitude of tensile stress decreases from figures a) to d) while the area of compressive region increases correspondingly.

5.3.3.3.2 Comparing the confinement in the Y direction for four layers under Option 1

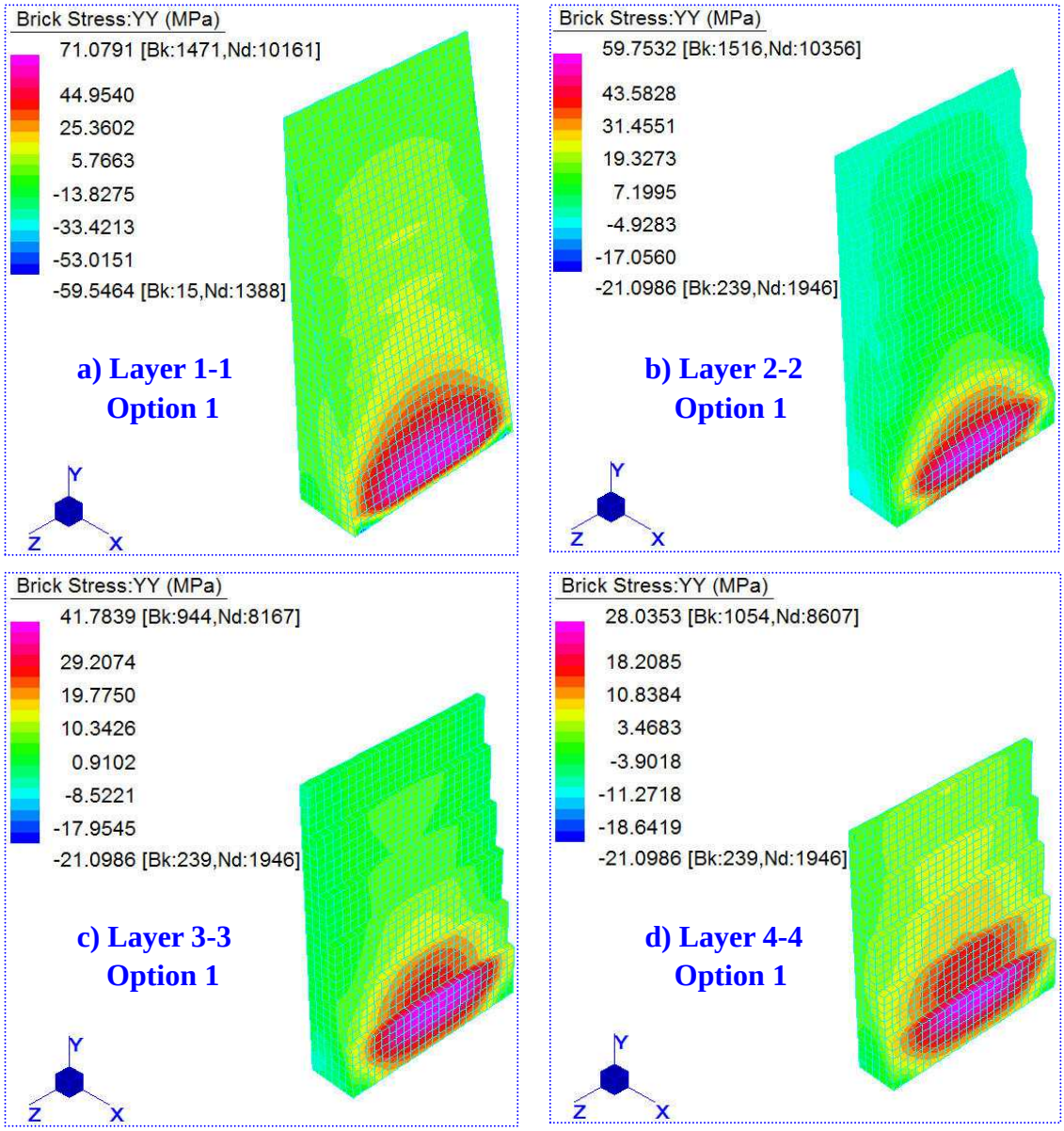

Figure 5.38: Isometric view of stress distribution in the Y direction for four layers under Option 1 (compression is (-)).

The isometric view of stress distribution in the Y direction under Option 1 is shown in

Figure 5.38. Similar to the stress distribution in the Z direction, the distribution of stresses in the Y direction are also quite similar for four layers. The magnitude of tensile stress decreases from figures a) to d) while the area of compressive region increases at the same time.

5.3.3.3.3 Comparing the confinement in the Z direction for four layers under Option 2

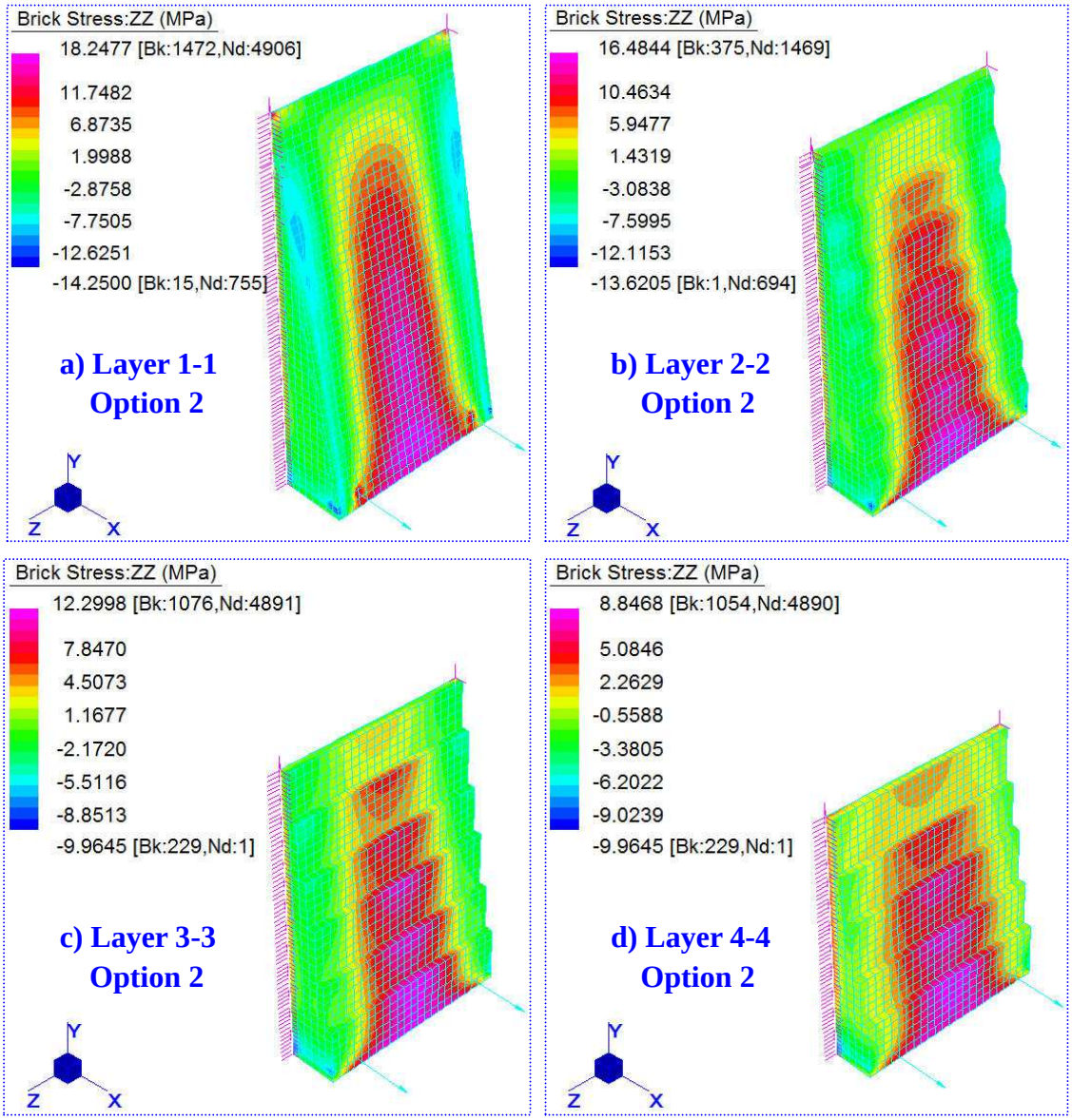

Figure 5.39: Isometric view of stress distribution in the Z direction for four layers under Option 2 (compression is (-)).

Figure 5.39 illustrates the isometric view of stress distribution in the Z direction under Option 2. Similar to the stress distribution under Option 1, the distribution of stresses

in the Z direction are also quite similar to each other from figures a) to d). The magnitude of tensile stress decreases from figures a) to d) while the area of compressive region increases correspondingly.

5.3.3.3.4 Comparing the confinement in the Y direction for four layers under Option 2

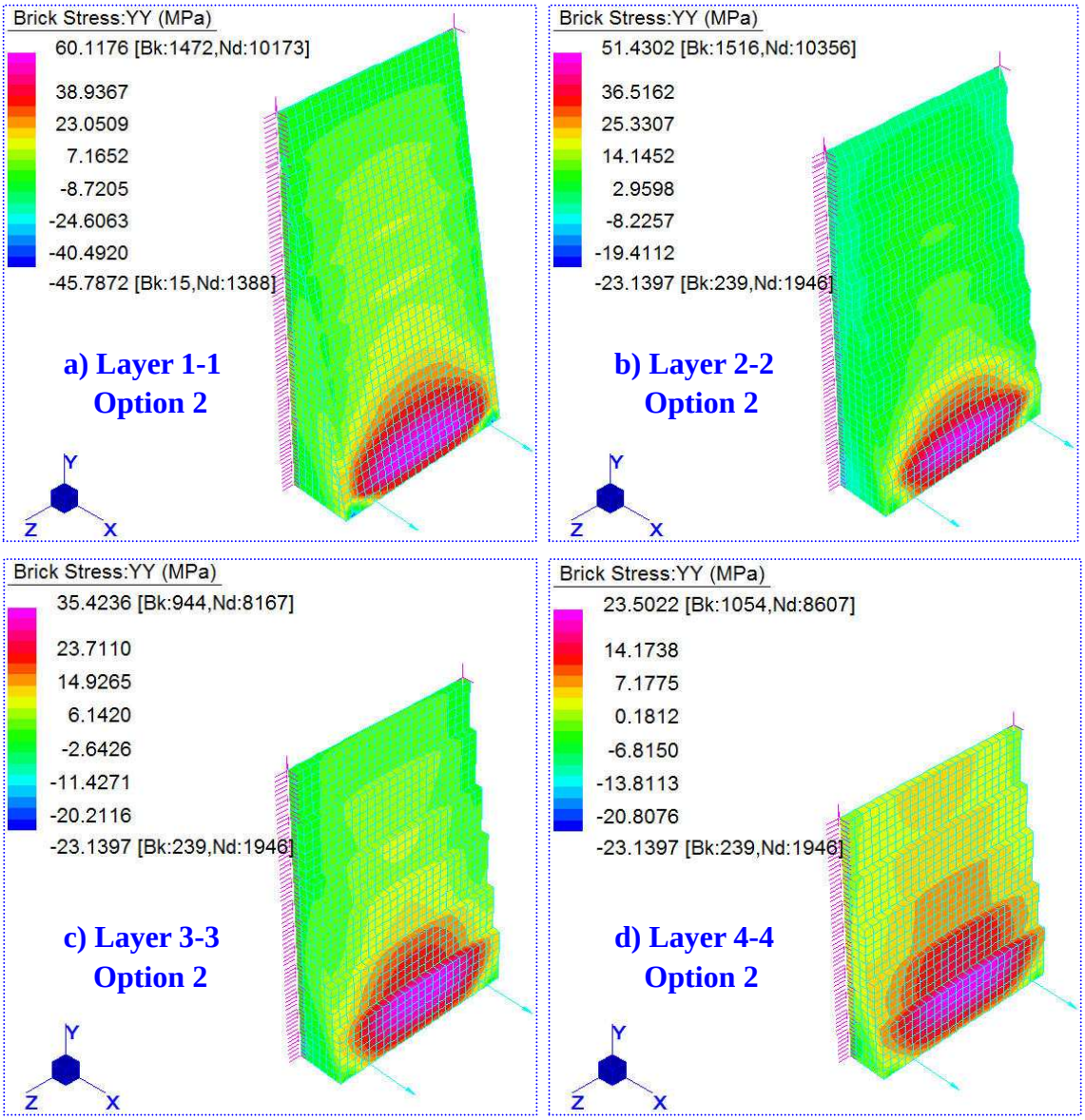

Figure 5.40: Isometric view of stress distribution in the Y direction for four layers under Option 2 (compression is (-)).

The isometric view of stress distribution in the Y direction under Option 2 is shown in Figure 5.40. Similar to the stress distribution in the Z direction, the distribution of

stresses in the Y direction are also quite similar for four layers. The magnitude of tensile stress decreases from figures a) to d) while the area of compressive region increases at the same time.

For the confinement in the Z direction, it can be seen from Figures 5.37 and 5.39 that the confinement region is larger for the elements close to the back plate of the hidden corbel. However, the magnitude of compressive stresses in the Z direction reduces as the location moves away from the back or side plates which indicate a potential reduction of the bond stress. The reduction of the compressive stresses is caused by the stiffness of the corbel.

Figure 5.2 shows the stress distribution in the support region and indicates that the magnitude of stresses reduces as the location moves further away from the face of the support. The increased area of compressive stress (Figures 5.37 to 5.40) indicates that a better confinement is provided for the elements close to the back plate of the hidden corbel. Also, the reduction of the reaction stresses leads to a reduction of the stresses in the Z direction, which in turn reduces the bond stress.

Similar to the confinement in the Z direction, Figures 5.38 and 5.39 indicate that the area of confinement increases with the elements closer to the back plate of the hidden corbel while the magnitude of the compressive stresses in the Y direction reduces correspondingly.

There is not a significant difference in the stress patterns as obtained from the two analysis options. The general trend is therefore established. The area of confinement that is in favour of the bond stress is located only close to the back and side plates. Only bars located approximately within 30mm from the side plates will be subjected to an increased bond stress.

5.4 Summary and conclusions

This chapter analyzed and verified the 2D FE model. By comparing the model with hand calculations, the 2D FE model provides a good representation of the stress distribution in the connection zone.

In order to provide the same loading conditions in a 3D model as in a 2D model, loads obtained from the 2D model were applied to the 3D model. By comparing the different thicknesses of triangular side plate, it is concluded that a thicknesses of more than 10 mm does not affect the confinement of concrete in the corbel zone.

By comparing the stress distribution results for the two options in the tension zone of the 3D model, the following conclusions were drawn:

- The concrete nearer to the triangular side plate are more confined, which can improve the bond stress in this region.
- The concrete nearer to the intersection of the triangular side plate and the bottom plate are more confined, which will improve the bond stress in this region.
- It is therefore important that tensile reinforcement be located in this region to benefit from any improved bond stress.

The next chapter analyzes the anchorage length and further verifies whether the anchorage length can be reduced through a laboratory experiment.

CHAPTER 6

COMPARISON BETWEEN EXPERIMENTAL AND NUMERICAL RESULTS

6.1 Introduction

Chapter 5 presented the FE modelling and verified the FE results with theoretical calculations. The tensile force at the bottom of the beam was calculated based on the 2D FE model.

In this chapter, the end anchorage length of tension reinforcement was investigated as calculated from the FE results and from the different design codes. A laboratory experiment was then setup to further verify if the end anchorage length of reinforcement bars for simply supported beams can be reduced from the specification of SABS 0100-1 (2000).

6.2 Comparing the end anchorage length between the FE results and the different design codes

The tensile force at each cross section along the beam can be calculated according to equation 2.5 and the corresponding anchorage length can be calculated through equation 2.6. Based on the conditions and dimensions in Appendix A and on the results of the FE modelling, the anchorage length of the tension reinforcement was calculated and then compared between the FE results, Eurocode 2 (2004), and SABS 0100-1 (2000).

Two alternative support conditions were investigated for the support conditions. The *first condition* is that there is a stress concentration near the face of support as

indicated in Figure 5.1. The *second condition* is that the stress is distributed along the support as shown in Figure 5.2. The anchorage length of tension reinforcement for the FE result is only compared with the design codes under the second condition because the FE results are based on the stress distribution under the second condition. By assuming the bond stress to be 2.9 MPa, which comes from SABS 0100-1 (2000), the anchorage length is compared assuming the two conditions.

6.2.1 Comparing the end anchorage length between Eurocode 2 (2004) and SABS 0100-1 (2000) under the first condition (rigid support)

The hidden corbel is 100 mm long and the beam is symmetric, therefore, the required anchorage length calculated at different positions along the beam is plotted from the face of the support to the centre of the beam as shown in Figure 6.1:

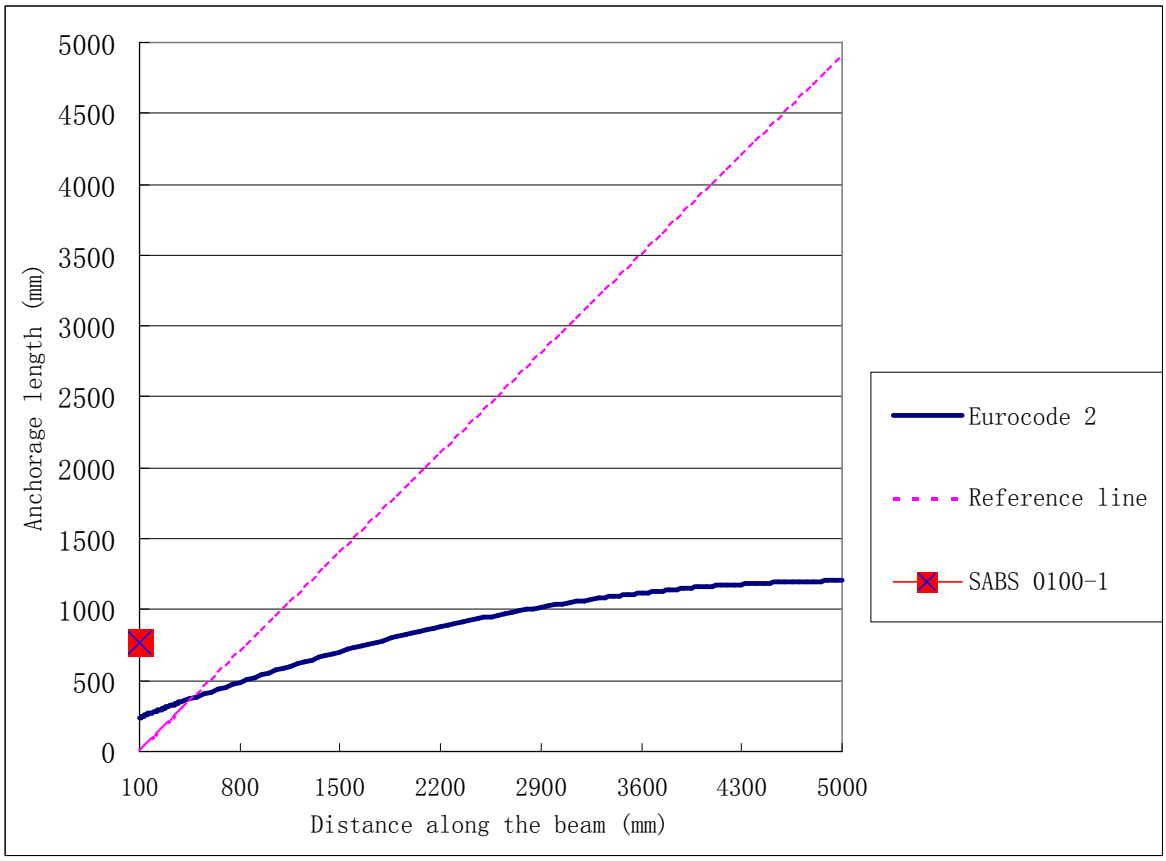

Figure 6.1: Required end anchorage length based on Eurocode 2 (2004) and on SABS 0100-1 (2000) assuming the rigid support. (first alternative)

As indicated in Figure 6.1, the anchorage length specified in SABS 0100-1 (2000) for the end support and introduced in Section 1.1, is much larger than that of Eurocode 2 (2004).

The dashed line in Figure 6.1 is the reference line which means the values for the X and Y coordinates are identical. Therefore, if the requirement line is located below the dotted line, it means that sufficient anchorage length is available between the specific location and the end of the beam.

6.2.2 Comparing the tensile force between the model results, Eurocode 2 (2004), and SABS 0100-1 (2000) assuming the second condition (soft support)

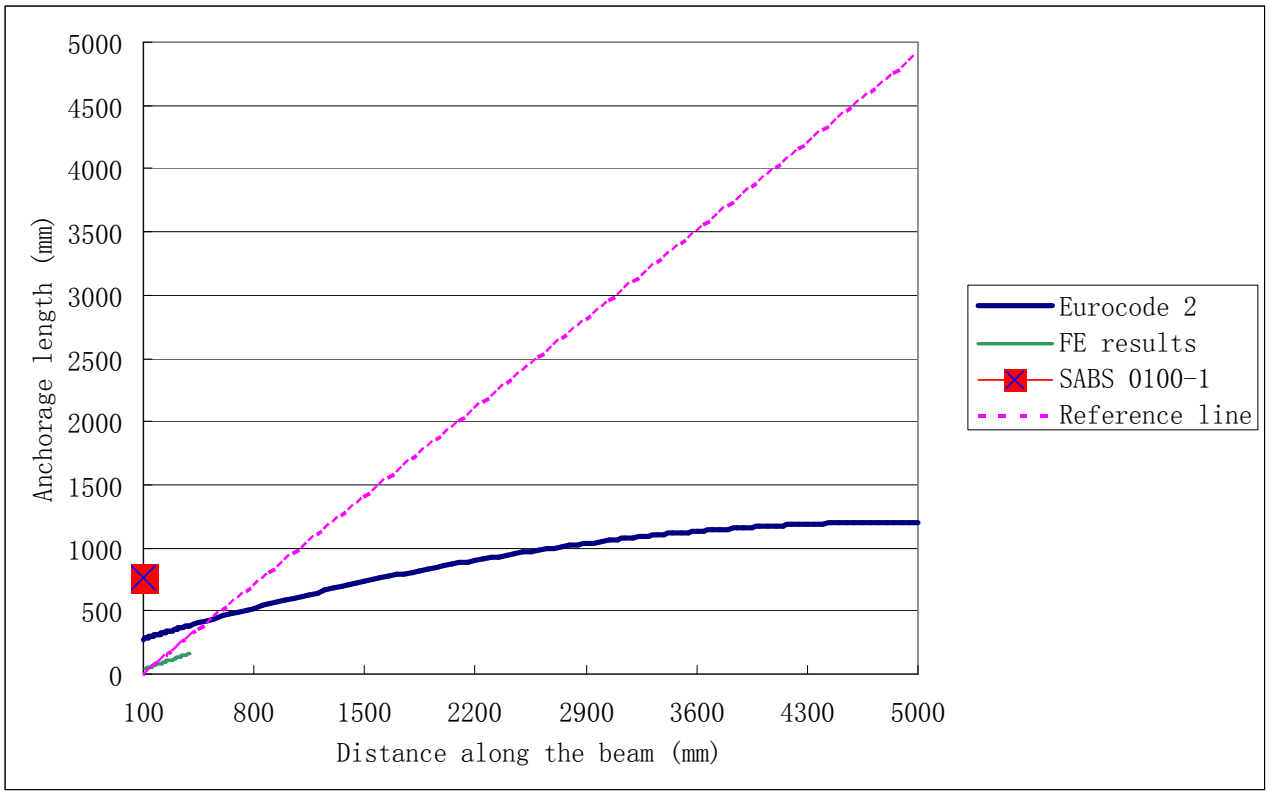

Figure 6.2: Required end anchorage length based on the model results, Eurocode 2 (2004) and on SABS 0100-1 (2000) assuming a flexible support. (second alternative)

It can be seen from Figure 6.2 that the anchorage length based on the Eurocode 2 (2004) and on the SABS 0100-1 (2000) are similar to that of Figure 6.1. However, the

anchorage length from the model results is much smaller than that of the Eurocode 2 (2004) and the SABS 0100-1 (2000). In order to compare the end anchorage length based on the Eurocode 2 for the two conditions, the end anchorage length with a distance from 100 mm to 800 mm along the end of the beam was plotted in Figure 6.3.

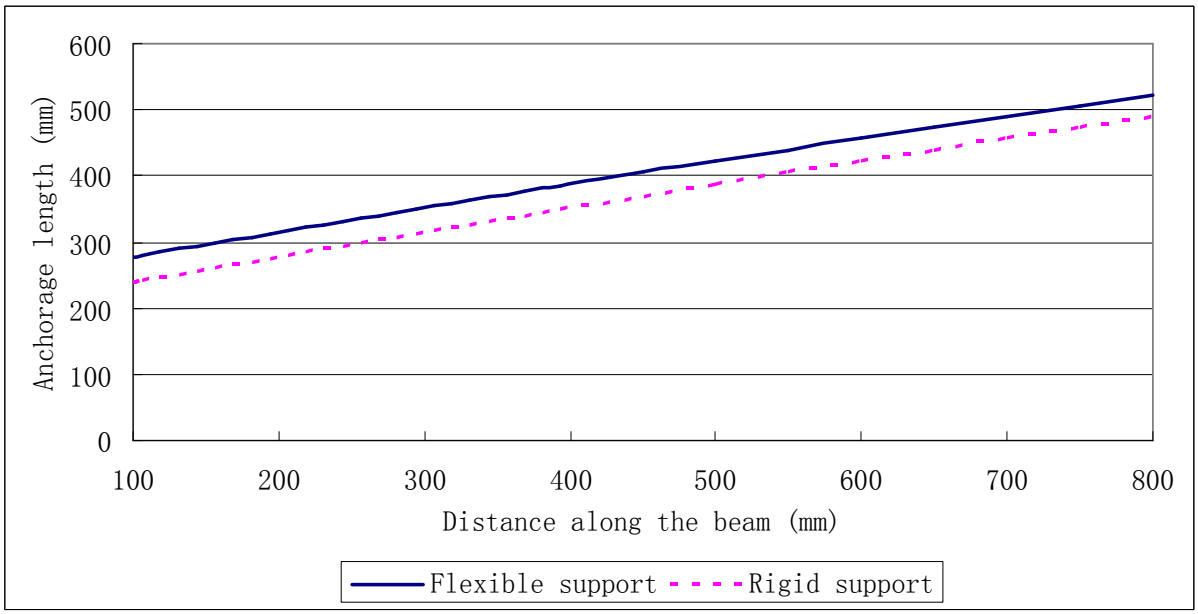

Figure 6.3: Comparing the required end anchorage length based on the Eurocode 2 for the two conditions (rigid support and flexible support).

The required end anchorage length for the tension reinforcement is slightly longer for the flexible than for the rigid condition (Figure 6.3). This is because the lever arm of the bending moment resulting from the support reaction in the second condition (flexible support) is longer, which is explained in Section 6.3.4 and shown in Figure 6.22.

For the modified hidden corbel connection, the anchorage length is required for Stage Ⅰ (installation stage) as indicated in Section 2.6.1, which is only required temporarily during the erection stage. This characteristic makes that the modified HCC is only slightly affected by the long term effects such as creep and shrinkage. Because the modified HCC do not need to consider the long term effects, it is reasonable that the required end anchorage length of tension reinforcement obtained from the FE results

would be smaller than that of the design codes.

In order to verify if the anchorage length can be shortened from code specifications, a laboratory experiment was set up with different types of support conditions and with different anchorage lengths for the tension reinforcement after the critical section.

6.3 Comparing the end anchorage length using a laboratory experiment

The standardized formwork in the laboratory of Stellenbosch University can provide at most 4 beams at the same time. In order to conduct the experiment under the same conditions, 4 specimens were cast. Each specimen includes a beam with two ends, therefore, four specimens can provide eight results for further comparison.

In order to control the concrete strength, a trial mix was executed. After curing for 7 days, the concrete strength was tested to ensure that the design strength of 30 MPa is reached. A simplified pull out test is then used to obtain the value of bond stress.

Based on the size of the beam, the bending moment and shear force for a certain cross section could be calculated. In order to compare the end anchorage length of tension reinforcement, the anchorage length was calculated according to equation 2.5. An anchorage length of 23 mm is calculated based on the tension forces obtained in the FE results. With the anchorage length of 23 mm, four types of beams with different support conditions and required end anchorage lengths were designed for the laboratory test. The laboratory setup for the beam test is shown in Figure 6.4.

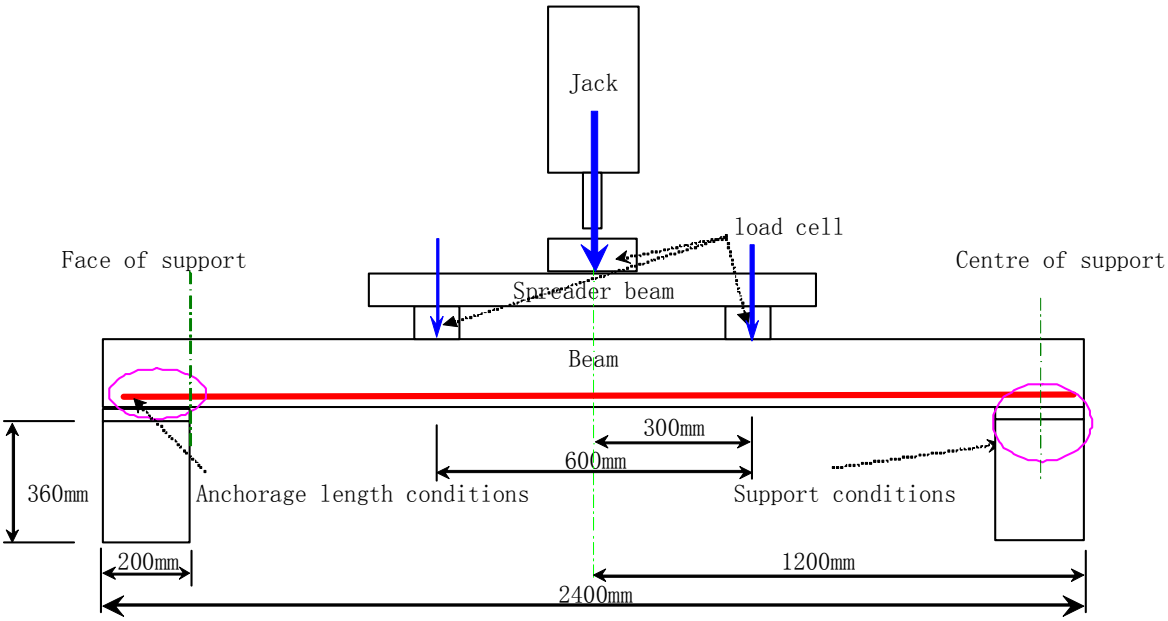

Figure 6.4: Sketch for the experiment setup and beam conditions.

As indicated in Figure 6.4, the force is transferred from the jack to the spreader beam and then transferred to the beam as two concentrated loads. The support conditions can be changed by the position of the rubber pad. The anchorage length of tension reinforcement was compared by extending different anchorage lengths after the face of the support or the centre of the support.

6.3.1 The concrete trial mix

The concrete trial mix was designed according to Addis (2005: 109) and the data is listed in Appendix E. The water to cement ratio was taken as 0.55 with a target concrete strength of 43 MPa after 28 days. According to the previous records of concrete mixes at Stellenbosch University, the strength of the concrete can reach 70% of the strength at 28 days after 7 days. Therefore, the concrete was supposed to reach 30.1 MPa after 7 days.

A total of 21 l of concrete trial mix was made. The slump test had a value of 60, which met the casting requirement. A total of 6 cubes with dimensions of 150×150×150 mm

were cast. Three of the concrete cubes were used to test the strength and three were used for pull out tests.

6.3.1.1 Concrete strength testing results

The results of concrete cube strength are shown in tables 6.1.

Table 6.1: Concrete cube strength.

Cube number	Force (kN)	Revising factor	True dimensions		Strength (MPa)
			width (mm)	height (mm)	
1	705	0.995	151	145	32.0
2	724	0.995	151	145	32.9
3	722	0.995	151	145	32.8
Average strength (MPa)					32.6

6.3.1.2 Bond stress testing equipment and results

The pull out tests were performed on the Zwick machine, which has a capacity of 250 kN (Figure 6.5).

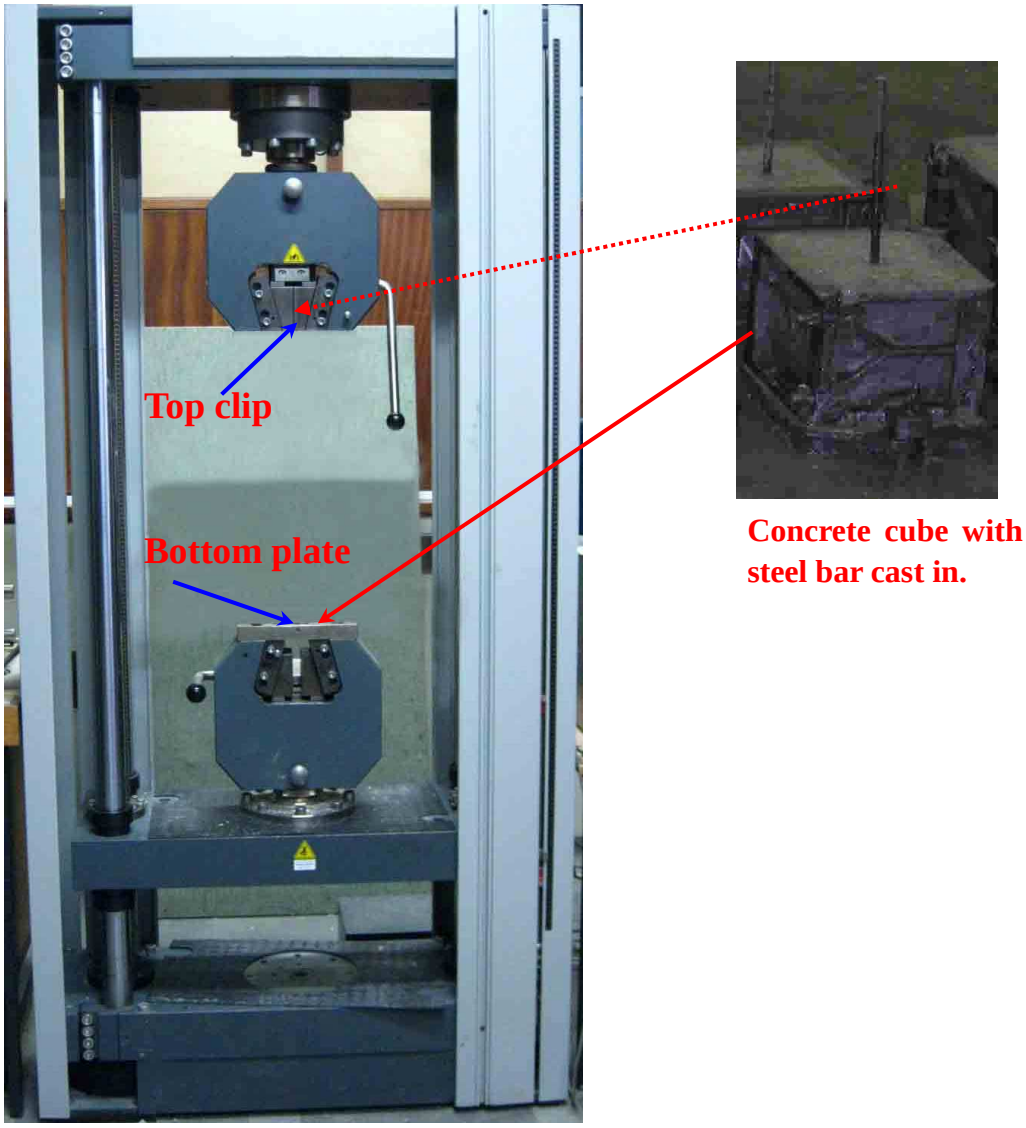

Figure 6.5: The Zwick machine and testing methods pull out test.

As demonstrated in Figure 6.5, the concrete cube with cast-in steel bar was placed on the bottom plate of the Zwick machine as indicated in the arrow. The top of the cube was covered with a thick steel plate with a hole to allow the reinforcement to protrude. The thick steel plate was fixed to the bottom plate of the Zwick machine with bolts and nuts. Between the top of the cube and the thick steel plate, a rubber pad is used to avoid eccentricity and to reduce the effect of Poisson's ratio, which can create confinement and stresses around the reinforcement bar. The steel bar outside the cube was clipped to the top clip of the Zwick machine as indicated by the dotted arrow.

ASTM (2003: 515) specifies that after the test is started, failure should occur after 3 minutes. The first pull-out test failed at a low force value because the loading rate was too high and under force control. The loading rate was then adjusted and set up to 1 mm/min to meet the specifications of the test. The results of the bond stress of the concrete trial mix are shown in table 6.2.

Table 6.2: Bond stress for the concrete trial mix.

Cube number	F_{max} (kN)	Bonding length (mm)	Bond stress (MPa)
4	fail	136	None
5	22.9	150	3.2
6	22.9	145	3.4
Average bond stress (MPa)			3.3

As indicated in table 6.2, the bond stress was calculated according to the following formula derived from equation 2.6. The factor of 1.5 in equation 6.1 is the concrete material factor for design in the ultimate limit state.

$$f_b = \frac{F}{\pi \cdot \phi \cdot l_b} / 1.5 \qquad (6.1)$$

From the results of the concrete trial mix, the allowable bond stress is approximately 3.3 MPa for the concrete strength of 32.6 MPa. These results are quite similar to the value that is given in table 24 of SABS 0100-1 (2000) (A bond stress of 2.9 MPa for the concrete strength of 30 MPa).

6.3.2 Preparing for the laboratory experiment

Before the experiment was conducted, several procedures were executed. First, the layout of the reinforcement and stirrups were calculated. Second, the end anchorage length for tensile reinforcement was calculated and then four types of beam conditions

were chosen for comparison. Third, reinforcement was ordered and then the reinforcing cages were fixed. Fourth, the experimental setup was prepared in the laboratory and finally, the concrete was mixed and four beams were cast.

6.3.2.1 Beam dimensions and reinforcement layout

Based on the formwork available in the laboratory, beam dimensions with 200 mm wide, 280 mm high and 2400 mm long were used. The detailed calculations are shown in Appendix F. The bottom tension reinforcement is selected as reinforcement bars 2-Y-20 and 2-Y-10.

Bangash (2003: 66) showed that the detailing of reinforced concrete beams between BS 8110 (1997), Eurocode 2, and the American design code (ACI) are not the same. By comparing the curtailment of bars in beams, 50% of reinforcement that extends into the support is a requirement only by BS 8110 (1997). A tensile force exists and it must be anchored.

6.3.2.2 Determining the anchorage length for four types of beams

From the FE results, the tensile force calculated at the face of the support is approximately the same as when the angle θ in equation 2.4 from Eurocode 2 (2004) is equal to 68 degrees. Therefore, an anchorage length of 23 mm after the face of support was calculated for a bond stress of 3 MPa and a load of 62 kN from the jack (Appendix F).

In order to compare different anchorage lengths for the tension reinforcement, four types of beam conditions were chosen as shown in Appendix G. The beams were numbered and the corresponding conditions were as follows:

***Beam 1*:** The calculated anchorage length after the face of the support with a rigid support.

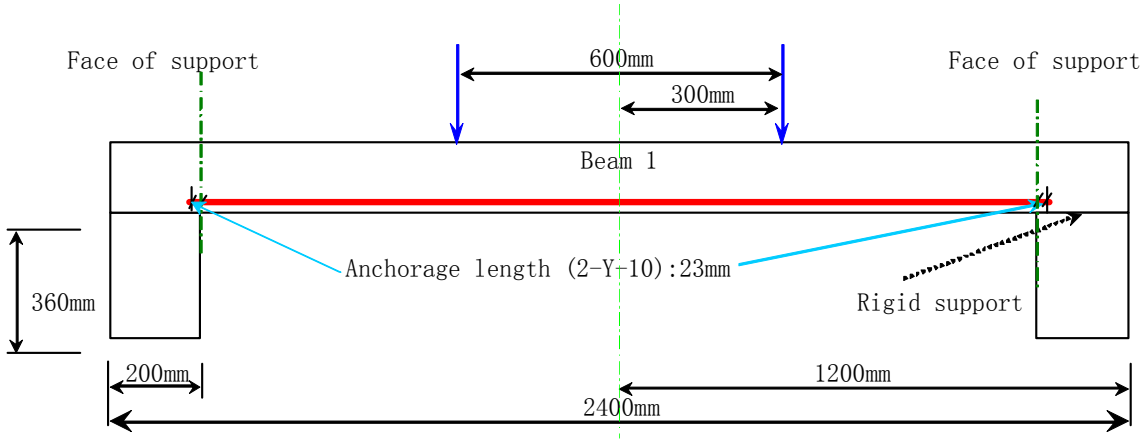

Figure 6.6: Sketch for end anchorage length of tension reinforcement and support conditions for beam 1.

As indicated in Figure 6.6, 2-Y-10 reinforcement bars extend 23 mm after the face of the support on each end of the beam. For the support conditions, beam 1 is directly laid on the concrete support that simulates a rigid support.

***Beam 2*:** The calculated anchorage length after the face of the support using a rubber pad as support.

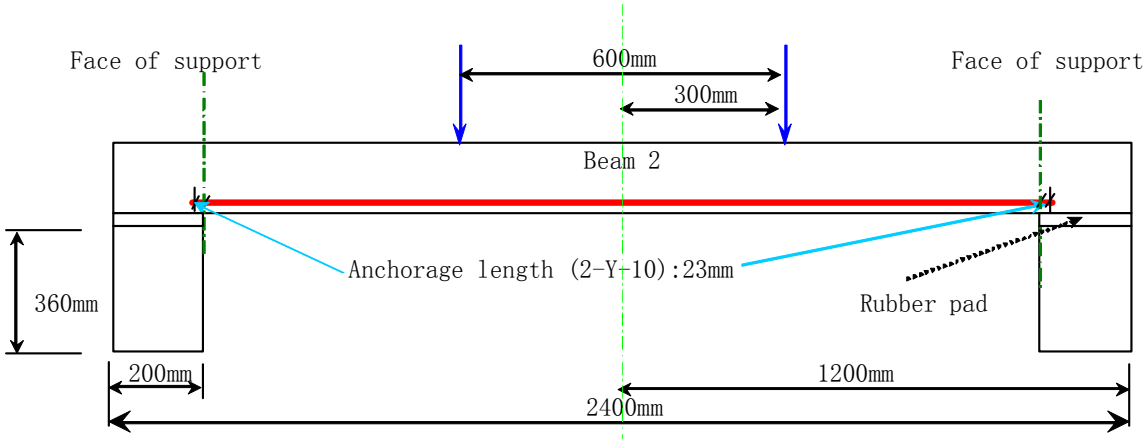

Figure 6.7: Sketch for end anchorage length of tension reinforcement and support conditions for beam 2.

As indicated in Figure 6.7, 2-Y-10 reinforcement bars extend 23 mm after the face of

the support on each end of the beam. A rubber pad is used on each end of the beam as support conditions between beam 2 and the concrete support.

***Beam 3*:** The calculated anchorage length after the centre of the support using a rubber pad as support.

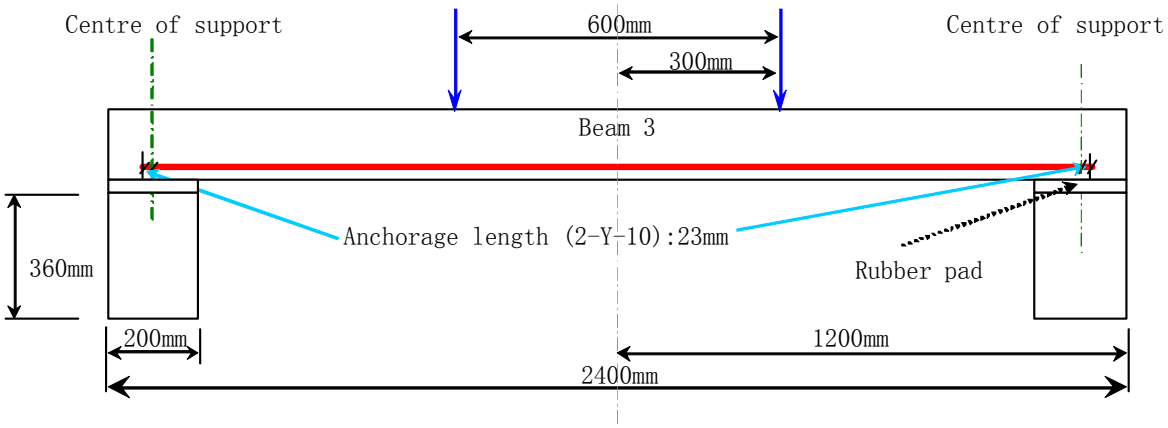

Figure 6.8: Sketch for end anchorage length of tension reinforcement and support conditions for beam 3.

As indicated in Figure 6.8, 2-Y-10 reinforcement bars extend 23 mm after the centre of the support on each end of the beam. A rubber pad is used on each end of the beam as support conditions between beam 3 and the concrete support.

***Beam 4*:** The anchorage length of 12 times bar diameter after the centre of the support with a rubber pad.

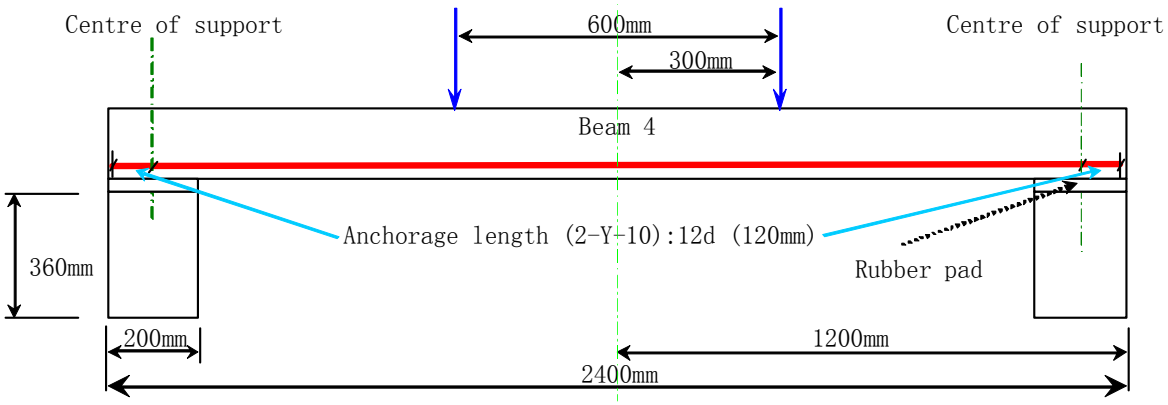

Figure 6.9: Sketch for end anchorage length of tension reinforcement and support conditions for beam 4.

As indicated in Figure 6.9, 2-Y-10 reinforcement bars extend 120 mm (12 times diameter of Y-10) after the centre of the support on each end of the beam. A rubber pad is used on each end of the beam as support conditions between beam 4 and the concrete support.

The type of rubber pad used for the laboratory experiment is reinforced rubber. In order to match the dimension of the hidden corbel as designed in Appendix A, a 200 mm wide and 100 mm length rubber pad was used. In order to determine whether the rubber pad can be used in order to avoid either a too stiff support or a too soft support, a test was conducted. A stiffness of 15333 N/mm for a 100 mm $\times$ 100 mm rubber was obtained through the test. Then a FE model was conducted and proved that under the load range between 30 kN to 300 kN, the beam end was in full contact with the rubber pad without lifting at the end of the beam.

6.3.2.3 Ordering reinforcement and binding the reinforcing cages

The reinforcement and stirrups were ordered from Winelands Reinforcing Ltd in South Africa. The reinforcing cages were then fixed according to the calculation from Section 6.3.2.2. The detailed information on the layout of beams and test conditions are listed in Appendix G.

Figure 6.10: Reinforcing cages in the formwork.

Figure 6.10 shows the reinforcing cage inside the formwork. The circled block shows a wire protruding from the beam. The wire is located in the middle of the beam, which enabled the location of the tension reinforcement at the support to be determined after the beam is cast. This allowed the loads on the beam to be positioned as symmetric as possible when putting the pre-cast beam on the support. In addition, knowing exactly the layouts of reinforcement will also help to analyze the mechanisms after the test.

6.3.2.4 Preparing experimental setup in the laboratory

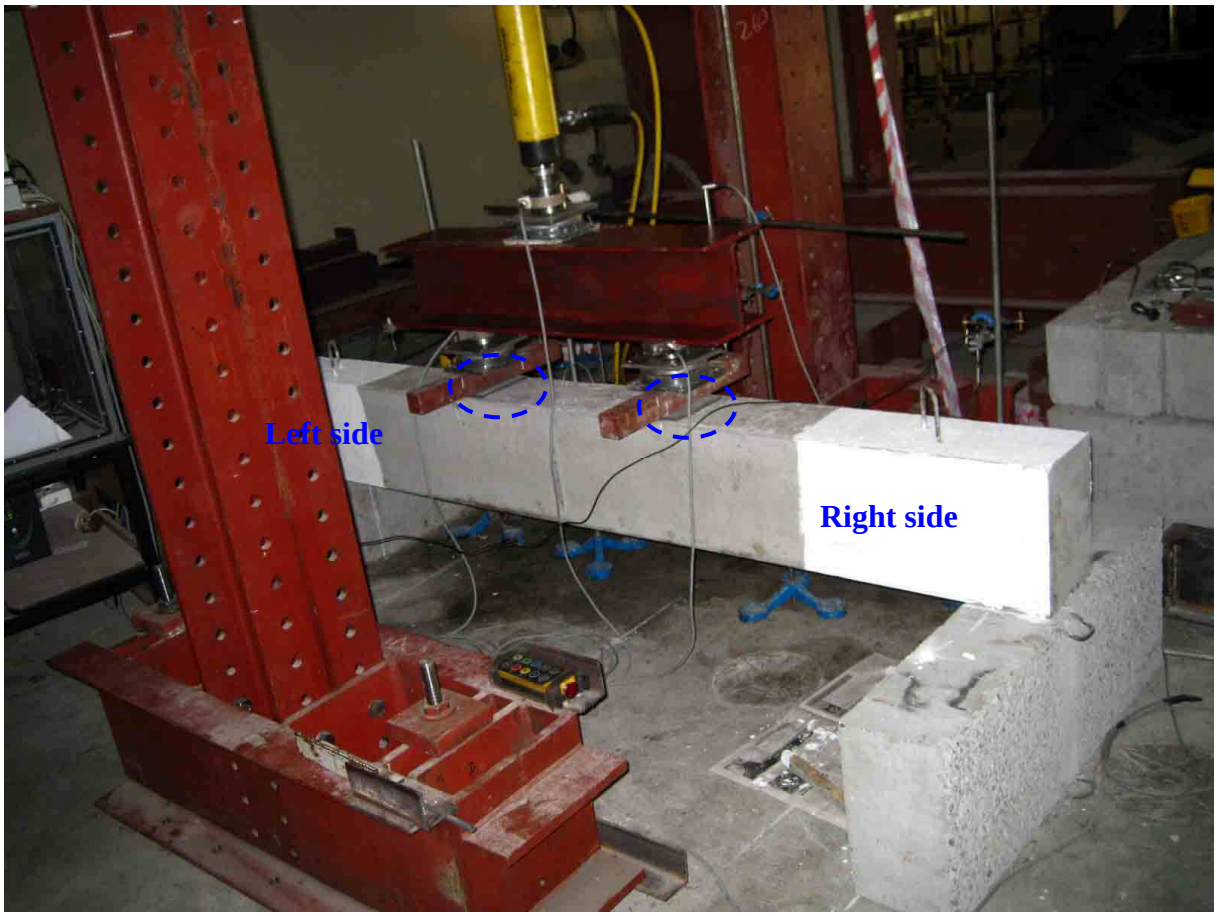

Figure 6.11: Experimental setup in the laboratory.

The test arrangement in the laboratory is shown in Figure 6.11. The jack was fixed to the steel frame and the load was transferred from the jack to the beam through a spreader beam. A total of three load cells were used. One load cell was located

between the spreader beam and the jack to obtain the force from the jack. The other two load cells were located between the spreader beam and the concrete beam to obtain the loads on the beam. In order to prevent the crushing of concrete caused by the force as indicated in the dashed circle, two rubber pads were placed. Because this test does not focus on deflections, the rubber pads did not affect the results. Four LVDTs were used at the beam ends and at the location of the dashed circle (Figure 6.11). With the relative displacement between the beam end and the location where loads were applied, the applied load can be plotted as a force displacement relationship. The four point bending moment in Figure 6.11 has the advantage of reducing the maximum bending moment.

6.3.2.5 Mixing the concrete and casting the beam

The concrete was cast into 4 beams together with 18 concrete cubes. Twelve of these concrete cubes were used to test the concrete strength. Six of these concrete cubes with cast-in steel bars were used to test the bond stress. The concrete beams and cubes were then covered with wet blankets for curing.

6.3.3 Analyzing the mechanisms of the laboratory experiment

Before testing the beams, compression tests were performed to obtain the concrete cube strength and pull out tests were executed to obtain the bond stress. As indicated in Appendix I, the average concrete cube strength was 29 MPa and the average bond stress was 5.1 MPa. Because the value bond stress increases from 2.9 MPa to 5.1 MPa, the corresponding applied load from the jack is then increased from 60 kN to 108 kN in order to provide the same calculated end anchorage length of tension reinforcement that extends after the face of the support. The test was started by setting up the support with a 23 mm anchorage length of tension reinforcement.

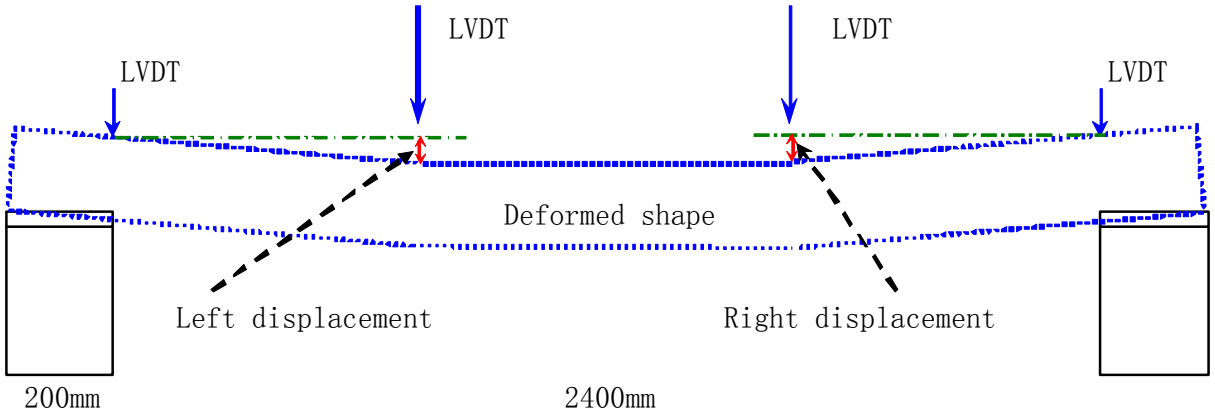

Figure 6.12: Sketch for the displacement of the beam.

As shown in Figure 6.12, the dotted line indicates the deformed beam shape after the load was applied. Four LVDTs can measure the relative displacement on each side of the beam. The data can then be plotted the force displacement relationship on each side of the beam. In addition, the total force displacement relationship can also be plotted. Here, the total force is the force from the jack and the corresponding displacement is the mean value of the left displacement and the right displacement (Figure 6.12).

6.3.3.1 Testing beam 1

Beam 1 has 23 mm of anchorage length of tension reinforcement after the face of the rigid support. Beam 1 failed in bond on the right side of the beam with the ultimate load approximately equals to 288 kN. Figure 6.13 shows the total force-displacement curve of the beam.

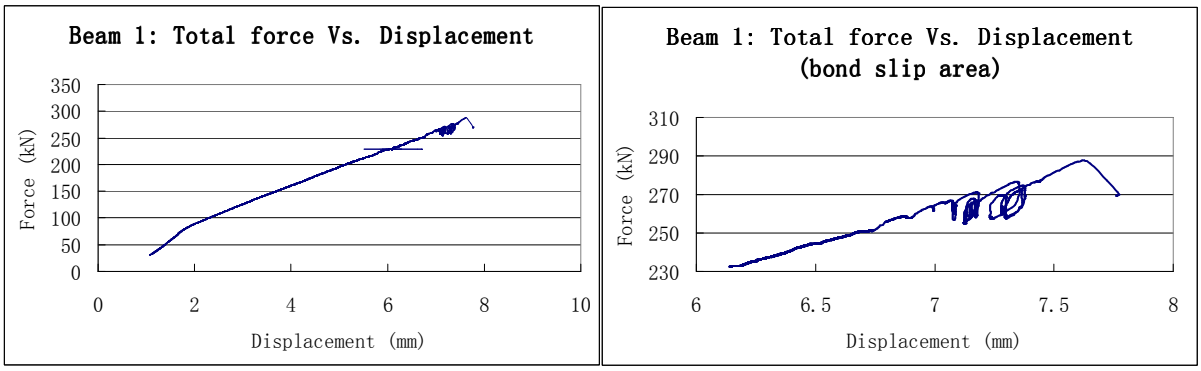

a) Total view b) Closer view of bond slip area

Figure 6.13: Total force-displacement curve for beam 1.

It can be seen from Figure 6.13 that the force-displacement curve becomes helically when the applied load reaches approximately 270 kN, which indicates a bond slip mechanism in the beam. In order to compare the force on each side of the beam, the force-displacement curve on the bond slip area for each side was plotted.

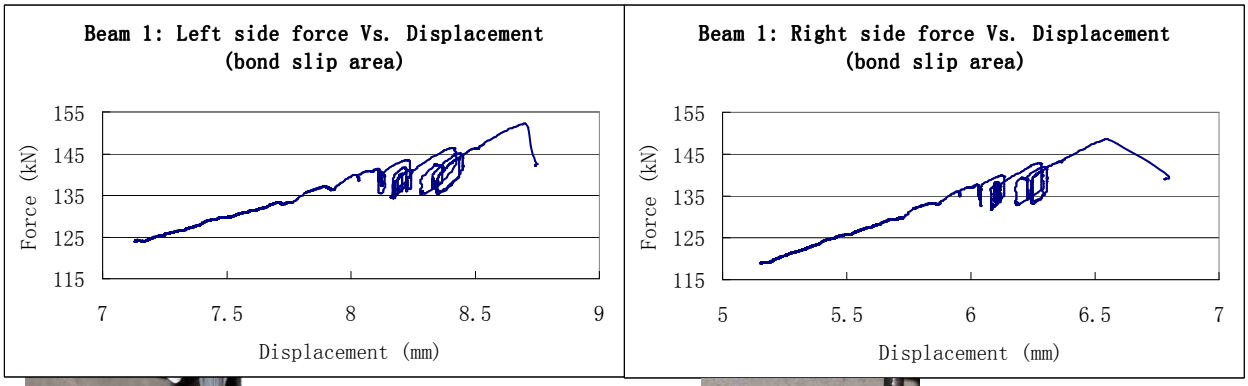

Plan view of bottom reinforcement at left support

Plan view of bottom reinforcement at right support

Figure 6.14: Force-displacement curve for each side of beam 1.

The bottom part of Figure 6.14 shows the reinforcement conditions at the beam end corresponding to each side of the beam. Figure 6.14 also demonstrates that the shear force on the right side of the beam is smaller than on the left side. However, the bond failure occurs earlier on the right than on the left side (Figure 6.14). This is because the end of the reinforcement bars on the left end was slightly bent (unintentionally)

and this increased the bond capacity.

The helical curve demonstrated the bond slip behaviour between the tension reinforcement and the surrounding concrete. Due to the slip, the reinforcement pulled out slightly which resulted in the reduction of the load. At the same time, the relative displacement between the beam end and the adjacent dashed circle (Figure 6.11) remained the same. However, with an increase of the load, the reaction force increased, which in turn increased the lateral pressure on the reinforcement bars over the support with a resulting improvement of the bond stress. Therefore, the bonding force resisted the tensile force after the initial slip. After that, with an increase of the tensile force, the bonding force can not resist the tensile force and the slip starts again. After several repetition of this bond slip mechanism, the bonding force could not resist the tensile force any longer and the beam failed.

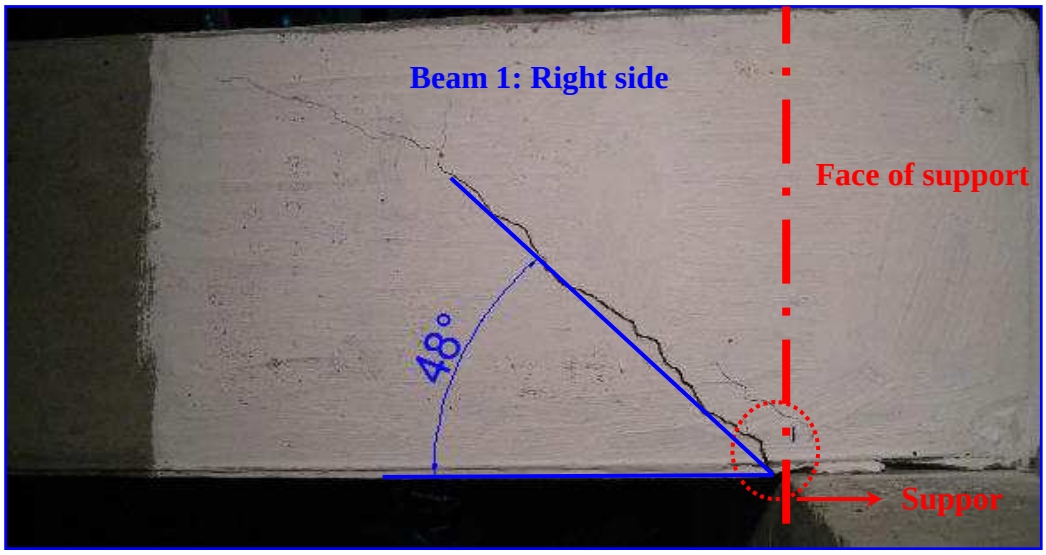

Figure 6.15: Bond failure on the right side of the beam.

It is shown in Figure 6.15 that the crack, resulting from bond failure in the tensile reinforcement is approximately at 48 degrees. Because the bond failure started from the bottom reinforcement at the beam end, there is a sign of relative horizontal displacement as can be seen in the dotted circle (Figure 6.15).

6.3.3.2 Testing beam 2

Beam 2 has 23 mm of anchorage length of tension reinforcement after the face of the support using a rubber support pad. Beam 2 experienced a bond failure at the right support with the ultimate load approximately equal to 230 kN as indicated in Figure 6.16.

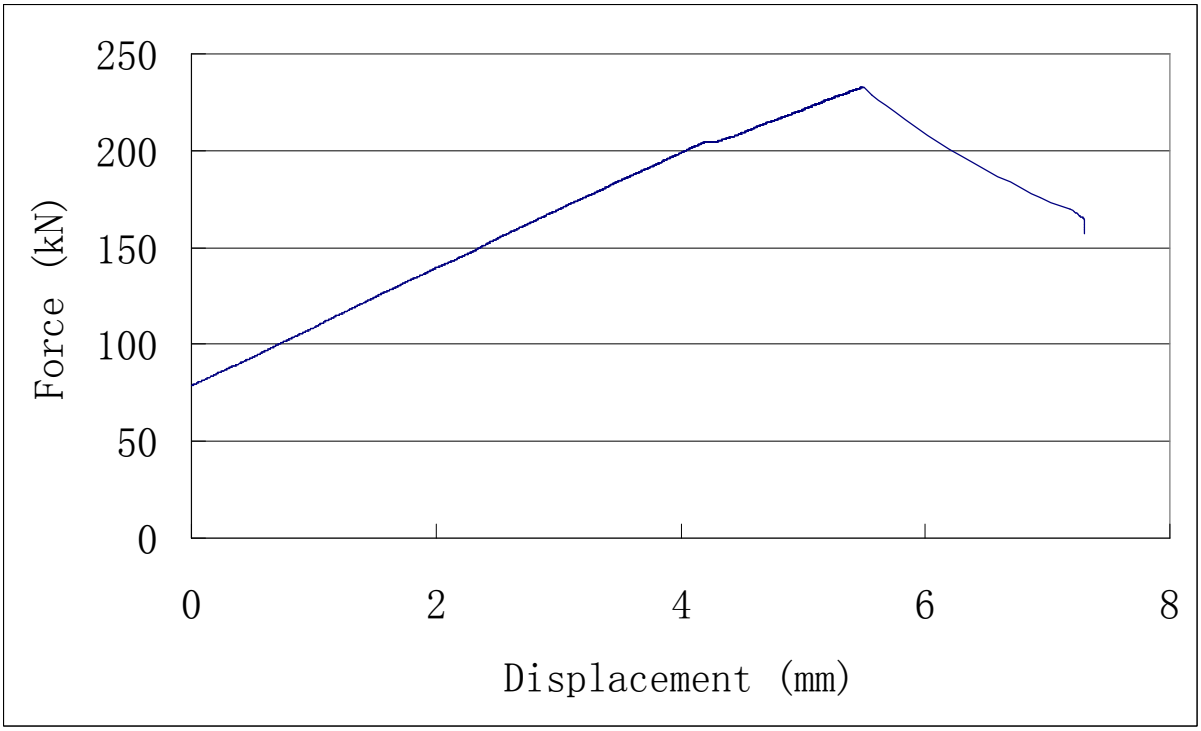

Figure 6.16: Total force-displacement curve for beam 2.

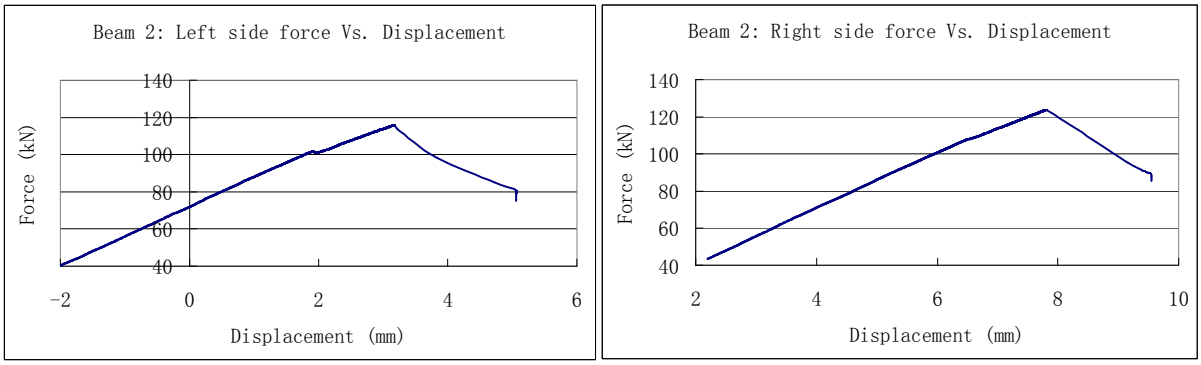

Figure 6.17: Force-displacement curve for each side of beam 2.

Figure 6.17 shows the force-displacement relationship for each side of beam 2. The

reinforcement condition on each end was nearly identical. The right side of the beam failed first because the force on that side was larger. A bond failure occured when the reaction force reached approximately 121 kN on the right side of the beam.

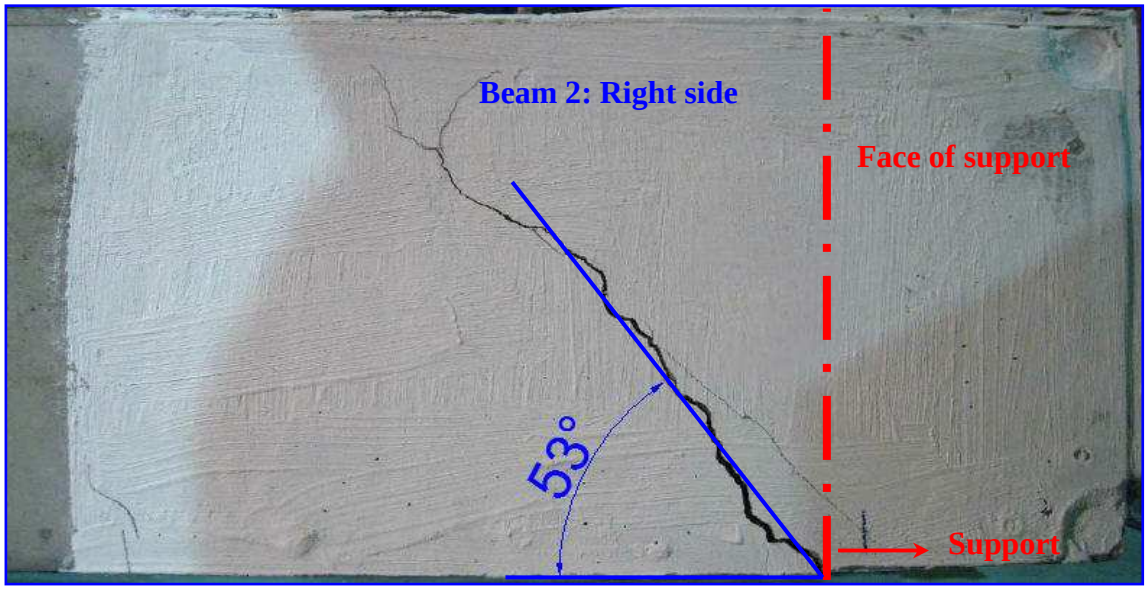

Figure 6.18: Bond failure on the right side of the beam 2.

Figure 6.18 shows the bond failure of beam 2. The angle of cracking in beam 2 is quite steep and similar to that of beam 1. The cracking starts at the bottom reinforcement at the beam end and a relative displacement occurs at the bottom of the beam.

6.3.3.3 Testing beam 3

Beam 3 has 23 mm of anchorage length of tension reinforcement after the centre of the support using a rubber pad as support. The first two beam tests indicated that the bond failure occurred when the total load nearly reach 300 kN. Beams 3 and 4 have much longer anchorage lengths of the tension reinforcement and should fail in shear. The electrical jack used in the tests on beam 1 and 2 can at most provide 300 kN, therefore, a hand jack with the capacity of 500 kN was used with the same experimental setup.

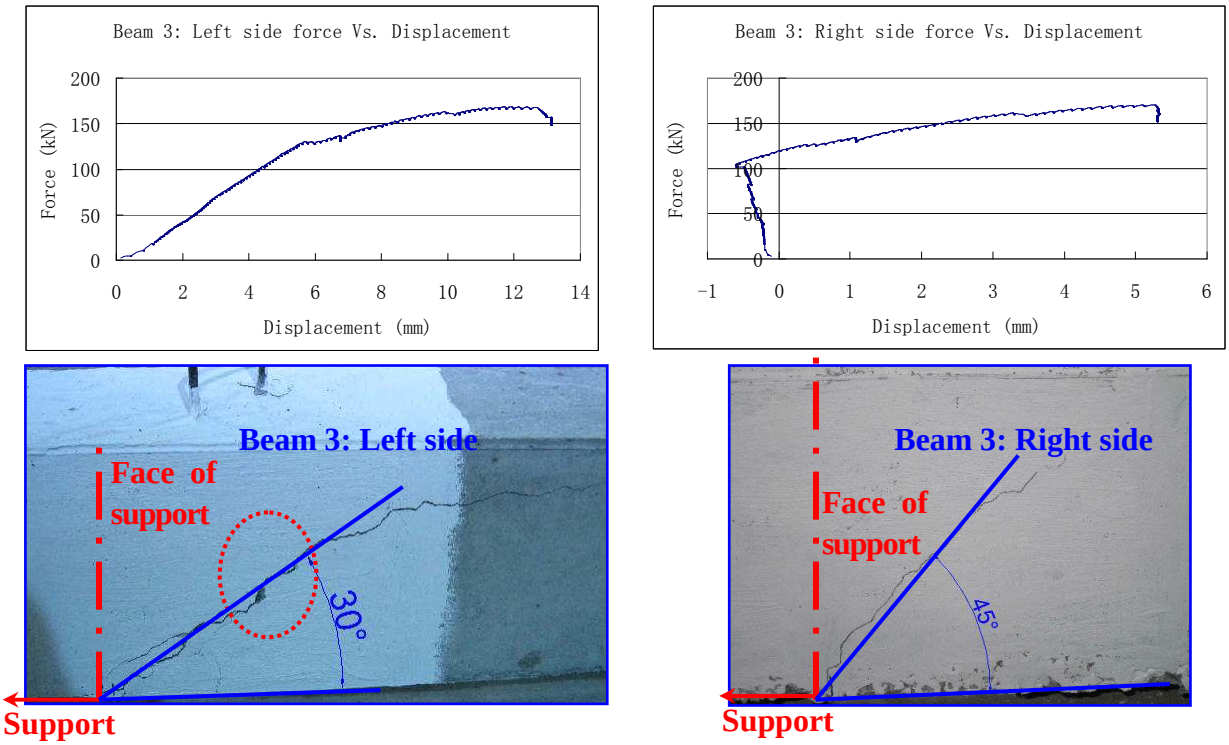

Figure 6.19: Force-displacement curve for each side of beam 3.

The force-displacement relationship and its corresponding cracks are shown in Figure 6.19. Beam 3 has a shear failure on the left side of the beam. The bottom left part of the Figure indicates the shear crack is approximately 30 degrees, while the bottom right part shows a bond crack of nearly 45 degrees. The load distributed on each side is nearly the same according to the force-displacement curve and the maximum shear force equals approximately 170 kN. As shown in the dotted circle, the shear failure started from the centre of the beam in the vertical direction and extended to the extreme fibres of the beam.

6.3.3.4 Testing beam 4

Beam 4 has 120 mm of anchorage length of tension reinforcement after the centre of the support using a rubber pad as support. Beam 4 has the same support condition as that of beam 3, but provides longer anchorage length of tension reinforcement. Figure 6.20 shows the force-displacement relationship for each side of the beam and shows the corresponding cracks beneath the curve.

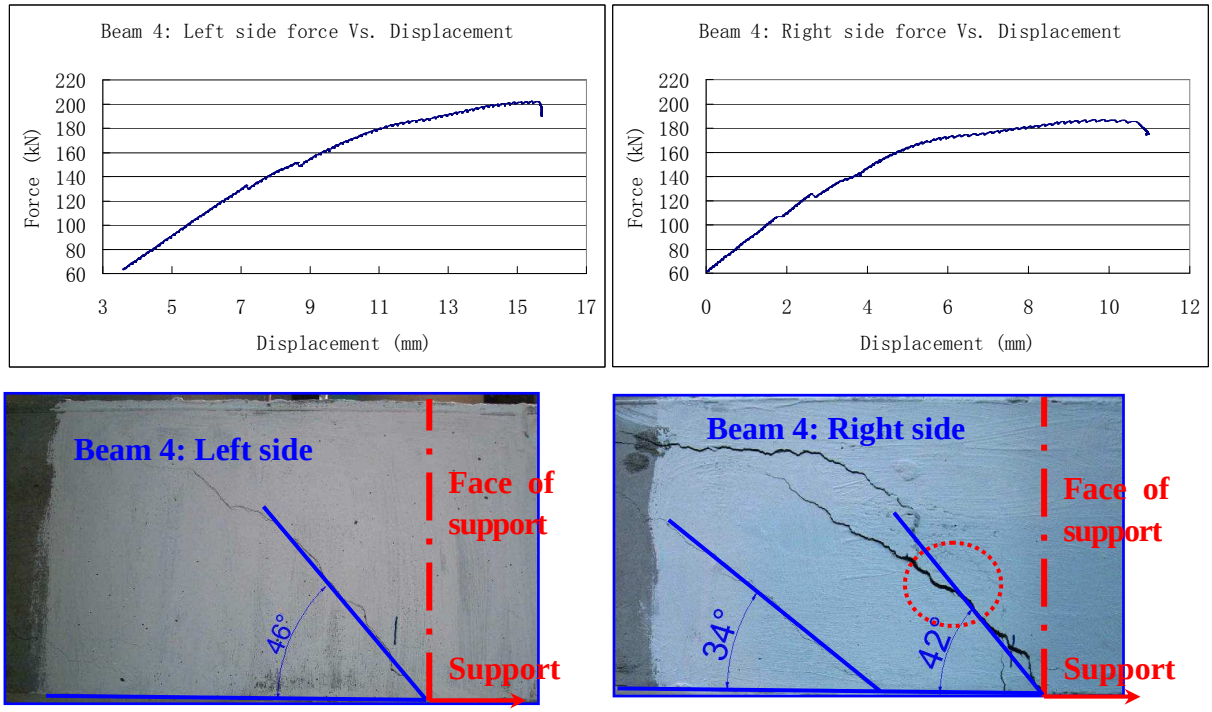

Figure 6.20: Force-displacement curve for each side of beam 4.

The beam failed in shear on the right side of beam 4 as indicated in Figure 6.20. The shear cracks on the right side of the beam were approximately 42 and 34 degrees, while the bond cracks on the left side of the beam were approximately 46 degrees. The ultimate shear force was approximately 185 kN on the right side. The shear failure mechanism is identical with that of beam 3 and started in the dotted circle.

6.3.3.5 Testing beam 1 for the second time

The testing of beam 1 was initially stopped when bond failure occurred at the loud sound of the crack formation. Subsequently, beam 1 was tested for a second time under the same conditions to determine if the resistance could be increased. The results of the force-displacement curve for each side of the beam and corresponding cracks are shown in Figure 6.21.

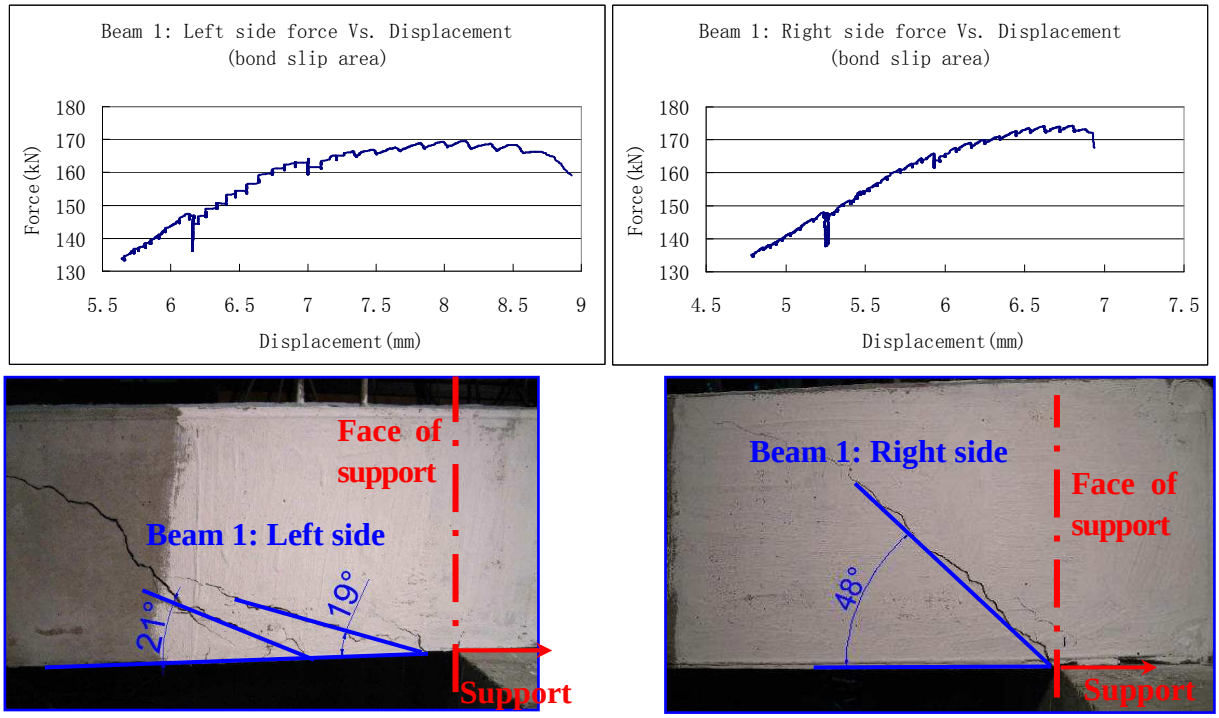

Figure 6.21: Force-displacement curve for bond slip area on each side of beam 1.

After several repetitions of bond slip behaviour, the bond resisted the tensile force before shear failure. The shear crack was approximately 20 degrees while the bond crack remained the same as that of the first test. The shear failure for this test was based on two reasons. The first reason is that the reaction force was in the critical point between bond failure and shear failure. The second is that the shear crack already developed under the first loading, which caused an ultimate shear resistance reduction for the second loading. The ultimate force for the shear failure was approximately 168 kN.

6.3.4 Comparing the results from the laboratory experiment

From the first two tests, it was found that the tension resistance at bottom bars for a simply supported beam with a rigid support is better than that of a flexible support. In the first test of beam 1, the reaction forces were concentrated near the face of the support as shown in Figure 5.1. For the second test (beam 2), the reaction forces were distributed along the support and had a stress distribution similar to that

indicated in Figure 5.2. Based on equation 2.5, the bending moment at the face of the support for beam 2 is larger than that of beam 1 because the lever arm in beam 2 is larger than in beam 1 as shown in Figure 6.22. With the same shear force, reaction force and angle θ, the tensile force that develops in the bottom reinforcement in beam 2 is larger than that of beam 1. Therefore, the bond failure occurs in beam 2 at a lower ultimate load.

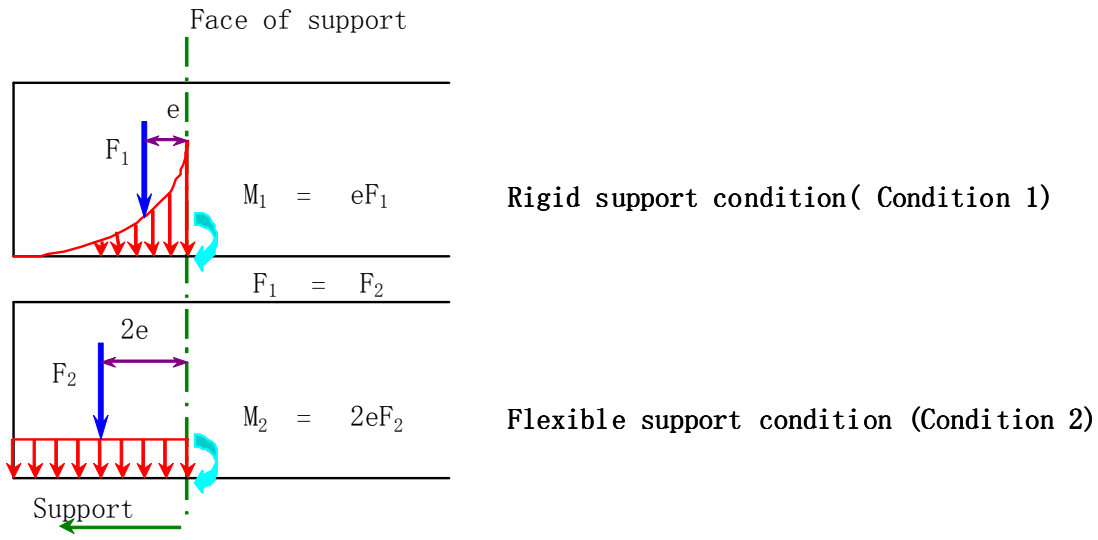

Figure 6.22: Stress distribution and bending moment for the rigid and flexible support conditions.

Because the bond failure in beam 2 is similar to that obtained with the FE analysis, the bond stress can be obtained from the FE analysis. According to Section 6.3.2.2, the bond stress was calculated to be approximately 16.9 MPa, which is 4 times more than that from the pull out test. However, by using equation 2.4, which comes from Eurocode 2 (2004), the bond stress value was calculated to be approximately 103.6 MPa, which is about 20 times that of the pull out test. This indicates that as the reaction force increases the vertical confinement pressure increases and improves the bond strength significantly.

For beams 3 and 4, because of the increase in bond stress, they are only beams

subjected to shear failure. Another finding is that the resistance of the beam under the ultimate bending moment and shear force is much higher than that of the theoretical calculations. However, this was not part of this investigation and is therefore not discussed here.

6.4 Summary and conclusions

This chapter introduced the relationship between the mechanisms in the connection zone. The end anchorage length of tension reinforcement is then compared between the design codes and further compared with the FE model analysis. A laboratory experiment was introduced to verify whether the end anchorage length of tension reinforcement can be reduced.

The experimental procedures of four beam specimens are described. By comparing the test results and analyzed data, the following conclusions can be drawn:

- The end anchorage length of the tension reinforcement as specified in SABS 0100-1 (2000) can be reduced if adequate concrete confinement is provided to increase the bond strength.
- The tensile force at the beam end for a rigid support is smaller than that of flexible supports which results in comparatively shorter anchorage lengths needed for the tension reinforcement after the face of the support.
- The bond stress increases with the increasing of vertical pressure from the support reaction.

Therefore, the laboratory experiment confirmed that a shorter anchorage bond length can be used as was demonstrated with the finite element analyses. The role of concrete confinement and well as the actual tensile force in the reinforcement is demonstrated as identified with the finite element analyses.

CHAPTER 7

CONCLUSIONS AND RECOMMENDATIONS

This thesis investigated a beam-column connection in pre-cast concrete. This chapter summarizes this investigation as described in the previous chapters. The main conclusions are drawn and some topics are recommended for further research.

7.1 Summary

This investigation aimed to obtain a better understanding of the mechanisms in the connection zones of pre-cast beams where built-in hidden corbels are used. A total of five mechanisms were identified. It was found that the mechanism of tensile force in reinforcement in the connection zone needs an in-depth investigation. This tensile force directly affects the end anchorage length of tension reinforcement.

End anchorage length of tension reinforcement at the support of a simply supported beam plays an important role in the stability and strength of structures. By comparing different design codes, it was found that the required end anchorage length of tension reinforcement calculated from Eurocode 2 (2004) is shorter than that specified in SABS 0100-1 (2000).

The anchorage of bottom reinforcement was evaluated for a hidden corbel connection (HCC) in pre-cast beams. Based on theoretical analyses and FE modelling, the anchorage for tension reinforcement at the support regions for the modified HCC only needs to be considered for Stage Ⅰ (Installation stage). If beams are designed as continuous members in the permanent condition, there is not a similar problem of bond failure in tension. Therefore, the conditions based on Stage Ⅰ were investigated further.

By allowing plate elements in a finite element analysis to take both compressive and tensile stress, the tensile force was calculated at certain cross sections in the connection zone. The tensile force was then converted to the end anchorage length by assuming the value of the bond stress from the design code. The tensile force after the face of the support obtained with a 2D FE model indicated that the value was smaller than that calculated from Eurocode 2 (2004). The stress contributions obtained with a 3D FE model identified the location inside the corbel that will have the best bond stress.

After the FE modelling, a laboratory experiment was used to verity the FE results. By comparing four beams with different support conditions and different lengths of reinforcement anchorage, the following conclusions were drawn:

7.2 Conclusions

1) Main reinforcement anchor length:

- The end anchorage length of reinforcement bars as required by SABS 0100-1 (2000) can be reduced from the face of the support for a simply supported beam.
- A requirement that at least 50% of tension reinforcement should extend into the support, is not necessary as specified by SABS 0100-1 (2000).
- The Eurocode 2 (2004) can be used to determine the tensile force in the reinforcement from where the anchorage length can be determined. This will result in a shorter anchorage length than the 12 diameter of tension reinforcement past the centre of support as specified by SABS 0100. The method from Eurocode 2 (2004) in calculating end anchorage length of tension reinforcement is recommended to be considered in the South African design code.

2) Confinement and reinforcement layout:

- The bond stress increases with an increase in lateral pressure on the reinforcement. The results from this investigation provide a clear indication that the confinement in the support region increases the bond stress. These values however need to be quantified.
- The confinement region for bars is only in the close proximity of the triangular side plates of the modified HCC. If more than two bars are used, the confinement can not be considered for bars located towards the centre of the modified HCC.

3) Support flexibility (stiff and flexible options):

- The resistance of tensile force by reinforcement at the beam end for a rigid support is better than that of a softer support. It would be prudent to design as if the support is soft, simulating the crushing of concrete in the support region.

4) It is conservative to consider the critical section from where reinforcement should be anchored to be at the centre of the support when calculating the end anchorage length of tension reinforcement from the FE result. When considering the critical section to be at the face of the support, the support conditions (either rigid or soft) determine the end anchorage length of tension reinforcement. It would be conservative to assume a soft support, which would be consistent with an assumption that the average bearing pressure is distributed over the full length of the support.

5) It was verified that the specific modified HCC with a length of 100 mm considered in this investigation can provide sufficient end anchorage length for the tension reinforcement in the simply supported condition.

6) All the mechanisms in the connection zone need to be verified according to the design code when designing the modified HCC. The tensile force, which determines

the end anchorage length of the tension reinforcement, is the dominant factor that determines the size of the hidden corbel in most cases.

7.3 Recommendations for future research

This research focused on the end anchorage length of tension reinforcement for a simply supported beam. For the modified HCC, the end anchorage length of tension reinforcement determines the size of the hidden corbel, which plays an important role for the economy and potential usage. Hence, a further investigation was conducted by comparing different design codes and modelling and found that the end anchorage of tension reinforcement can be reduced after the face of the support. However, this investigation only focused on uniformly distributed loads on the beam. Some further research is recommended:

- More laboratory experiments are needed to find the exact relationship between the effect of the confinement and the lateral pressure on the bond stress.
- Investigate the effect of concentrated load on end anchorage length of tension reinforcement.
- Investigate long term effects such as creep and shrinkage for the end anchorage of tension reinforcement for a simply supported beam.
- Investigate the dynamic effect on the end anchorage length for the modified HCC.
- Investigate the non-linear material 3D modelling for the modified HCC.
- Determine parameters for a definition of a rigid or soft support.
- From the test results, it was shown that the bond stress increases significantly due to confinement pressure. However, these values have not been quantified and further research is necessary.
- The effect of tensile forces ("negative confinement") in the 3D FE model has not been studied and needs further research to determine the effect on bond stress.

Reference list

Books and Publications

Addis, B. 2005. *Fundamentals of concrete*. Midrand: Cement and Concrete Institute.

Bangash, M. Y. H. 2003. Structural detailing in concrete. 2nd ed. London: Tomas Telford Ltd.

British National Pre-cast Concrete Association. 2006. A guide to the one hundred advantages of precast concrete. [Online]. Available: http://www.precast.org/100_adantages_of_precast_concrete.pdf [2008, October 20].

Craig, J. R. and Roy, R. 2000. Mechanics of materials. 2nd ed. United States: John Wiley & Sons, Inc.

Desayi, P. and Krishnan, S. 1964. *Equation for Stress Strain Curve of Concrete*. ACI. Proceedings, 61 (3): 345-350.

Hubber, U. 2005. Reliability of reinforced concrete shear resistance. Unpublished master's thesis. Stellenbosch: University of Stellenbosch.

International Federation for Structural Concrete. 2000. *Bond of reinforcement in concrete*. Switzerland: International Federation for Structural Concrete.

International Federation for Structural Concrete. 2008. *Structural connections for precast concrete buildings*. Switzerland: International Federation for Structural Concrete.

Jurgens, C. 2008. An investigation into the feasibility of hybrid concrete construction in South Africa. Unpublished master's thesis. Stellenbosch: University of Stellenbosch.

JVI 2009. *BSF introduction*. [Online]. Available: http://www.jvi-inc.com/home. shtml [2008, October 20].

Kooi, L. 2004. Behaviour of precast concrete beam-to-column connection with hidden corbel. Unpublished master's thesis. Malaysia: Universiti Teknologi Malaysia.

Kaewunruen, S. and Remennikov, A. 2006. *Nonlinear finite element modelling of railway prestressed concrete sleeper*. [Online]. Available: http://ro.uow.edu.au/ cgi/viewcontent.cgi?article=1320&context=engpapers [2008, October 18].

Kong, F. K. and Evans, R. H. 1987. *Reinforced and Prestressed Concrete*. 3rd ed. Hong Kong: Van Nostrand Reinhold Co. Ltd.

Mosley, B., Bungey, J., & Hulse, R. 2007. *Reinforced Concrete Design to Eurocode 2*. 6th ed. New York: Palgrave Macmillan.

Nawy, E. 2009. Reinforced concrete: A fundamental approach. 6th ed. London: Pearson Education Ltd.

Oehlers, D. 1995. *Composite steel and concrete structural members: fundamental behaviour*. Great Britain: Elseviser Science Ltd.

Prokon. 2008. Available: http://www.prokon.com [2008, March 12]

Robins, P.J. and Standish, I.G. 1982. *The effect of lateral pressure on the bond of round reinforcing bars in concrete*. International Journal of Adhesion and Adhesives, 2 (2): 129-133.

Strand7. 2005. *Using Strand7*. 2nd ed. Sydney: Strand7 Pty Ltd.

Strand7. 2009. *Strand7 online help.* [Online]. Available: http://www.strand7.com/ [2009, March 18].

Yasojima, A. and Kanakubo, T. 2004. *Effect of lateral confinement in bond splitting behavior of RC members*. 13th World Conference on Earthquake Engineering. Vancouver, B.C., Canada. (August 2004).

National Standards

ASTM. 2003. *Stand Test Method for Comparing Bond Strength of Steel Reinforcing Bars to Concrete Using Beam-End Specimens*. ASTM international, 01 (04): 513-516.

"BS 8110: Structural use of concrete - Part 1. Code of practice for design and construction". BSI, 1997.

"Eurocode 2: Design of concrete structures - Part 1-1: General rules and rules for buildings". CEN, 2004.

"SABS 0100-1: The structural use of concrete. Part 1: Design". Pretoria: South African Bureau of Standards, 2000.

"SANS 10162-1: South African National Standard – The structural use of steel Part 1: Limit-state design of hot-rolled steelwork". Pretoria, Standards South Africa, 2005.

"Southern African Steel Construction Handbook". 6th ed. Johannesburg: South African Institute of Steel Construction, 2008.

APPENDIX A

DESIGN OF A TYPICAL SKELETAL FRAME BUILDING STRUCTURE

Design of a typical structure

1. Description of the building

Purpose of the building: Typical skeletal frame building
The span for the beam is: 10m
The span for the floor is: 5m
Density of beam: 24 kN/m^3
Density of floor slab(according to Echo): Slab depth Density
150mm 2.75 kN/m^2
Dead load: 1) Beam loads: 5.36 kN/m
2) Floor loads: slab density*slab span= 13.75 kN/m
3) Brick wall loads: 2.7kPa
4) Partition: 1.5kPa
Live load: 1) Nominal imposed floor loads: 2.5kPa (According to SABS 10160-1989 Table 4)

Characteristic strength of reinforcement: f_y = 450Mpa
Characteristic strength of shear reinforcement: f_y = 250Mpa
Characteristic strength of concrete: f_{cu} = 30Mpa

2. Preliminary design of dimensions

Based on the span/effective depth ratios, select the ratio as follows:
(SABS 0100-1 talbe10)

28 with both ends continuous beams
24 with one end continuous beams
20 simply supported beams with norminal restrained ends

effective depth d=L/ratio= 10000/28 = 0.357m
= 10000/24 = 0.417m
= 10000/20 = 0.5m

Fire resistance (SABS 0100-1 table 43) fire resistance

Siliceous aggregate concrete:

Fire rating: 1.5

Concrete cover (mm)	Beam width (mm)
35	140

3. Calculate the bending moment and shear force of the beams

Step 1: load case 1: (installation stage) self-weight of beams and slabs

In this stage, regard the beam as simple supported beam.

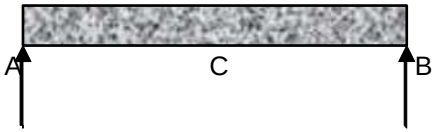

Beam area: The beam cross-section(preliminary):

Beam height	0.500	m
Beam width	0.333	m
Beam area	0.167	m^2

(Rule of thumb 2/3 of effective height)

Actual beam area

Beam height	0.620
Beam width	0.360
Beam area	0.223
effective h	0.569

$$d \geq \sqrt[3]{\frac{3M}{2 \times 0.156 \times f_{cu}}} = 0.5527 \text{ m}$$

Load case 1:

	Dead load
Unfactored	19.107kN/m
Factored	22.928kN/m

The maximum bending moment occurs at C: $M_{max} = \frac{WL^2}{8} = 286.60$ kN.m

The maximum shear occurs at A,B: $V_{max} = \frac{WL}{2} = 114.64$ kN

Diagram

bending moment

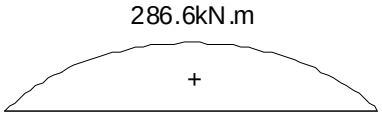

shear

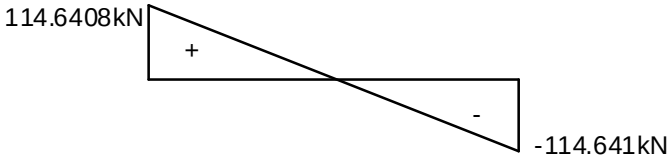

Step 2: Load case 2:combination of load case 1, imposed loads and partitions.
Load case 1 is calculated above, this step calculates imposed loads and partitions.
Continuous beam simplification:

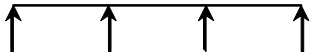

Dead load: Total dead load: 4.200 kN/m

Live load: Total live load: 13kN/m

1.2D (kN/m)	1.6L (kN/m)
5.040	20kN/m

Load case 1

live load	20	20	20
dead load	5.040	5.040	5.040
Total	25.040	25.040	25.040

Load case 2

live load	20		20
dead load	5.040	5.040	5.040
Total	25.040	5.040	25.040

Load case 3

live load		20	
dead load	5.040	5.040	5.040
Total	5.040	25.040	5.040

1)Bending moment

Regard the beam as a continuous beam, span is: 10m
(SASCH table 5.20 combined with Prokon analysis)

Use prokon analysis for the load case2 bending moment and shear, then combine with the bending moment and shear with load case1 to obtain the ultimate load case.

The maximum and minimum bending moments can be obtained from the graphical output of the Prokon analysis.

	Bending moment			Shear		
	Maximum	Minimum		Maximum	Minimum	
Load case1	480.93	-250.40	kN.m	264.88	-264.88	kN
Load case2	526.67	-150.40	kN.m	254.88	-254.88	kN
Load case3	449.20	-150.40	kN.m	239.84	-239.84	kN
Result	526.67	-250.40	kN.m	264.88	-264.88	kN

4. Calculate the required reinforcing steel bars

d= 0.569m b= 0.36m

$$K = \frac{M}{bd^2 f_{cu}} = 0.151 \quad \text{Ok}$$

$$z = d\left\{0.5 + \sqrt{(0.25 - \frac{k}{0.9})}\right\} = 0.448$$

$$A_s = \frac{M}{0.87 \cdot f_y \cdot z} = 3002 \ \text{mm}^2$$

Analysis	Diameter	Area(mm^2)	Number
	32	804	3.7

Reinforcement	
diameter	32
number	4
total area(mm^2)	3216.99

$100 A_s / A_c$ = 0.0144 < 4% **OK**

5. Calculate the required stirrupts, corbel length

Full penetration weld

$$\left.\begin{array}{l} V_r = \phi A_v f_s \\ f_s = 0.66 f_y \end{array}\right\} V_r = 0.66 \cdot 0.9 A_v f_y \geq V_{\max} \Rightarrow A_v \geq \frac{V_{\max}}{0.66 \cdot 0.9 f_y} = 1783.7 \text{ mm}^2$$

According to SASCH table 2.23, minimum thickness of steel plate is 4.5 mm.

The required height of corbel weld to the vertical plate $h \geq \frac{A_v}{2t}$ = 198 mm. **OK**

Fillet weld

Weld the web use 6 mm fillet weld: E70XX: $X_u = 480 MPa$

Base metal:

X_u	480	MPa
f_u	350	MPa

$$V_r = 0.67 \cdot \varphi_w \cdot A_m \cdot f_u \geq V_{\max} \Rightarrow A_m \geq \frac{V_{\max}}{0.67 \cdot \varphi_w \cdot f_u} = 1685.9 \text{ mm}^2$$

Consider the plate at bottom. Area of the plate at bottom that resist the shear is (2b-2t)x12=6852 mm^2
If choose 5mm fillet weld the area is 5710 mm^2 **OK**

Weld metal:

$$V_r = 0.67 \cdot \varphi_w \cdot A_u \cdot X_u (1.00 + 0.5 \cdot \sin^{1.5} \theta) \geq V_{\max} \Rightarrow A_u \geq \frac{V_{\max}}{0.67 \cdot \varphi_w \cdot X_u (1.00 + 0.5 \cdot \sin^{1.5} \theta)} = 1229.3 \text{ mm}^2$$

Consider the plate at bottom. Area of the plate at bottom that resist the shear is (2b-2t)x6/sqrt(2)=2422 mm^2
If choose 5mm fillet weld the area is 2018 **OK**

Bearing resistance V_{max} = 264.88 kN

$$\frac{V_{max}}{b_{corbel} \cdot l_{corbel}} \le 0.4 \cdot f_{cu} \quad \Rightarrow \quad l_{corbel} \ge \frac{V_{max}}{0.4 \cdot f_{cu} \cdot b_{corbel}} = 0.076 \text{ m}$$

Taken 100 mm corbel length.

Stirrups The shear force from the distance d of the end of the corbel:

$$v = \frac{V}{bd} = 1.29 \text{ MPa}$$

$$\left(\frac{100\,A_s}{b_v d}\right)^{\frac{1}{3}} = 1.2$$

If the value larger than 3, take 3.

$$Vc = \frac{0.75}{\gamma_m}\left(\frac{f_{cu}}{25}\right)^{\frac{1}{3}}\left(\frac{100\,A_s}{b_v d}\right)^{\frac{1}{3}}\left(\frac{400}{d}\right)^{\frac{1}{4}} = 0.61 \text{ MPa}$$

$$\frac{A_{sv}}{s_v} \ge \frac{b(v - v_c)}{0.87\,f_{yv}} = 1.137$$

Choose R10@125 stirrups, where $\frac{A_{sv}}{s_v}$ = 1.256

Nominal

For nominal stirrups, $\frac{A_{sv}}{s_v} = 0.002b$ (for mild steel)

$\frac{A_{sv}}{s_v} = \frac{b(v - v_c)}{0.87\,f_{yv}}$ $\Rightarrow \quad v - v_c = 0.002 \cdot 0.87 \cdot f_{yv} = 0.435 \text{MPa}$

$$L_{nominal} = \frac{V_{max} - (v_c + 0.435) \cdot b \cdot d}{\omega} = 1.076 \text{ m}$$

In this case, $\frac{A_{sv}}{s_v}$ = 0.720

Choose R10@200 stirrups, where $\frac{A_{sv}}{s_v}$ = 0.785

Bolts

Shear resistance of bolts

$V_r = 0.7 \cdot 0.6 \cdot \varphi_b \cdot n \cdot m \cdot A_b \cdot f_u$ Steel code P44 13.12 b)

$\varphi_b = 0.8$

$V_r \geq V_{\max} \Rightarrow 0.7 \cdot 0.6 \cdot \varphi_b \cdot n \cdot m \cdot A_b \cdot f_u \geq V_{\max}$

$n \geq \frac{V_{\max}}{0.7 \cdot 0.6 \cdot \varphi_b \cdot \cdot m \cdot A_b \cdot f_u}$ = 3.0233

Diameter	Area(mm^2)	bolt class	strength	need number
20	314.16	8.8	830	4

APPENDIX B

CHECK THE SHEAR FORCES IN THE MODEL OF HCC SHOE

The following paragraphs describe the procedure on how to calculate the shear force in the model.

Step1: Collecting the magnitude and direction of principal stresses for elements in zones 2 and 3.

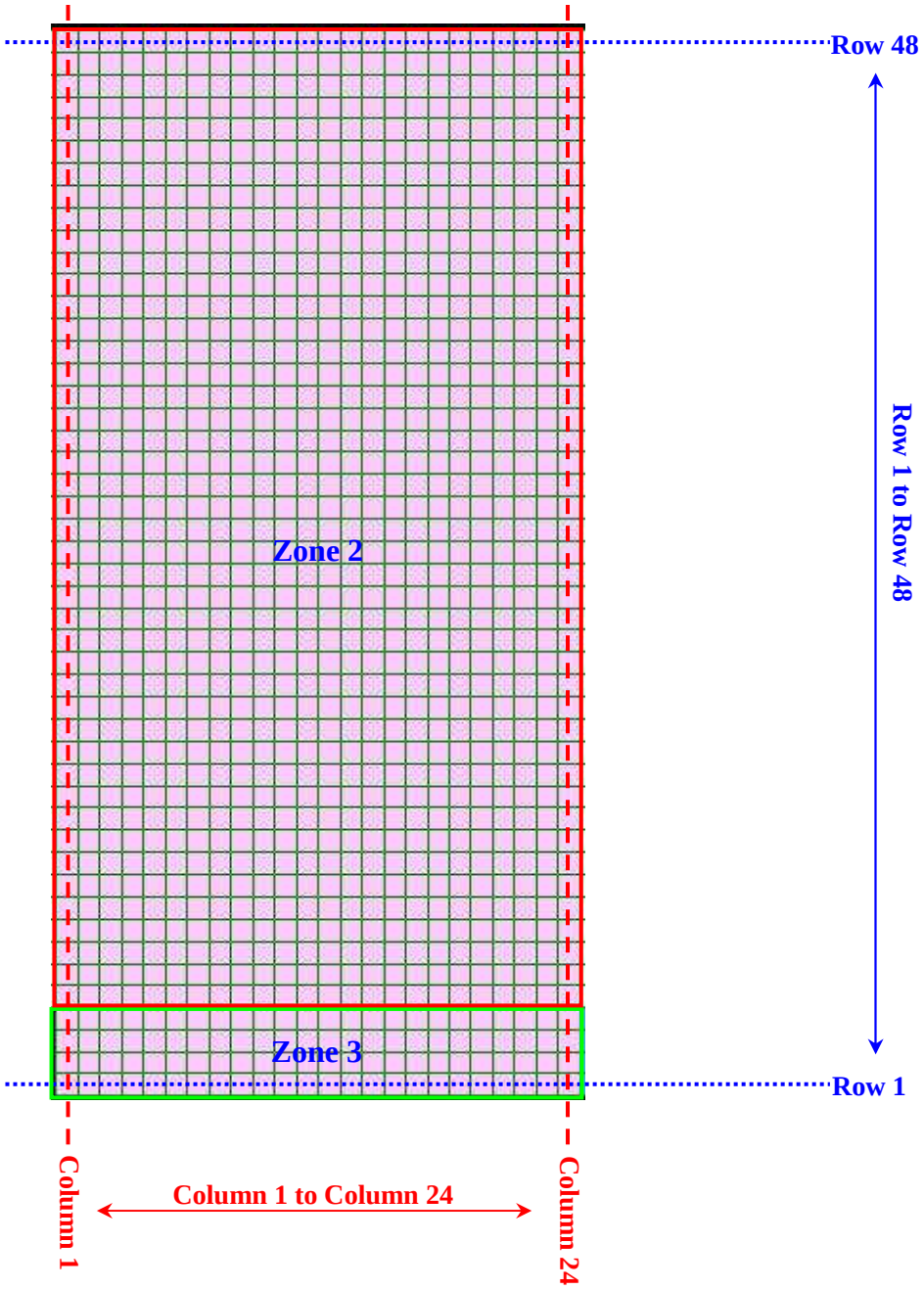

Figure B.1: Define rows and columns for hand calculations.

The rows and columns of plate elements were defined in Figure B.1, which shows the plate elements in zones 2 and 3. The magnitude of principal stress V11 and V22 and their direction for the elements depicted in Figure B.1, which were extracted from

STRAND7 database.

Step 2: Calculate the shear force

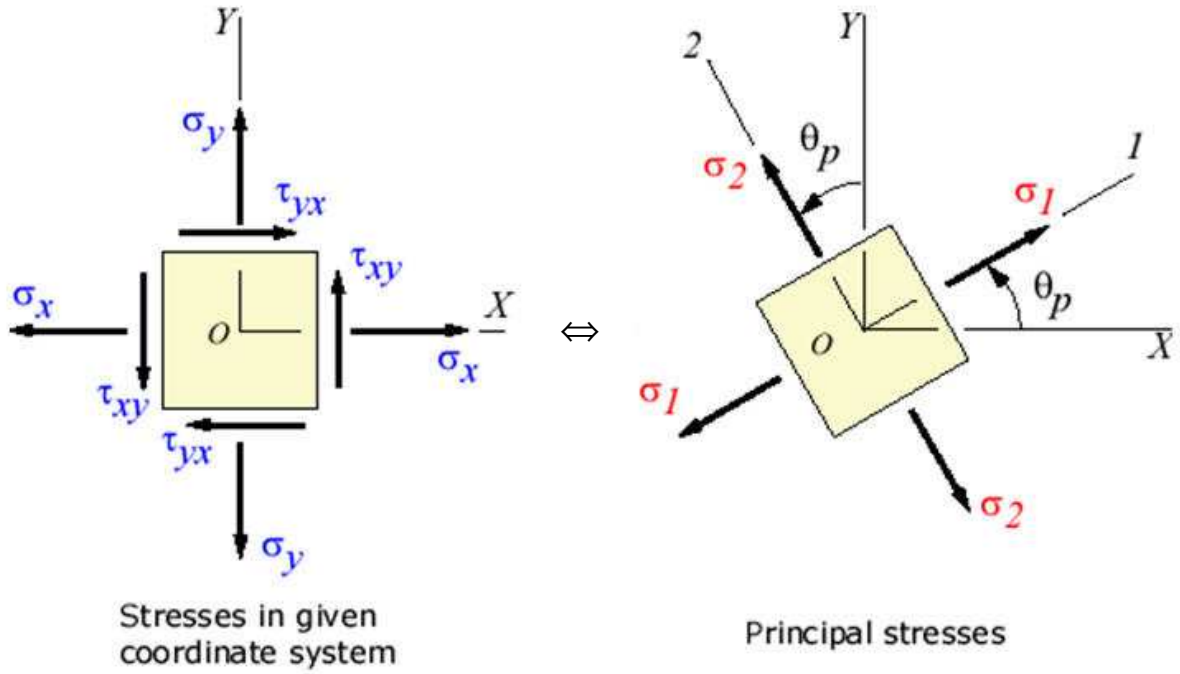

Figure B.2: Conversion of principal stresses and stress in a given coordinate.

Figure B.2 shows the conversion of principal stresses and stress in a given coordinate. The data collected from STRAND7 gives the magnitude and angle of principal stresses such as the right side of Figure B.2. In Figure B.2, the stress in the left side is equivalent to the right side and they just express the stress state in different coordinate system.

In order to calculate the shear force, the shear stress in the horizontal and vertical direction is calculated as indicated in the left side of Figure B.1. Mohr's circle introduces the direct view of the stress state for any given coordinate systems.

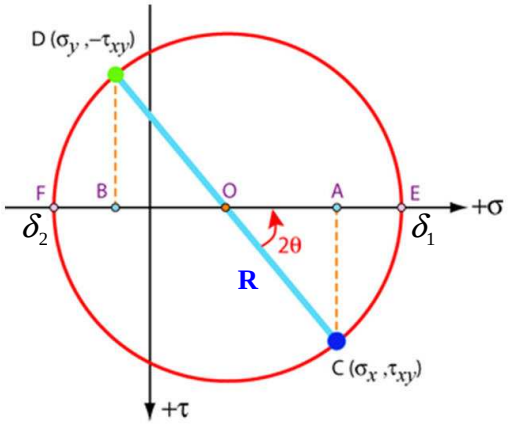

Figure B.3: Sketch for Mohr's circle.

In Figure B.3, the principal V11 indicates δ_1 at point 'E' and the principal stress V22 indicates δ_2 at point 'F'. The value of R can be derived from Figure B.3 as below.

$$R = \frac{\delta_1 - \delta_2}{2} \tag{B.1}$$

Where:

R : Maximum shear stress

δ_1 : Maximum principal stress

δ_2 : Minimum principal stress

The shear stress at any face CD (Figure B.3) can be then be calculated by the following formula:

$$\tau = -R\sin 2\theta \tag{B.2}$$

Where:

τ : Shear stress at a certain face CD in Figure B.3

Based on equations B.1 and B.2, the shear stress at each plate Q8 element was calculated.

There are a total of 1152 plate Q8 elements in zones 2 and 3. All the elements in the FE model were calculated using the same methods. The plate element (plate Q8 element 1414), which is the point of intersection between row 1 and column 1, was calculated and was used as an example.

For plate Q8 element 1414, V11 equals 8.9471 MPa, V22 equals 0.6964 MPa and the angle is -45.9855 degree. Therefore:

$$R = \frac{\delta_1 - \delta_2}{2}$$
$$= \frac{8.9471 - 0.6964}{2}$$
$$= 4.12535\ \text{MPa}$$

$$\tau = -R\sin 2\theta$$
$$= -4.12535 \times \sin[2 \times (-45.9855)]$$
$$= 4.122909\ \text{MPa}$$

The calculated shear stress value is the shear per unit length. The shear force in vertical direction is calculated as follows:

$$V = \tau \cdot b \qquad \text{(B.3)}$$

Where:

V : Shear force in the plate Q8 element.

b : The height of the plate Q8 element as indicated in Figure 4.6.

$$V = \tau \cdot b$$

$$= 4.122909 \times 12.75$$

$$= 52.56709 \text{ N}$$

Based on the same way, shear force on each element in zones 3 and 4 was calculated. The shear forces for all elements in the same column were summed up and were compared with the theoretical shear force on that cross section, such as location of column 1, column 2

Table: B.1 Comparison of shear force between the model analysis and theoretical calculation

Shear force		
Column	Model analysis	Theoretical calculation
1	112760.9	112752
2	112473.3	112464
3	112185.5	112176
4	111897.7	111888
5	111610	111600
6	111322.2	111312
7	111034.5	111024
8	110746.8	110736
9	110459.1	110448
10	110171.3	110160
11	109883.6	109872
12	109595.9	109584
13	109308.1	109296
14	109020.3	109008
15	108732.5	108720
16	108444.8	108432
17	108157	108144
18	107869.2	107856
19	107581.4	107568
20	107293.5	107280
21	107005.7	106992
22	106717.8	106704
23	106430	106416
24	106142.1	106128

APPENDIX C

VERIFYING THE TENSILE FORCE IN THE TENSION REINFORCEMENT USING EUROCODE 2

The bottom tensile forces for each cross section, which are resisted by the reinforcement, were calculated for those elements in that column (shown in B.2). The normal stress of each element in the direction X, which contributes to the tensile force at the bottom of the beam was calculated. In addition, the shear stress for each element was also calculated because the difference of shear stress between the adjacent elements also contributes to the tensile force at the bottom of the beam. All the tensile stress and difference of shear stress in the same column (B.2), which is contributing to the tensile stress, were summed up. The tensile force on the cross section of a certain column can thus be calculated.

The plate Q8 element 1414 and 1438, which are the bottom two elements in column 1 were then calculated as follows:

Step1: Calculating average stress δ_{avg}

Based on Figure B.3, the average stress can be calculated as follows:

$$\delta_{avg} = \frac{\delta_1 + \delta_2}{2} \qquad \text{(C.1)}$$

Where:

δ_{avg} : Average stress, point 'O' in Figure B.3.

Table C.1: Results of average stress for plate Q8 element 1414 and 1438.

Plate Q8 element	δ_1 (MPa)	δ_2 (MPa)	δ_{avg} (MPa)
1414	8.947	0.696	4.821
1438	77.246	-7.585	34.830

Step2: Calculating the horizontal normal stress δ_x

The normal stress can be derived from Figure B.3.

$$\delta_x = \delta_{avg} + R \cdot \cos(2\theta) \qquad \text{(C.2)}$$

Where:

δ_x: Normal stress in the horizontal direction (Figure B.3)

Table C.2: Results of normal stress (horizontal) for plate Q8 element 1414 and 1438.

Plate Q8 element	δ_{avg} (MPa)	R (MPa)	θ of V11 (degree)	δ_x (MPa)
1414	4.821	4.125	-45.985	4.679
1438	34.830	42.415	-56.115	18.783

Step3: Calculating the shear stress τ

Section 5.2.5.1 already shows how to calculate the shear stress. Because the shear stress τ_{xy} and τ_{yx} are equal, the value of τ is calculated to represent the shear stress in the plate Q8 element.

The shear stress for plate Q8 element 1414 is already calculated in Section 5.2.5.1. By using the same way, the shear stress in plate Q8 element 1438 equals to 42.41555 MPa. With the width b (Figure 4.6) equals to 12.75 mm, the corresponding shear force is 500.6 N.

Step4: Calculating the difference of shear stress τ between adjacent plate Q8 elements 1414 and 1438.

The direction of differentiate shear force determines if this difference will contribute to the tensile force. In order to show the effect of shear stress on the tensile force, the shear stress of plate Q8 elements 1414 and 1438 is shown in Figure C.1. Because this step only considers the difference of shear stress, the normal stress sigma x and y are not shown in Figure C.1.

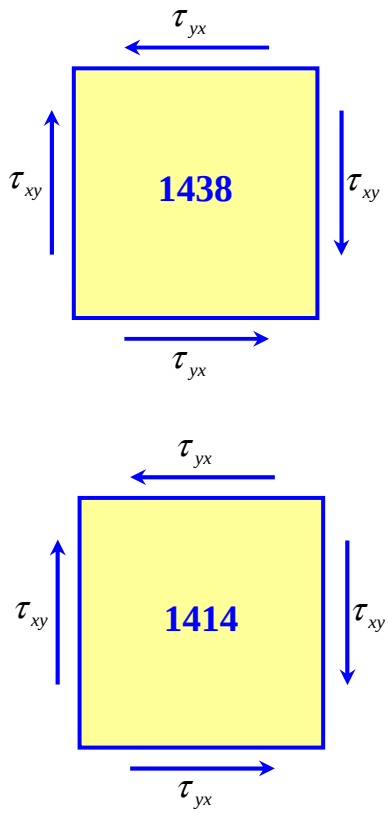

Figure C.1: Difference of shear stress for plate Q8 elements 1414 and 1438.

Only the shear stress for plate Q8 elements 1414 and 1438 is shown in Figure C.1. Between the interfaces of these two elements, the shear stress differs. In this section, the shear forces for these two elements were calculated based on the shear stress and width of elements. The shear force in element 1438 minus the shear force in 1414 obtains the difference of shear force between these two elements. The sign convention is used here to control whether the difference of shear stress is

contributed to the tensile force. If the value of difference is positive, it means that the direction of shear force is towards the right side. The difference of shear force is then contributed to the tensile force and is resisted by the tension reinforcement. If the value of difference is negative, it means that the direction of shear force is towards the left side. The difference of shear forces contribute to the compressive force and will is then resisted by the concrete.

Step 5: Calculating the tensile force at the bottom of the model.

The total tensile forces compose of two parts. One is the tensile force from normal stress δ_x as calculated in step 2. The other is the tensile force from the difference of shear force as calculated in step 4. By summing up all the tensile forces in one cross section as indicated in each column (Figure B.1), the tensile force on that cross section can be calculated. The detail calculations were listed in Appendix C.

The tensile force in column 1 (Figure B.1) is taken as an example. The total value of normal forces that are contributed to the tensile force in column 1 equals to 19232.9 N. The total value of differences of shear force that are contributed to the tensile force in the same column equals to 4566 N. Therefore, the total tensile force for the cross section that is located in column 1 equals to 23798 N.

Step 6: Calculating the angle θ based on equation 2.5.

The tensile force was calculated in step 5. The bending moment for each cross section were calculated in Appendix C. The shear force was calculated in Section 5.2.5.1 and the effective depth d was calculated in Appendix A. The angle θ was then calculated based on equation 2.5 and used for comparison.

Step 7: Estimating the angle between the model calculation and the rough theoretical calculation.

Table C.3: Estimating the angle between the model analysis and the actual calculation

Angle							
Column	**Distance (mm)**	**Model**			**Actual**		
		cotθ	θ(arc)	θ(degree)	cotθ	θ(arc)	θ(degree)
1	6.25	0.044	1.526	87.444	0.010	1.560	89.422
2	18.75	0.028	1.542	88.384	0.030	1.540	88.267
3	31.25	0.031	1.539	88.191	0.050	1.520	87.114
4	43.75	0.044	1.526	87.435	0.070	1.500	85.963
5	56.25	0.060	1.510	86.558	0.090	1.480	84.815
6	68.75	0.075	1.495	85.683	0.110	1.460	83.672
7	81.25	0.090	1.480	84.808	0.131	1.440	82.534
8	93.75	0.105	1.465	83.976	0.151	1.420	81.401
9	106.25	0.120	1.451	83.136	0.171	1.401	80.275
10	118.75	0.134	1.436	82.330	0.191	1.381	79.157
11	131.25	0.149	1.422	81.503	0.211	1.362	78.047
12	143.75	0.163	1.408	80.697	0.231	1.342	76.946
13	156.25	0.178	1.394	79.881	0.252	1.323	75.855
14	168.75	0.193	1.379	79.059	0.272	1.305	74.774
15	181.25	0.207	1.365	78.260	0.292	1.286	73.704
16	193.75	0.222	1.351	77.432	0.312	1.267	72.645
17	206.25	0.238	1.337	76.607	0.332	1.249	71.599
18	218.75	0.253	1.322	75.800	0.352	1.231	70.566
19	231.25	0.267	1.309	75.001	0.372	1.213	69.545
20	243.75	0.283	1.294	74.168	0.393	1.196	68.537
21	256.25	0.299	1.280	73.349	0.413	1.178	67.544
22	268.75	0.314	1.266	72.544	0.433	1.161	66.564
23	281.25	0.329	1.252	71.752	0.453	1.144	65.599
24	293.75	0.344	1.238	70.970	0.473	1.128	64.648

APPENDIX D

NORMAL AND SHEAR STRESSES FOR TWO SUPPORT CONDITIONS FOR THE 3D MODEL

Table D.1: Normal and shear stress for compression zone

Row (Refer to Figure B1)	Normal stress (MPa)	Shear stress (MPa)
1	-0.011	-0.189
2	-0.032	-0.179
3	-0.061	-0.225
4	-0.096	-0.316
5	-0.137	-0.447
6	-0.571	-1.261
7	-0.678	-1.623
8	-0.786	-2.009
9	-0.894	-2.415
10	-1.003	-2.839
11	-1.842	-4.535
12	-1.982	-5.095
13	-2.120	-5.662
14	-2.259	-6.236
15	-2.397	-6.815
16	-2.536	-7.400
17	-3.582	-9.582
18	-3.734	-10.233
19	-3.886	-10.884
20	-4.039	-11.534
21	-4.191	-12.185
22	-4.342	-12.836
23	-5.423	-15.054
24	-5.562	-15.706
25	-5.691	-16.346
26	-5.802	-16.974
27	-5.889	-17.585
28	-6.705	-19.424

Table D.2: Normal and shear stress for tension zone (Option 1)

Row (Refer to Figure B1)	Normal stress (MPa)	Shear stress (MPa)
29	-6.657	-19.963
30	-6.524	-20.474
31	-6.276	-20.961
32	-5.873	-21.429
33	-5.267	-21.894
34	-5.005	-23.476
35	-3.958	-24.222
36	-2.664	-25.227
37	-1.144	-26.635
38	0.528	-28.631
39	-0.828	-31.84
40	-0.294	-35.506
41	0.334	-40.363
42	3.494	-48.529
43	13.419	-49.972

Table D.3: Normal and shear stress for tension zone (Option 2)

Row (Refer to Figure B1)	Normal stress (MPa)	Shear stress (MPa)
29	-6.075	-20.065
30	-6.186	-20.534
31	-6.280	-20.961
32	-6.357	-21.344
33	-6.418	-21.692
34	-7.022	-23.121
35	-7.154	-23.661
36	-7.349	-24.403
37	-7.657	-25.491
38	-8.137	-27.108
39	-9.549	-30.307
40	-10.728	-33.673
41	-12.313	-38.141
42	-14.852	-45.305
43	-14.185	-45.121

APPENDIX E

CONCRETE TRIAL MIX

Concrete trial mix for the experiment

	Materiaal	FM	CBD (kg/m^3)	RD	K
Cement	OPC 42.5		1500	3.14	
	Surebuild 32.5		1500	3.04	
Sand	Philippi	1.5		2.69	
	Crusher dust	3.6		2.71	
	Malmesbury	2.3		2.60	
Stone	6 mm		1535	2.70	
	13 mm		1495	2.70	0.9
	19 mm		1577	2.72	1

Where:

FM = fineness modulus of sand calculated from sieve analysis

CBD = compacted bulk--density is a measure of packing capacity

CBD_{St}= dry compacted bulk density of stone determined in accordance with SABS Method 845:1994, kg/m^3

RD = Relative density is needed to calculate solid volume

Input data:

W/C ratio	**0.55**
water	**225liter**
sand	**Philippi**
Stone size	**13 mm**
Cement	**OPC 42.5**

		Quantity	
Water requirement	Mass (kg)	225	
	Volume (Litre)	225	
Sement requirement	Mass (kg)	409.091	C = W/(W/C)
	Volume (Litre)	130.284	V=C/RD
Stone content	Mass (kg)	1121.250	St = CBDst(K-0.1FM)
	Volume (Litre)	415.278	V=St/RD
Sand requirement	Mass (kg)	617.190	m=RD*v
	Volume (Litre)	229.438	$V=1000-V_{(w+se+st)}$

	Volume (litre)	Mass (kg)
Total	1000	2372.530

21 Litre	Volume (litre)	Mass (kg)
water	4.725	4.725
Cement	2.736	8.591
Stone size	8.721	23.546
sand	4.818	12.961

Result:

28 day	43	MPa	
7 day	30.1	MPa	70% strength of 28 days

APPENDIX F

DESIGN OF CONCRETE BEAMS FOR THE LABORATORY EXPERIMENT

Calculation for the experiment

1) Dimension of the beam

Input value		
b:	**200**	mm
h:	**280**	mm
L:	**2400**	mm
d:	**242**	mm

A_{beam} = 56000 mm^2 = 0.056 m^2

V_{beam} = 1E+08 mm^3 = 134.4 L

Concrete density= 24 kN/m^3

f_{cu}	**30**	MPa
f_{ck}	**25**	MPa
f_y	**450**	MPa

2) Load calculation

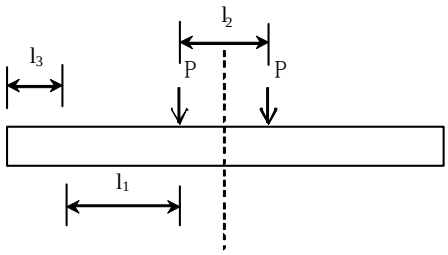

Self weight = 1.344 kN/m

l_1= 700 mm (face of support to point load)

l_2= **600** mm (point load to point load)

l_3= **200** mm (support length)

$l_{e=}$ **2200** mm (effective length)

Point load = 30 kN

R_{beam} = 60/ 2 + 1.344 × 2.4/ 2 = 31.613 kN

Jack force needed: **60** kN <= **134.62** kN (Max force the beam can take)

Longitudinal reinforcement

$M=0.156bd^2f_{cu}$ = 54.816 kNm

Bending

Max	Total	24.968	kNm
	M_{load}	24	kNm caused by applied load
	M_{beam}	0.9677	kNm caused by self weight

M= 24.968 kNm

$$K = \frac{M}{bd^2 f_{cu}} = 0.0711 < 0.156$$

$$z = d\left\{0.5+\sqrt{(0.25-\frac{k}{0.9})}\right\} = 221.09 \text{ mm}$$

$$A_s = \frac{M}{0.87 \cdot f_y \cdot z} = 288 \text{ mm}^2$$

	Dia	Area	Number	Total	Sum
phi	**10**	78.54	**2**	157.08	785.4
	20	314.16	**2**	628.32	

V_{face} = 31.478 kN $V_{face(1)}$= 31.344 kN

V_{ed} = 31.153 kN

v/2cot θ = **6.359** kN

$V_{Rd,max(22)}$ = 135.04 kN θ = 4.6205

$V_{Rd,max(45)}$ = 196.02 kN θ choose 22

$$l_{bondage} \geq \frac{F_s}{\pi \cdot \phi \cdot f_{cu}}$$ 34.899 mm /1.5 = 23.266 mm Bond stress: **2.9** MPa

phi	**10**	mm
As	78.54	mm^2
F(0.87Asfy)	30.748	kN

$l_a = n\Phi$ = 33.733 ϕ

$l_{anchorage}$(mm) = 3.4882 ϕ /1.5 = 2.3254 ϕ

Shear

$$Vc = \frac{0.75}{\gamma_m}\left(\frac{f_{cu}}{25}\right)^{\frac{1}{3}}\left(\frac{100A_s}{b_v d}\right)^{\frac{1}{3}}\left(\frac{400}{d}\right)^{\frac{1}{4}} = 0.7585 \text{ Mpa}$$

$$\left(\frac{100A_s}{b_v d}\right)^{\frac{1}{3}} = 1.1751$$

$$v = \frac{V}{bd} = 0.6532 \text{ Mpa} \qquad \frac{A_{sv}}{s_v} \geq \frac{b(v - v_c)}{0.87 f_{yv}} = -0.054$$

Nominal shear stirrups:

$$L_{nominal} = \frac{V_{max} - (v_c + 0.435) \cdot b \cdot d}{\omega}$$

$\frac{A_{sv}}{s_v}$ = 0.002b = 0.4

Choose R8@175 stirrupts, where $\frac{A_{sv}}{s_v}$ = 0.575

0.081= 176 mm

Total volume: 537.6 + 3 = 540.6 Litre Take: **600** Litre

APPENDIX G

BEAM END CONDITIONS CHOSEN FOR THE EXPERIMENT

Beam 1 : Tension reinforcement anchor after the face of support (Rigid support)

top

2Y10		
length 1	2390	mm
length 2	2390	mm

Bottom

2Y10		
length 1	2130	mm
length 2	2130	mm

2Y20		
length 1	2004	mm
length 2	2005	mm

Stirrups

Face of support

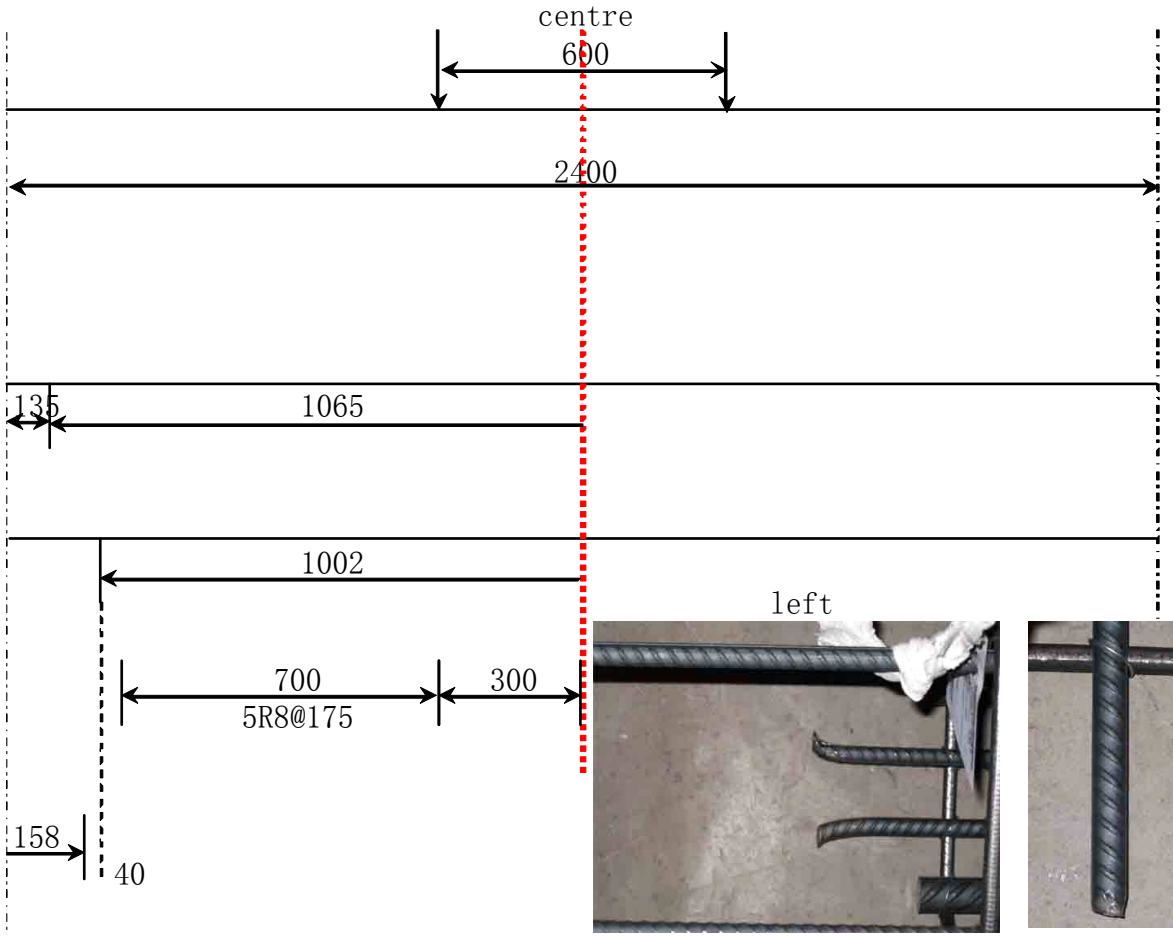

Beam 2 : Tension reinforcement anchor after the face of support (Rubber support)

top

2Y10		
length 1		mm
length 2		mm

Bottom

2Y10		
length 1	2130	mm
length 2	2130	mm

2Y20		
length 1	2025	mm
length 2	2025	mm

Stirrups

Face of support

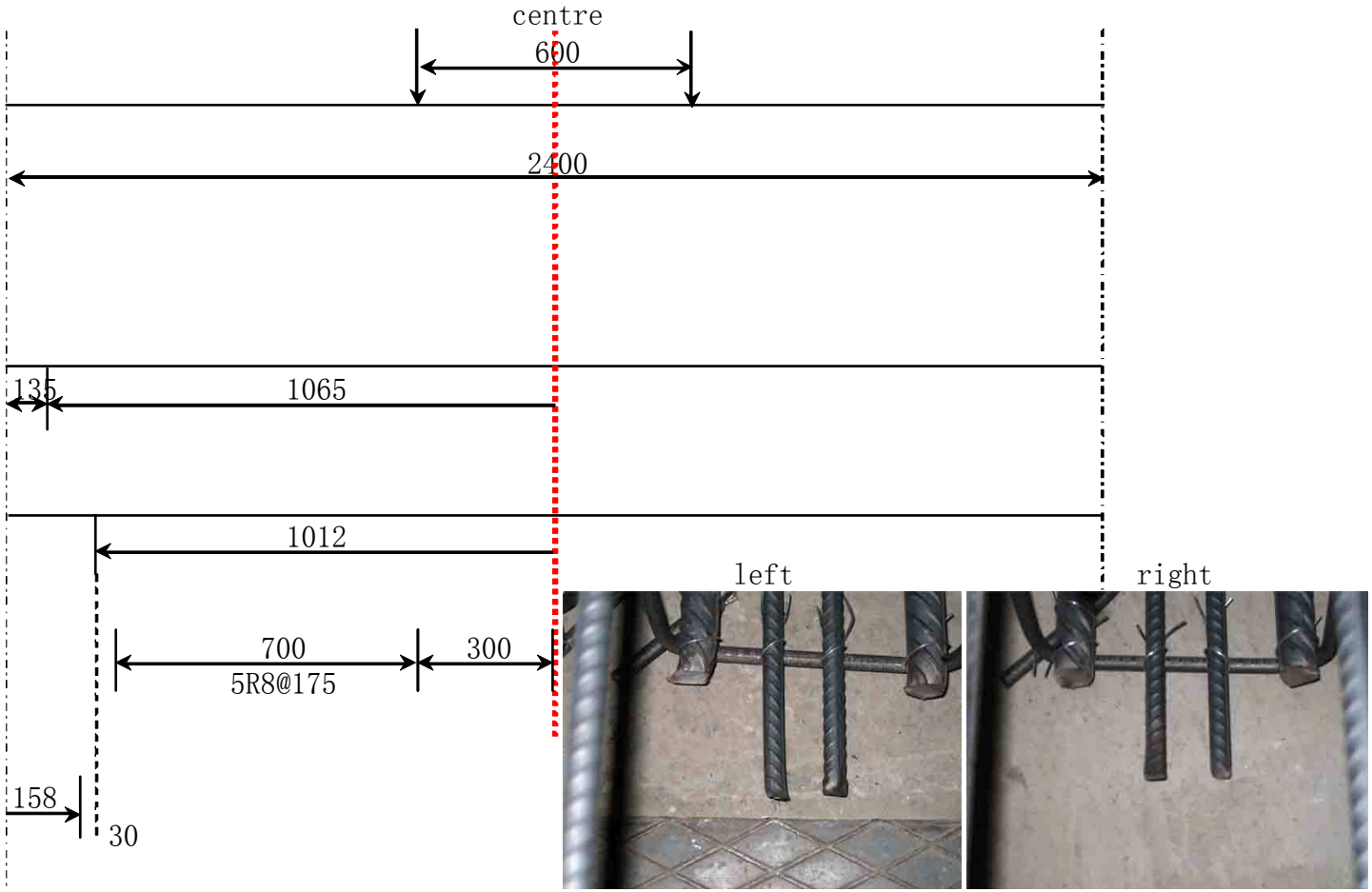

Beam 3 : Tension reinforcement anchor after the centre of support (Rubber support)

top

2Y10		
length 1	2393	mm
length 2	2395	mm

Bottom

2Y10		
length 1	2224	2230flaw
length 2	2224	mm

2Y20		
length 1	2030	mm
length 2	2026	mm

Stirrups

Face of support

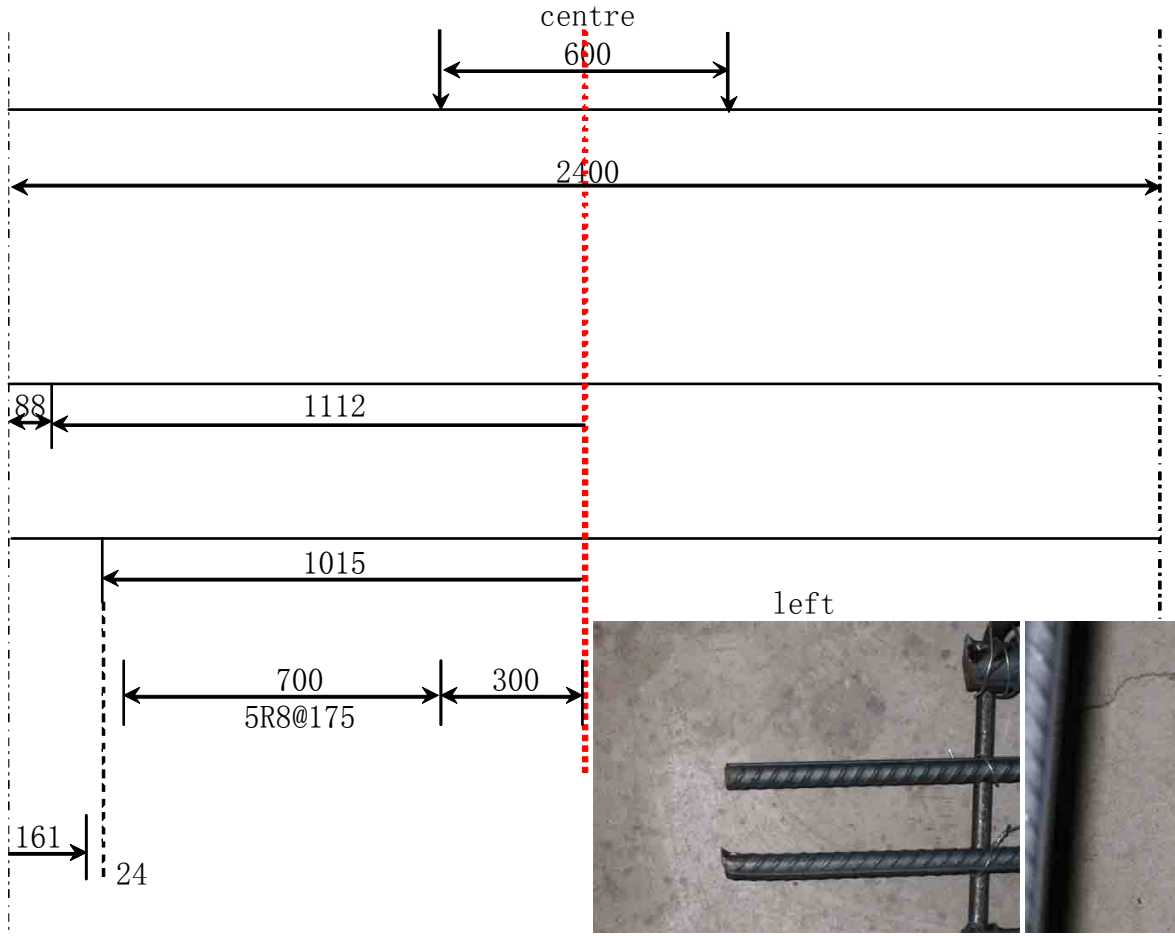

Beam 4 : Tension reinforcement anchor 12d after the centre of support (Rubber support)

top

2Y10		
length 1	2394	mm
length 2	2395	mm

Bottom

2Y10		
length 1	2392	mm
length 2	2392	mm

2Y20		
length 1	2028	mm
length 2	2028	mm

Stirrups

Face of support

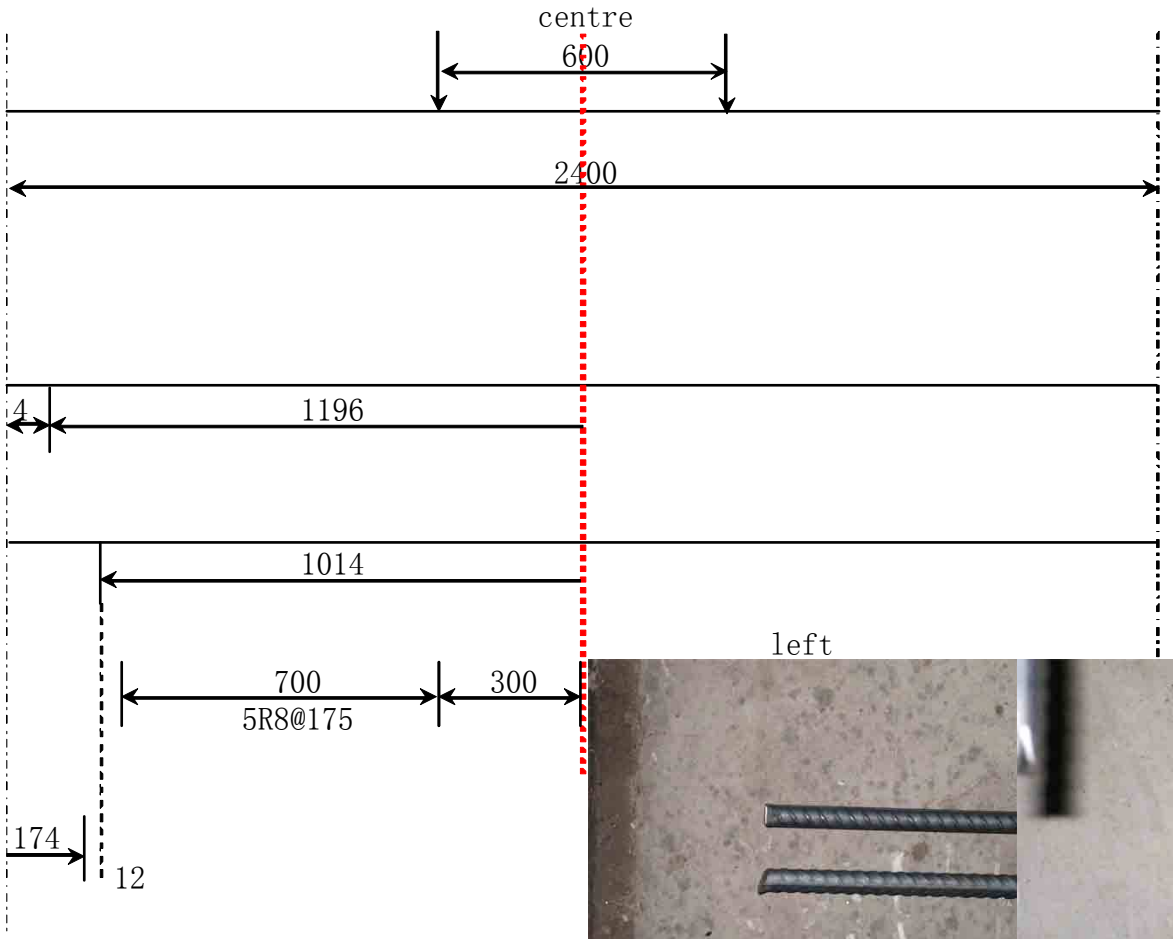

APPENDIX H

CONCRETE MIX FOR EXPERIMENT

W/C ratio	0.55
water	185liter
sand	Malmesbury
Stone size	13 mm
Cement	OPC 42.5

		Quantity	
Water requirement	Mass (kg)	185	
	Volume (Litre)	185	
Sement requirement	Mass (kg)	336.364	C = W/(W/C)
	Volume (Litre)	107.122	V=C/RD
Stone content	Mass (kg)	1001.650	St = CBDst(K-0.1FM)
	Volume (Litre)	370.981	V=St/RD
Sand requirement	Mass (kg)	875.930	m=RD*v
	Volume (Litre)	336.896	$V=1000-V_{(w+se+st)}$

	Volume (litre)	Mass (kg)
Total	1000	2398.944

120 Litre	Volume (litre)	Mass (kg)
water	22.2	22.2
Cement	12.855	40.364
Stone size	44.518	120.198
sand	40.428	105.112

Result:

28 day	**43**	MPa	
7 day	30.1	MPa	70% strength of 28 days

APPENDIX I

RESULTS OF CONCRETE STRENGTH AND BOND STRENGTH OF TEST CUBES WITH EMBEDDED REINFORCING BAR

Pull out test 2009/10/19 load rating: 1 mm/min

Concrete cube 1

b	d	h
150	150	150

mm

Concrete cube 2

b	d	h
100	100	100

mm

reinforcement Y 10 bar

Pull out test

cube	time	F_{max} (kN)	bond(mm)	bond stress
1	9:35	28.963	130	4.728
2	10:00	34.781	144	5.125
3	10:16	40.599	147	5.861
4	10:34	34.035	136	5.311
5	10:58	32.999	137	5.111
6	11:12	33.319	147	4.810

$$l_b = \frac{F}{\pi \cdot \phi \cdot f_{cu}} \Rightarrow f_{cu} = \frac{F}{\pi \cdot \phi \cdot l_b}$$ /1.5 safety factor

average 5.158 MPa

Strength

cube	time	F (kN)	factor	stress	true dimension	
1	8:14	28.8	1.005	28.657	100	101
2	8:24	28.7	1.005	28.558	100	101
3	8:29	28.2	1.005	28.341	100	100
4	8:33	29.4	1.005	29.845	99	100
5	8:37	28.4	1.005	28.830	99	100
6	8:40	29	1.005	28.856	100	101
7	8:44	29.6	1.005	29.748	100	100
8	8:50	29.5	1.005	29.066	100	102
9	8:57	28.5	1.005	28.359	100	101
10	9:02	30.9	1.005	30.747	100	101
11	9:06	28.7	1.005	28.003	100	103
			average	29.0011	MPa	